

Chemistry of Alkylaromatics in Crude Oil Upgrading

By

Lawrence Tin Chi Lai



B.S.E in Chemical Engineering, University of Michigan, 2012

M.S. Chemical Engineering Practice, Massachusetts Institute of Technology, 2016

Submitted to the Department of Chemical Engineering
in Partial Fulfillment of the Requirements for the Degree of
Doctor of Philosophy in Chemical Engineering

at the

MASSACHUSETTS INSTITUTE OF TECHNOLOGY

June 2019

© 2019 Massachusetts Institute of Technology. All rights reserved.

Signature redacted

Signature of Author.....

Department of Chemical Engineering
5/14/2019

Signature redacted

Certified by.....

William H. Green
Hoyt C. Hottel Professor in Chemical Engineering
Thesis Supervisor

Signature redacted

Accepted by.....

Patrick S. Doyle
Robert T. Haslam (1911) Professor of Chemical Engineering, Graduate Officer
Committee for Graduate Students

Chemistry of Alkylaromatics in Crude Oil Upgrading

By

Lawrence Tin Chi Lai

Submitted to the Department of Chemical Engineering
on May 14th in Partial Fulfillment of the Requirements for the
Degree of Doctor of Philosophy in Chemical Engineering

Abstract

Due to the rise in demand of crude oil over the long term, technologies to upgrade crude oil need to be developed to ensure maximum use efficiency of future oil sources. In typical carbon rejection processes, coke formation is a common phenomenon that would lead to decreased yield of upgraded oil. As a result, the chemical behavior of coke formation is a potent area of research. Due to the high complexity of the composition of crude oil and coke, this work simplifies the study of supercritical water upgrading of crude oil to a hexylbenzene pyrolysis system. The pyrolysis of hexylbenzene at process conditions of 450°C and 75 creates several hundred products resolved by GCxGC, and the analysis is intractable if one considers only the experimental data, which does not reveal reactive intermediates or reaction paths. However, introducing theoretical considerations using the Reaction Mechanism Generator (RMG) allows analysis of a vast number of species while retaining information of elementary reaction steps and reactive intermediates. Information on these steps and intermediates can be obtained from Quantum Chemistry

Hexylbenzene pyrolysis was characterized using RMG with key steps computed using Quantum Chemistry. The results indicate that the retro-ene reaction, previously thought to carry an important role in hexylbenzene pyrolysis, is much slower than reported in literature. Furthermore, alkylaromatic chemistry at 450°C is extremely sensitive to species thermochemistry. Further investigation was done on the formation of 2-ring aromatic species in hexylbenzene pyrolysis, likely precursors of coke. Thermochemistry and rate calculations were made for 2-ring species as a result of the intramolecular and intermolecular addition pathways, resulting in 27 thermochemistry group additivity values to allow for extrapolation of this work's calculations to analogous species. In addition, 25 training reactions were added to allow rate rules calculated in this work to be extrapolated to similar reactions.

Finally, all this new chemical knowledge was incorporated into RMG, and a detailed kinetic model for hexylbenzene pyrolysis was constructed. The generated model was able to predict the total molar yield of bridged 2-ring aromatics, and fused 2-ring aromatics. However, many individual species had inaccurate molar yield predictions, and some key pathways to form 2-ring species were found to be missing. Additional quantum calculations were performed after the construction of this kinetic model to attempt to resolve these mispredictions.

Thesis Supervisor: William H. Green

Title: Hoyt C. Hottel Professor of Chemical Engineering

Acknowledgements

I would like to express gratitude to my thesis advisor, Professor William Green, who displayed incredibly deep expertise in a vast variety of subjects, trusted his students with freedom to pursue their research goals, and invested in each of his individual students patiently as we slowly developed our niches. My work in particular took many iterations to reach its current form; for a while I exclusively worked on experiments, and I spent more time than I would like to admit to study my predecessors' work in excruciating detail, and Professor Green gave me the appropriate guidance, trust, and patience for me to overcome the learning curve I had to pick up all the necessary research skills.

My thesis committee members, Michael Timko, Roger Summons, and Yuriy Roman, each had their own expertise relevant to this work. I would always refer new experimentalists to talk to Professor Timko and Professor Roman's students for their great experience in reactor engineering in different settings. Professor Summons is an invaluable expert on separations with a non-chemical engineering point of view that gave a different perspective on problems and classes of compounds of interest.

My former mentors Adam Carr and Caleb Class gave me an early transition to the lab group. Adam took time off his work at Aerodyne corporation to come back to the Green Group every Friday to make sure that I am well transitioned to the experimentalist's job (apart from finishing his own work). Caleb left me with his RMG Java model of hexylbenzene, which was an extremely important starting point for my thesis work, and to learn about the technicalities of RMG.

Throughout the years, my undergraduate partners, Tamba Monroe, Alison Lui, Perman Jorayev, and Isaiah Borne were all extremely hard-working individuals. I'd often find myself taking the supporting role to these students' research goals, cleaning apparatus and doing the janitor's work (which are traditionally thought of as an undergraduate student's job) so that I could enable them on their valuable work in their short summer schedules. It was a pleasure seeing these students exploring their ideas and learning from them.

My peers, have provided me with support and key pieces of knowledge. Without them, my work was not possible. These peers include Soumya Gudiyella, Mengjie Max Liu, Allen Mark Payne, Sarah Khanniche, Zachary Buras, Jim Chu, Nathan Yee, Mark Goldman, Kehang Han, Matt Johnson, Ryan Gillis, Hao-Wei Pang, Agnes Jocher, Phalgun Lolur, Yi-Pei Li, Alon Grinberg Dana, Nick Vandewiele, Connie Wu, Lisa Hsieh, Enoch Dames, Jianghuai Cai, and Duminda Ranasinghe.

On my personal life, I would like to thank my parents, Anthony Lai, and Josephine Ip, and brothers, Joseph Lai, and Sunny Lai (also my roommate for the last five years). Everybody from my extended family thought I would be the med student, just like my mother. None of my siblings became a doctor; instead, we went our own ways to do our great things. Our family of five has very distinct personalities and traits from each other, and I'm sure that had a great role to play in my upbringing as a chemical engineer and scientist.

I used to be a president of two student organizations (at different times). I was the president of MIT's Hong Kong Student Society for three years. On the verge of the organization shutting down due to everybody in it graduating, I partnered with individuals with Godine Chan, Wang Chi Cheung, Alice Wong, Janice Chui, and Joanne Lee to regrow the organization. I eventually found Anfernee Lo and Crystal Tsui, where they could continue at where I left off. I shook hands with a few influential people from Hong Kong, learnt how to write a website (all on my own), publicize for events, and familiarized myself with many intricacies with the student activities office. I was once passionate about spreading Hong Kong's culture, and keeping this organization alive and trying to expand was a great experience.

I started MIT Sport Taekwondo when I was introduced to the sport by Yang Dai. Through many belt ranks, I survived a grueling black belt test, and became appointed to become the President of this organization. It was a rewarding experience to change the inner workings of the team that I felt didn't work, recruit the largest year since I've joined the team, and develop relationships with other taekwondo schools, but I had to leave my position due to this thesis and a few other rising conflicts that I faced in the team. I want to thank my former friends Jaz Harris, Elizabeth Zou, Peter Tran, Akwasi Owusu-Akyaw, Richard Joshua Murdock, Lorenz Baumgartner, Nina Anwar,

Samantha Amey-Gonzalez, Yaseem Rana, Anastasiia Uvarova, Michelle He, Silvia Knappe, Renee Zhao, Samuel Majors, Suzie Byun, Lillian Bu, Jiaying Liu, Yenthanh Le, Christopher Williams, who at one point or another helped me through my growth as an athlete or supported and appreciated my work.

Finally, I'd just like to thank others that I was/am close to. Jacynth Tate Agraan, June Lam, Hoiting Helen Cheung, Elizabeth Koze, Yang Dai, Wendy Lee Trattner, Tam Nguyen, Jennifer Wong, Stella So, and Coco Yiu. The tremendous personal growth that I've been through in my years of graduate school was made possible because of these individuals that I have met.

Contents

1. Chapter 1.....	15
1.1. Shortage of Oil.....	15
1.2. Crude Oil Upgrading.....	16
1.3. Hexylbenzene Model Compound System	18
1.4. Reaction Mechanism Generator (RMG)	20
1.5. Thesis Objectives	21
2. Chapter 2.....	23
2.1. Introduction.....	23
2.2. Methods.....	25
2.2.1. Batch Reactor	25
2.2.2. GC-FID Method for Gas Analysis	25
2.2.3. GC-MS/FID Method for Liquid Analysis	25
2.2.4. GCxGC-FID Method for Liquid Analysis.....	26
2.2.5. Overview of Computational Methods	26
2.2.6. Constructing Chemical Kinetics Simulations with RMG	26
2.2.7. CHEMKIN Simulations	27
2.2.8. Gaussian 03 Calculations	28
2.2.9. RMG – Arkane (formerly known as Cantherm).....	28
2.3. Results and Discussion	28
2.3.1. New Experimental Results	28
2.3.2. Changes to Carr et al. Model	30
2.3.3. Overview of new Reaction Pathway	33
2.3.4. Kinetic Sensitivity Analysis of Hexylbenzene	35
2.3.5. Kinetic Rates of Sensitive Reactions.....	40
2.3.6. Thermochemistry Sensitivity of Hexylbenzene	42
2.3.7. Thermodynamics of Key Species	45
2.3.8. Uncertainty of species thermochemistry.....	49
2.4. Conclusions	51
3. Chapter 3.....	53
3.1. Introduction.....	53
3.2. Computational Details	57
3.2.1. RMG – Cantherm.....	57
3.2.2. Group Additivity Estimates.....	57
3.2.3. Uncertainty Analysis.....	59
3.3. Results and Discussion	59
3.3.1. Fused Two Ring Aromatic Formation Mechanism.....	59
3.3.2. Thermochemistry of Fused Two Ring Aromatic Species.....	62
3.3.3. Derived Group Values.....	67
3.4. Conclusions	73
4. Chapter 4.....	75
4.1. Introduction.....	75

4.2.	Methods.....	77
4.3.	Results and Discussion	77
4.3.1.	Aromatic Intermolecular Addition Reactions of Interest.....	77
4.3.2.	Thermochemistry of Intermolecular Addition Products.....	79
4.3.3.	Derived Thermochemistry Group Values for Intermolecular Addition Products	81
4.3.4.	Future work for thermochemistry estimations in intermolecular addition.....	85
4.3.5.	Kinetics of Intermolecular Addition	86
4.3.6.	Summary to rate coefficients of Aromatic Intermolecular Addition	92
4.4.	Conclusions	92
5.	Chapter 5.....	93
5.1.	Introduction.....	93
5.2.	Experimental Methods	95
5.2.1.	GCxGC-qMS/FID Method for Liquid Analysis.....	95
5.2.2.	Constructing Chemical Kinetics Simulations with RMG	95
5.3.	Results and Discussion	97
5.3.1.	GCxGC Analysis of 2-ring aromatics.....	99
5.3.2.	Bridged 2-Ring Aromatics	103
5.3.3.	Fused 2-Ring Species.....	109
5.3.4.	Species Beyond 2 Rings	117
5.3.5.	Hexylbenzene Isomers.....	119
5.4.	Conclusions	120
6.	Chapter 6.....	122
6.1.	Summary of chapter conclusions	122
6.2.	Future of CBS-QB3 calculations	124
6.3.	Additional Chemical Systems to Study.....	125
6.4.	Future of Hexylbenzene Model for 2-Ring Aromatics.....	126
6.5.	Fully automated chemical mechanism generation of alkylaromatic pyrolysis	126
6.6.	Improvements in Gas Chromatography Instrumentation	127
6.7.	Improvements in Batch Reactor Method	128
6.8.	Incorporation of Water to investigation.....	129
6.9.	Transition from 2-Ring Species to Coke	130
7.	References	131

List of Figures

- Figure 1 Growth in oil demand projected by the OPEC WOO 2018 for Eurasia, developing countries (DCs), India, China, Organization for Economic Cooperation and Development (OECD) and the World. 15
- Figure 2 Products of a) hexylbenzene + water, 450°C and 300 bar, and b) hexylbenzene, 450°C, 70 bar. The color of products is visually different, indicating the suppression of coke formation in conditions where water is present. 17
- Figure 3 GCxGC-FID chromatograms of a) crude oil, and b) supercritical water treated crude oil at 450°C and 300 bar, 30 minutes. 18
- Figure 4 GCxGC-FID chromatograms for a) Pure hexylbenzene, and b) SCW treated hexylbenzene at 450°C, 300 bar, 40 minutes. 20
- Figure 5 Carr et al. model (Lines) comparison with Carr et al. experiments (no fill symbols ○) and this work's experiments (filled symbols ●) for conversion of hexylbenzene (left) and molar yield of major aromatic products(right), including toluene (blue line/circles), styrene (black dashed line/triangles), and ethylbenzene (red dotted line/squares). Reaction conditions are at 22.6.mL volume, temperature ramp up to 450°C over 10 minutes based on experimental pressure profile (30-350 bar). Aromatic molar yield is defined here as moles aromatic compounds present in product divided by starting moles of hexylbenzene. Error bars denote the standard deviation of duplicated experiments. For instances where duplicates were not performed, error bars are averaged from other time points of the same study. 29
- Figure 6 Schematic of 4-membered ring "retro-ene" described by Burklé-Vitzthum [33], and 6-membered ring retroene reaction described by Klein and Virk [34]. The 4-membered ring "retro-ene" reaction is used in Carr et al.'s model, and its rate is highly overestimated. 30
- Figure 7 Conversion comparison between model by Carr et al (black dotted), Lai version 1 after removal of 4-membered ring "retro-ene" reaction and introduction of RMG-Py database (red dashed), and Lai version 2 (blue solid) after all revisions discussed in this article are applied. Experimental data points (circles) included for comparison. Reaction conditions are at 22.6.mL volume, temperature ramp up to 450°C over 10 minutes based on experimental pressure profile (30-350 bar). 32
- Figure 8 Overview of the chemical mechanism of the pyrolysis of Hexylbenzene in Lai Version 2 at short reaction times. The full chemical mechanism can be found in the supporting information and involves >200 reactions and >2500 reactions. 33
- Figure 9 Moles of aliphatic hexylbenzene radicals in Lai Versions 1 (black) and 2 (white) at 16 minutes. Reaction conditions are at 22.6.mL volume, temperature ramp up to 450°C over 10 minutes based on experimental pressure profile, initial pressure of helium and hexylbenzene scaled to experimental feed, and mass fractions of 0.833 Helium and 0.167 hexylbenzene. Radical species are defined below: 34
- Figure 10 Sensitivity of hexylbenzene with respect to rate coefficients for Lai Versions 1 (black) and 2 (white) at 16 minutes. Reaction conditions identical to Figure 9. Reactions are listed in descending order of sensitivity in Lai Version 1. 36
- Figure 11 Log rate of formation of initiation reactions evaluated at 16 minutes reaction time for Lai Versions 1 (black) and 2 (white). Reaction conditions identical to Figure 9. 37

Figure 12. Relative reactive fluxes of beta scission of hexylbenzyl radicals evaluated at 16 minutes reaction time for Lai Versions 1 (black) and 2 (white). Reaction (3) in Lai Version 1 is set as 100% relative flux in this plot. Reaction conditions identical to Figure 9.	38
Figure 13. Conversion of Hexylbenzene in Lai Version 1 where the pre-exponential factor of reaction (2) is multiplied by 0.5, 1, 2, 5 10, and 100 times, denoted by the different colored curves. Reaction conditions identical to Figure 9.	40
Figure 14. Conversion of Hexylbenzene in Lai Version 1 where the pre-exponential factor of reaction (3) is multiplied by 0.5, 1, 2, 5 10, and 100 times, denoted by the different colored curves. Reaction conditions identical to Figure 9.	41
Figure 15 Sensitivity of hexylbenzene with respect to species Gibbs free energy for Lai Versions 1 (black) and 2 (white) at 15 minutes. Reaction conditions identical to Figure 9. Species are listed in descending order of sensitivity in Lai Version 1.....	43
Figure 16. Model conversion of Hexylbenzene in Lai Version 1 with modified enthalpy of hexylbenzene (from -1kcal/mol to +10kcal/mol). It can be observed on this plot that a change as small as 1kcal/mol can significantly changes the conversion of hexylbenzene with respect to time. Reaction conditions identical to Figure 9.	44
Figure 17 Model predicted (lines) and experimental measured (symbols) molar yield of major aromatic species for Lai Version 2, including toluene (blue), ethylbenzene (red), and styrene (black). Horizontal axis is set as conversion of hexylbenzene to allow better comparison of species selectivity between model and experiments. Reaction conditions identical to Figure 9.	48
Figure 18 GCxGC chromatogram of hexylbenzene pyrolysis products at 450°C, 40 minutes. Chromatogram shows many peaks in regions with two or more aromatic rings.....	49
Figure 19. Error bounds of hexylbenzene conversion in Lai Version 2, computed by adding/substracting the root mean square deviation of enthalpy for the CBS-QB3 level of theory to Hexylbenzene's Gibbs free energy in Lai Version 2.	50
Figure 20 Gibbs free energy comparison of Hexylbenzene using CBS-QB3 method (blue solid line) and M06-2x/cc-pVTZ method (red dashed line). At the temperature of interest (723K), there is a 10.1 kcal/mol difference.....	51
Figure 21 Proposed formation mechanism for propylindene from the third hexylbenzene radical	60
Figure 22 Proposed formation mechanism of ethylnaphthalene from the fourth hexylbenzene radical	60
Figure 23. Proposed phenyl migration pathways from hexylbenzene to x-phenyl-1-hexyl radicals.	61
Figure 24 Distribution of Gibbs free energy deviation (kcal/mol) for 83 calculated fused two ring species up to 12 carbon atoms. Distribution for previous RMG estimates (white) and with updated group values (black) are shown.	67
Figure 25 Distribution of Gibbs free energy deviation (kcal/mol) for 24 calculated aromatic intermolecular addition products. Distribution for RMG estimates previously (white) and after adding the aromatic pi radical group (black) are shown.	81
Figure 26 Evans-Polanyi relationship for aromatic intermolecular addition reactions calculated by CBS-QB3 (blue circles) and aliphatic intermolecular addition reactions approximated by RMG using propylene + radical (red squares). It can be observed that the two classes of reactions exhibit very different Evans Polanyi relationships.....	88

Figure 27 RMG estimated rate coefficients (dashed) and CBS-QB3 calculated rate coefficients (solid) for 1. Toluene + H (Blue), 2. Toluene + CH ₃ (Red), 3. Toluene + C ₂ H ₅ (Green), 4. Toluene + Benzyl (Purple), and 5. Toluene + 1-phenyl-1-ethyl (Orange). Rate coefficients for each class of reaction are averaged between four different addition sites. It can be observed that RMG's rate estimates are much faster than CBS-QB3 calculations because of RMG's questionable source.	88
Figure 28 CBS-QB3 calculated rate coefficients for toluene + H (Blue Solid) and hexylbenzene + H (Black dashed) in the substituted position. Rate coefficients for two reactions differ by no more than factor of 1.5 across all temperatures shown.	89
Figure 29 Rate coefficients for 1. Toluene + H (Blue Solid), 2. Hexylbenzene + H (Black Dashed), 3. Toluene + CH ₃ (Red Dotted), 4. Toluene + C ₂ H ₅ (Green Dash Dotted), 5. Toluene + Benzyl (Purple Dash Double Dotted), and 6. Toluene + 1-phenyl-1-ethyl radical (Orange Solid). Rate coefficients for each class of reaction are averaged between four different addition sites. The calculated rate coefficient is slower for the addition of larger radical species.	90
Figure 30. Rate coefficients for 1. Toluene + H (Ortho) (Blue Solid), 2. Toluene + H (Meta) (Red Dashed), 3. Toluene + H (Para) (Purple dotted), and 4. Toluene + H (Substituted) (Black Dash Dotted). Differences in the rate coefficients up to an order of magnitude can be observed.	91
Figure 31 a) Experimental conversion of hexylbenzene for previous work [29] (red crosses), this work (blue circles) and model predicted conversion of hexylbenzene for previous work [29] (red dashed lines), this work (blue solid lines); b) molar yield of toluene (red), ethylbenzene (blue), and styrene (green) for previous work [29] (crosses) and this work (circles). Reactor temperature of 450°C with 10 minutes heat up time. Reactor pressure 55 bar. Error bars represent standard deviation in replicated experiments.	97
Figure 32 GCxGC chromatogram of products produced by hexylbenzene pyrolysis at 40 minutes, 450°C, and 55 bar. Key compounds and groups labelled.	99
Figure 33 GCxGC chromatograms of hexylbenzene pyrolysis, 15 minutes, 450°C, and 55 bar.	100
Figure 34 GCxGC chromatograms of hexylbenzene pyrolysis, 20 minutes, 450°C, and 55 bar.	100
Figure 35 GCxGC chromatograms of hexylbenzene pyrolysis, 30 minutes, 450°C, and 55 bar.	101
Figure 36 GCxGC chromatograms of hexylbenzene pyrolysis, 40 minutes, 450°C, and 55 bar.	101
Figure 37 GCxGC chromatograms of hexylbenzene pyrolysis, 60 minutes, 450°C, and 55 bar.	102
Figure 38 GCxGC chromatogram of hexylbenzene pyrolysis, 90 minutes, 450°C, and 55 bar.	102
Figure 39 a) Experimental (circles) and model predicted (line) total molar yield of bridged 2-ring aromatics, b) experimental molar yield of bibenzyl (red circles), 1,3-biphenylpropane (blue squares), 1,4-biphenylbutane (green diamonds), biphenyl (orange crosses), sum of selectivities of C ₂₀ H ₂₆ (purple triangles), and total alkyl biphenyl (grey dashes). Model predicted molar yield of bibenzyl (red lines), 1,3-biphenylpropane (blue line), 1,4-biphenylbutane (green line), biphenyl (orange line), sum of molar yield of of C ₂₀ H ₂₆ (purple line), and sum of molar yield of alkylbiphenyl compounds (grey line). Batch reactor conditions of 450°C, and 55 bar.	103
Figure 40 The two C ₂₀ H ₂₆ species seeded in the kinetic model.	104
Figure 41 Proposed formation pathway for biphenyl compounds by (1) addition of phenyl radicals to aromatic bonds, followed by beta scission of an aliphatic radical, (2) radical recombination of two phenyl radicals, (3) cyclization of a phenylhexenyl radical, (4) Diels-Alder addition	

	between styrene and 1,3-butadiene, or (5) intramolecular hydrogen abstraction followed by phenyl radical addition to the second aromatic ring in bridged aromatics	106
Figure 42	Phenyl + ethylbenzene pathway studied to model the behavior of biphenyl formation in hexylbenzene pyrolysis	107
Figure 43	Rate coefficients of phenyl radical + ethylbenzene (in $\text{cm}^3/\text{mol}\cdot\text{s}$) (blue) and ethylbiphenyl radical beta scission (in s^{-1}) (red) estimated by RMG (dashed) and calculated by CBS-QB3 (solid).....	108
Figure 44	Molar yields of biphenyl (blue), methylbiphenyl/hexylbiphenyl (red). Experiments are represented in circles/squares, model yield in dashed lines, and model yield with updated kinetics from Figure 43 in solid lines.	109
Figure 45	Total molar yield of all fused 2-ring aromatics (including non-fully and fully aromatic species) for experiments (circles) and model (line). Batch reactor conditions of 450°C , and 55 bar.....	110
Figure 46.	Experimental molar yield of propylindane (red circles), ethyltetralin (blue squares), indane (green diamonds), methylindane (purple triangles), and tetralin (orange crosses). Model predicted molar yields of indane (red solid line) and ethyltetralin (blue dashed line). Batch reactor conditions of 450°C , and 55 bar.....	111
Figure 47	Most plausible formation pathway for naphthalene from ethyltetralin.	112
Figure 48	Experimental molar yield of naphthalene (red circles), methylnaphthalene (blue squares), ethylnaphthalene (green triangles), and benzocycloheptatriene (purple crosses). Model molar yield of naphthalene (red solid line) and ethylnaphthalene (green dashed line). Batch reactor conditions of 450°C , and 55 bar.	113
Figure 49	Proposed formation pathway of benzocycloheptatriene.	114
Figure 50	Rate coefficient of hexylbenzene intermolecular addition ($1/\text{s}$) to form methylbenzocycloheptene radical precursor (in shown in Figure 49) estimated by RMG (dashed) and calculated by CBS-QB3 (solid).....	115
Figure 51	Experimental molar yield of benzocycloheptatriene (crosses). Model predicted molar yields of methylbenzocycloheptene using RMG estimates (dashed), and using CBS-QB3 calculations (solid).	117
Figure 52 a)	Total molar yield of > 2 ring species, and b) molar yield of methylfluorene (blue circles), phenylnaphthalene (red squares), terphenyl (green diamonds), methylterphenyl (purple triangles). Batch reactor conditions of 450°C , and 55 bar.	118
Figure 53	Proposed formation pathways for methylfluorene, phenylnaphthalene, and terphenyl/methylterphenyl in this work's batch reactor conditions.	119
Figure 54	Total molar yield of hexylbenzene isomers (excluding n-hexylbenzene) measured by experiments (circles) and predicted by model (line). Batch reactor conditions of 450°C , and 55 bar. Exact identity of hexylbenzene isomers unknown due to lack of reference data.	120

List of Tables

Table 1. Rate of 4-membered ring “retro-ene” reaction by Burklé-Vitzthum [33] and this work, rate of 6-membered ring retroene reaction by this work, and RMG estimate of C-C scission rate. Calculations in this work done using the CBS-QB3 level of theory for propylbenzene.	31
Table 2. Model Version Description.....	32
Table 3 RMG rate estimation for Beta-Scission Reactions.....	39
Table 4 Rate constant parameters in modified Arrhenius format for reaction (3) estimated by RMG’s group estimates and calculated by CBS-QB3 level of theory. Temperature range of 300-2500K.	42
Table 5 Table of thermochemistry values for all species calculated in this work at 723K. Full NASA polynomials are available in the Supporting Information.	45
Table 6 Table of thermochemistry values at 298.15K, in comparison with literature values.	47
Table 7 Summary of thermochemical databases and their various characteristics	54
Table 8 Thermochemical data of species calculated in this work.....	62
Table 9 Thermochemical data comparison between this work and other literature sources (all data available).	65
Table 10. Original and updated values of polycyclic groups and the sources of RMG’s original group values.....	68
Table 11. Original and updated HBI groups for radicals, with their respective enthalpy/entropy values and the source of RMG’s original value. Enthalpy values in kcal/mol, and entropy values in cal/mol K.	70
Table 12 All available comparisons between this work’s hydrogen bond increments compared to Handbook of Bond Dissociation Energies in Organic Compounds [71].	72
Table 13 Aromatic intermolecular addition pairings considered for this work; possible resulting species are listed.	77
Table 14 Thermochemical data of species calculated in this work. Heat capacities given in supporting information.	79
Table 15 Various resonance structures estimated by RMG for Toluene + H products and how RMG classified them due to the lack of specify in radical groups. On the top, products of addition in the ortho, meta, and substituted position all feature the “bisallylic radical between pi bonds” as the lowest energy resonance structure. On the bottom, the product of Toluene + H in the para position, RMG identifies this radical as either a “secondary allyl radical” or “tertiary alkyl radical” depending on the resonance structure, and therefore mispredicts the energy of this species by a greater deviation.	83
Table 16 Comparison of enthalpy and entropy for the hydrogen bond increments for the aromatic pi radical (this work), secondary radical between two pi bonds, secondary allyl radical, and tertiary alkyl radical ³⁴	84
Table 17 Modified Arrhenius rate parameters and rate at 723K for aromatic intermolecular addition reactions in CBS-QB3 level of theory.....	86
Table 18 Thermochemistry of biphenyl, ethylbenzene, ethylbiphenyl, ethyl radical, and phenyl radical.	107
Table 19 Thermochemistry of fused 2-ring species with seven membered secondary rings; including benzocycloheptene, benzocycloheptadiene, benzocycloheptatriene, and various radical species.	115
Table 20 Group Additivity Values Developed in chapter 5.....	116

1. Chapter 1

Introduction

1.1. Shortage of Oil

Based on the Organization of the Petroleum Exporting Countries' (OPEC) World Oil Outlook (WOO) of 2018 [1], the growth in oil demand of the world is projected to decrease from 1.5 mb/d to 0.3 mb/d, shown in Figure 1. While the Organization for Economic Cooperation and Development (OECD) is a major player in slowing down the world's oil demand growth, this growth is projected to continue up to year 2040, and efforts must be made by oil producers to match this demand.

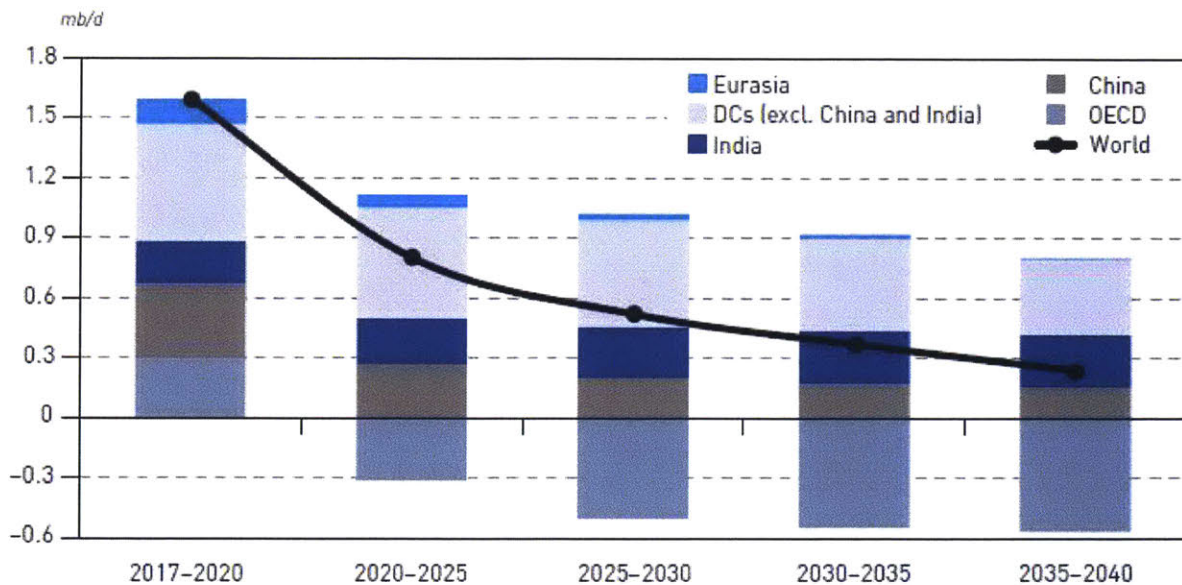


Figure 1 Growth in oil demand projected by the OPEC WOO 2018 for Eurasia, developing countries (DCs), India, China, Organization for Economic Cooperation and Development (OECD) and the World.

Part of the increase in the world's oil demand is to be met by heavy crude and shale oil [2]. In order to effectively use these heavy oil sources, crude oil must be chemically upgraded [3] [4] to oils with lower molecular weight and lower heteroatom content for the following reasons:

- Heavy oil is difficult to vaporize; pyrolysis takes place instead of combustion [5].
- Combustion of heavy oil is not as clean, due to the requirement of more equivalents of oxygen at the oil and air interface . [6]
- Heavy oil is extremely viscous, and transport of heavy oil in internal combustion engines is inefficient [7].
- High heteroatom content in heavy crude, such as sulfur [8] [9], nitrogen, and metals [3], are hazardous to the environment

1.2. Crude Oil Upgrading

Methods of crude oil upgrading include catalytic hydrogenation and petroleum coking [3]. The former process involves treatment at high hydrogen pressures with CoMo/NiMo catalyst [10], with the disadvantage that it uses expensive hydrogen [11], and is easily prone to deactivation of catalyst [3]. The latter process involves treatment at $\sim 500^{\circ}\text{C}$, pressures slightly higher than atmospheric, and avoids the requirement of using hydrogen or catalysts, but generates the unattractive side product of coke [12]. According to Ancheyta et al. [13], 15-30% of the crude oil's weight becomes coke in petroleum coking processes. In the interest of conserving the world's supply of oil and maximizing economic efficiency, upgrading technologies that avoid coke formation in crude oil upgrading is extremely crucial.

To avoid coke formation, Saudi Aramco developed supercritical water upgrading of crude oil [4], where supercritical water (water in conditions higher than the critical temperature and pressure of 647K and 220.6 bar [14]) is fed alongside crude in a process similar to petroleum coking, leading to upgraded oil with reduced coke formation. The coke suppression behavior of this process is modelled in this work, and shown in Figure 2, where the pyrolysis of hexylbenzene at 450°C in presence of water results in a much lighter color product than the pyrolysis of hexylbenzene in absence of water at 450°C .

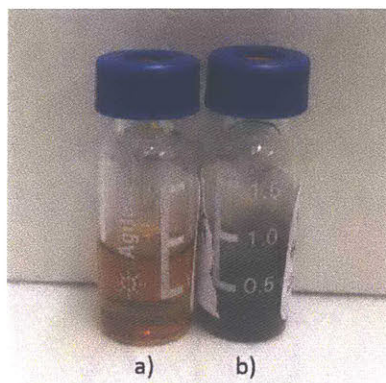
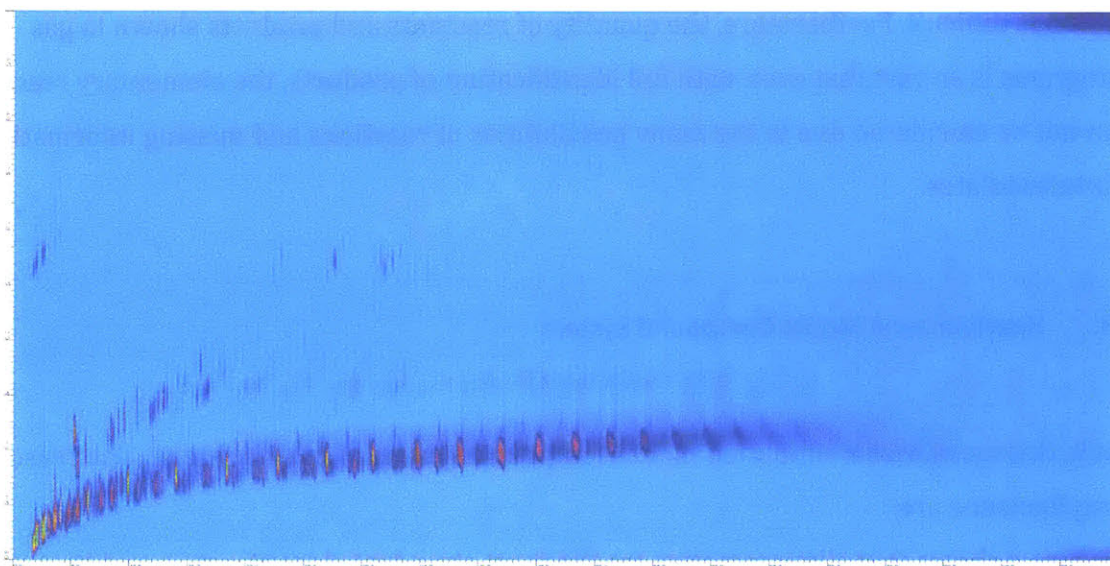
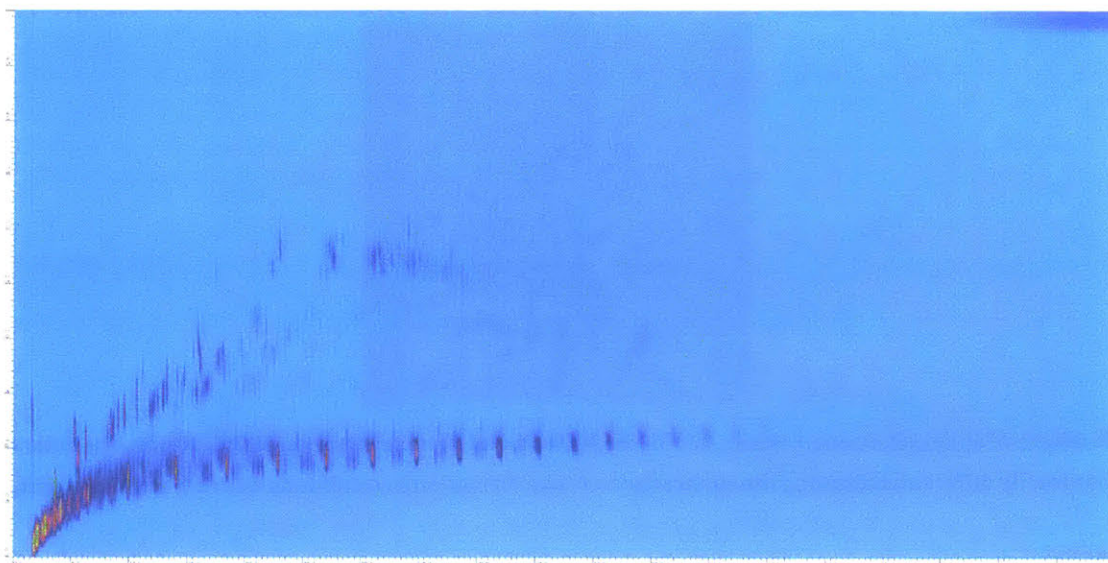


Figure 2 Products of a) hexylbenzene + water, 450°C and 300 bar, and b) hexylbenzene, 450°C, 70 bar. The color of products is visually different, indicating the suppression of coke formation in conditions where water is present.

To understand the behavior of coke formation and suppression, the early efforts of this work surround experimental work with crude oil. 2-dimensional gas chromatography with flame ionization detector (GCxGC-FID) was used as an analytical technique to analyze the reactant and product composition of crude oil. Figure 3 shows the GCxGC chromatograms of reactants and products of the supercritical water treatment of crude oil.



(a)



(b)

Figure 3 GCxGC-FID chromatograms of a) crude oil, and b) supercritical water treated crude oil at 450°C and 300 bar, 30 minutes.

A problem that Figure 3 presents towards characterizing coke formation is multifold. First, the complicated feed composition of crude oil cannot be fully characterized, and identifying changes in composition is difficult. Furthermore, the quantity of reactants and products shown in gas chromatograms is so vast that even with full identification of products, the elementary reaction steps can not be elucidated due to the many possibilities of reactions and missing information of radical intermediates.

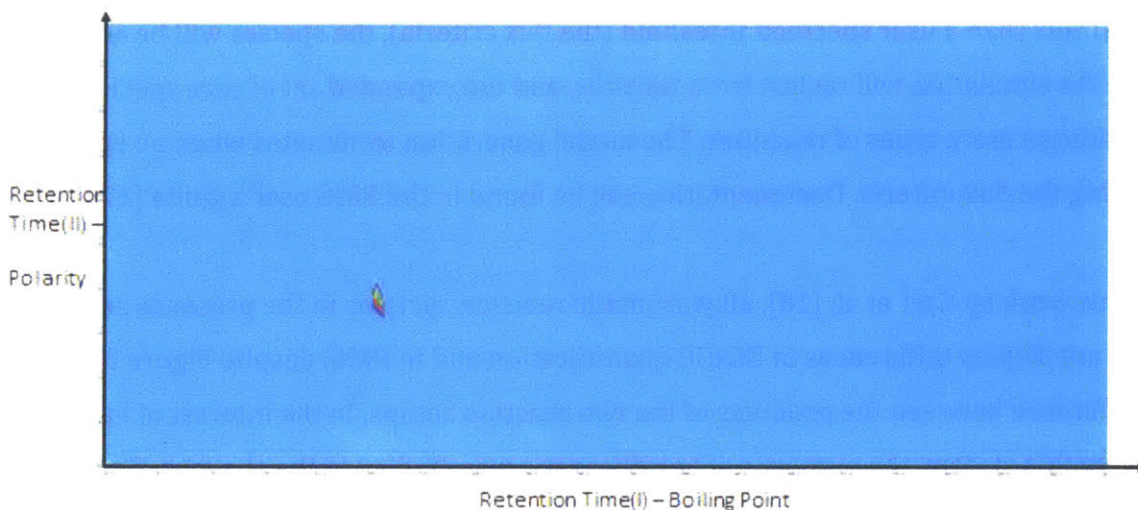
1.3. Hexylbenzene Model Compound System

As a result, this work uses a simplified model compound system of hexylbenzene. The reasons for using hexylbenzene are:

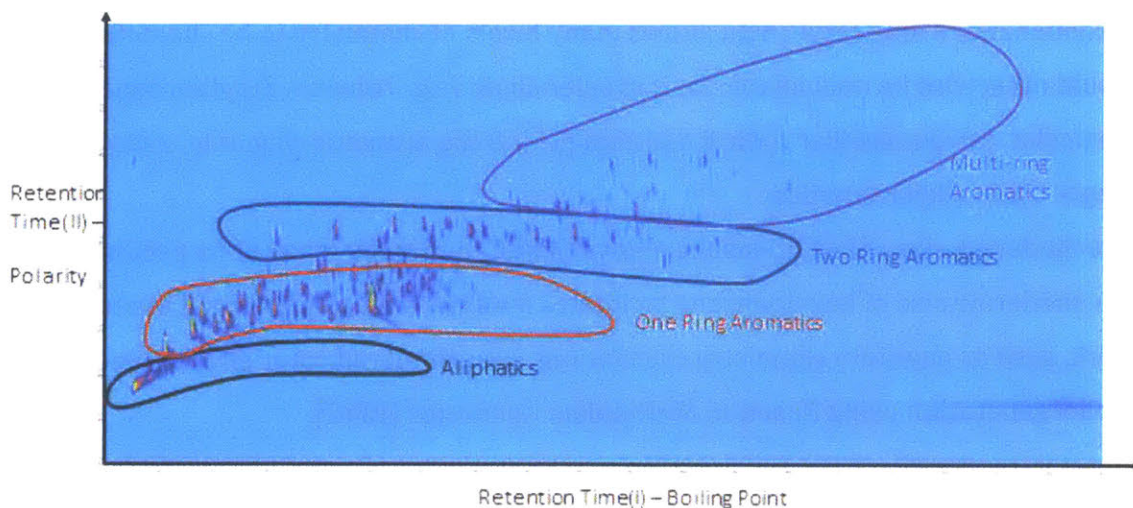
- Figure 3 shows that alkylaromatics are the most abundant class of compound in crude oil. Hexylbenzene is a good surrogate to model the behavior of alkylaromatics, and its behavior can be extrapolated to predict the behavior of other alkylaromatics.

- Hexylbenzene's long alkyl chain allows many facets of chemistry to be characterized that would otherwise be unavailable for a shorter chain (e.g. Toluene, Ethylbenzene, etc.). In particular, intramolecular radical addition [15] to the aromatic ring only takes place for longer chain alkylaromatics.
- The moderate size of hexylbenzene allows GCxGC to identify many of its products.
- The moderate size of hexylbenzene facilitates many of the computational aspects of this work, such as quantum chemistry calculations (less hindered rotor effects), and kinetic model generation using Reaction Mechanism Generator (RMG).

Figure 4 mirrors Figure 3 for the hexylbenzene system. However, this set of figures still highlights the problem of a very complicated product composition that cannot be easily characterized. Figure 4b contains more than 500 species, many of which are formed through multiple reaction pathways. In addition, unstable reaction intermediates such as radical species, are not observable on the GCxGC. This intractable experimental behavior suggests that a purely experimental approach is not sufficient to characterize hexylbenzene's formation of coke, or its 2-ring aromatic precursors. The Green Group software Reaction Mechanism Generator (RMG) is used to generate detailed kinetic models for the hexylbenzene system throughout this work in order to characterize the formation of 2-ring aromatic species because it circumvents many of the problems that an experimental approach would encounter.



(a)



(b)

Figure 4 GCxGC-FID chromatograms for a) Pure hexylbenzene, and b) SCW treated hexylbenzene at 450°C, 300 bar, 40 minutes.

1.4. Reaction Mechanism Generator (RMG)

RMG is a flux based chemical mechanism generator developed by the Green Group [16]. Given input conditions of species concentrations, temperature, and pressure, RMG will generate all possible reactions that can take place based on a user specified subset from 75 reaction families and 50 reaction libraries using the model's core species. If any species from the model's edge form at a higher flux than a user specified threshold (the flux criteria), the species will be added to the core, and the simulation will restart from time=0s, and the expanded set of core species will be able to undergo more types of reactions. The model generation terminates when no species can be added using the flux criteria. Documentation can be found in the RMG user's guide [17].

In previous work by Carr et al. [18], alkylaromatic reaction systems in the presence and absence of water do not display differences in GCxGC quantification and in RMG, despite Figure 2 showing a visual difference between the products of the two reaction setups. In the interest of further simplifying this system, the pyrolysis of hexylbenzene was studied in the absence of water for the majority of this work; the justification for this decision is to first study the formation of 2-ring aromatics and coke in hexylbenzene pyrolysis in the absence of water; once chemical knowledge

surrounding the formation of these compounds is secured, the effect of water on coke formation suppression can then be investigated.

RMG covers many of the weaknesses highlighted in Figure 4 that an experimental approach is vulnerable to. Using the automated reaction generation, RMG models can easily include hundreds of species and thousands of reactions, thus handling the large number of species found in the product composition of hexylbenzene pyrolysis. Due to the computational approach, all information of different reaction pathways and radical species could be conserved.

1.5. Thesis Objectives

With the motivations of this project and the resources available defined, this chapter outlines the objectives of this thesis as follows:

1. Characterize the basic chemistry of alkylaromatic pyrolysis at 450°C. In particular, this work is interested in the limitations of modeling alkylaromatic pyrolysis, and correct any previous misconceptions. This work is described in Chapter 2.
2. Understand the mechanisms of formation of 2-ring aromatics, with the underlying goal that knowledge obtained from the formation of 2-ring aromatics can be extrapolated to the formation of >2 ring species, and potentially to coke. This objective is further divided into the following sections.
 - a. Formation for fused 2-ring species through aromatic intramolecular addition, described in Chapter 3.
 - b. Formation for bridged 2-ring species through aromatic intermolecular addition, described in Chapter 4.
 - c. Modelling the formation of 2-ring aromatics in hexylbenzene pyrolysis by RMG with experimental validation using GCxGC-qMS, described in Chapter 5.
3. Incorporate chemical knowledge to RMG. It is important that information found in this work is not limited to hexylbenzene or alkylaromatic pyrolysis, but generalizable to a variety of different alkylaromatic containing chemical systems. To this end, the following information was incorporated to RMG.

- a. Thermochemistry of species found in this investigation is stored in the Lai_Hexylbenzene thermochemistry library.
- b. Thermochemistry of species related to this work can be estimated using new or updated group additivity values. (Introduced in Chapter 2)
- c. Kinetics of species found in this investigation is stored in the Lai_Hexylbenzene kinetics library.
- d. Kinetics of reactions related to this work can be estimated using new training reactions and new reaction groups designed to separate this work's training reactions from previously existing reaction groups. (Introduced in Chapter 3).
- e. A full list of changes made to RMG by this thesis can be found in Appendix A.

Chapters 2 through 5 will highlight the specific work towards these thesis objectives. Chapter 6 will complete the discussion with recommendations on the future direction of studying the chemistry of alkylaromatics should proceed.

2. Chapter 2

Chemistry of Alkylaromatics Reconsidered

This chapter is closely related to the article Lai, Gudiyella, Liu, and Green, “Chemistry of Alkylaromatics Reconsidered” [19]. In this work, Dr. Soumya Gudiyella performed part of the experiments and GC analysis for hexylbenzene pyrolysis; her data was incorporated as part of the data set in this chapter. Mengjie Max Liu performed the calculations for different retroene and “retro-ene” reactions discussed in this work.

Chapter Abstract

To investigate upgrading crude oil, alkylaromatic compounds are often chosen as model compounds to better understand their reactivity. In recent kinetic models of this chemistry, the main reaction consuming the alkylaromatic is a 4-membered ring “retro-ene” reaction. Here, the transition state of that reaction is discovered to be inconsistent with 6-membered ring retroene reactions reported in literature, leading to inaccurate conclusions. A new detailed kinetic model is constructed using Reaction Mechanism Generator (RMG), and thermodynamic parameters of key compounds and radicals are identified to limit model accuracy. Thermochemistry for key species in the chemistry of hexylbenzene, including hexylbenzene, alkylbenzenes, alkylbenzene radicals, aliphatic radicals, and styrene was calculated using the CBS-QB3 quantum chemistry method to improve the accuracy of the hexylbenzene pyrolysis model. The kinetics of a key beta scission reaction was also calculated. The results of these calculations have led to an overall improvement in hexylbenzene pyrolysis model predictions.

2.1. Introduction

Due to the increase in global energy consumption, the demand for petroleum is continually increasing each year [1]. This will eventually deplete lighter oil sources, and increase demand for the use of heavy oils containing high amounts of heavy hydrocarbons and high concentrations of heteroatoms, including nitrogen, sulfur, and various metals [3]. In order to maximize the utility of such heavy oils, upgrading processes are necessary to convert high molecular weight species in

crude oil into low molecular weight species [4] to facilitate better combustion [5], to meet environmental and regulatory standards [3], to be compatible with modern combustion engines, and to produce high value chemicals for the chemical process industry.

Converting large hydrocarbons into lighter species requires breaking Carbon Carbon (C-C) bonds. The most common weak C-C bond in heavy oils is the alkylaromatic linkage. The pyrolysis of alkylaromatic linkages is therefore very important for understanding the chemistry of certain crude oil upgrading processes, such as supercritical water upgrading of crude oil [4]. In a recent study from our laboratory, hexylbenzene was used as a model compound to represent the chemistry of alkylaromatics in crude oil [18]. The previous work [5] outlines the hexylbenzene reaction mechanism, and product yields that result from hexylbenzene reactivity in pyrolysis and supercritical water environments. However, the predictive model of that study disagreed with the experimental yields of styrene, ethylbenzene, and various unsaturated alkenes. Therefore, this work revisits the model reported by Carr et al. [18], and identifies its chemical inaccuracies. Furthermore, this work utilizes ab initio calculations to improve the model predictions, while developing further knowledge of the chemistry behind the pyrolysis of hexylbenzene and other alkyl aromatic species.

Previous studies on the pyrolysis of hexylbenzene include work by Mandal et al. [20], where the authors experimentally measured the conversion and yield of hexylbenzene at 500°C and 50MPa in the presence of supercritical water, and compared product yields with that of heptylbenzene. Other studies on pyrolysis of alkyl aromatics include Leigh and Szwarc [21] and Khorasheh and Gray [22], where the point of focus was on product compositions. Our work is targeted towards understanding the elementary steps of alkylaromatic pyrolysis processes. Works dedicated to elementary step chemistry of alkylaromatic pyrolysis include Chen and Froment [23], Savage and Klein [24], and Freund and Olmstead [25], but since these works are rule based and do not involve ab initio quantum calculations; chemically less intuitive aspects of the reaction mechanism might be incorrect due to the assumptions made. This work looks into the detailed chemistry using ab initio methods to elucidate the hexylbenzene pyrolysis reaction mechanism.

2.2. Methods

2.2.1. Batch Reactor

A 22.6mL stainless steel batch reactor (SITEC Part number 740.8036) was loaded with 1mL of hexylbenzene, flushed with 30bar Ultrapure Helium, heated to 450°C using a Techne FB-05 fluidized sand bath. The pressure of this reactor was monitored using an Omegadyne pressure transducer (MMA5.0KV5P4B0T4A6), but not controlled; the typical pressure range during the reaction was 320-350bar. Post-reaction, the reactor was cooled by immersion in a water bath, and the gas phase products were collected using a multi-layer foil sampling bag by Supel-Inert. The gas and oil phase products were subject to analysis using gas chromatography described below.

2.2.2. GC-FID Method for Gas Analysis

Gas products were analyzed using a Shimadzu GC-2014, installed with a 5 μ L sample injection loop, an Rt-Q-Bond Column with dimensions of 30m x 530 μ m ID, 20 μ m film thickness, leading to a flame ionization detector (FID). The temperature program for the separation features an initial temperature of 40°C for 1 minute to separate light components, followed by a 10 °C/min ramp to 150°C for a hold time of 2min, and finally a 25°C/min ramp to 270°C for a final hold of 2 minutes. This temperature program is optimized to separate hydrocarbons containing 1 to 5 carbons. Gas phase calibrations were performed using a calibration standard mixture from Airgas containing alkanes, alkenes, aromatics, and sulfur compounds (Airgas part number X21HE99C15A0000)

2.2.3. GC-MS/FID Method for Liquid Analysis

The organic phase liquid product from the experiments was analyzed using a GC-FID/MS (Agilent 7890, 5975C), equipped with an RXi-5HT column with dimensions of 30m x 250 μ m ID x 0.25 μ m film thickness. The MS signal was used for identification of products, whereas the FID signal was calibrated and used for quantification of the identified species. The mole fraction of products was quantified based on response factors found through analysis of standards containing alkanes, alkenes, alkylbenzenes, and alkylnaphthalenes; for species where standards were not available, their response factors were interpolated from existing standards based on their number of carbons. 3-Chlorothiophene was used as an external standard to ensure the accuracy of quantification.

2.2.4. GCxGC-FID Method for Liquid Analysis

The organic phase liquid products from the experiments was also analyzed using a GCxGC-FID system to provide a view of the distribution of heavier species. The hardware of this instrument is an Agilent 7890, with modifications made by LECO Corporation. The primary column of this instrument is an RXi-5HT column with dimensions of 30m x 250 μ m ID x 0.25 μ m film thickness; a secondary column was used for separation through polarity, and is a BPX-50 column with dimensions of 2m x 250 μ m ID x 0.25 μ m film thickness. This analysis of the liquid products employs a modulation time of 16 seconds. Species were identified and quantified using a FID detector; the instrument is calibrated to quantify alkanes, alkenes, alkylbenzenes, and alkylnaphthalenes. Volume under GCxGC peaks are quantified using the software GC-Image, developed by Zoex Corporation. The quantification and identification of products were based on response factors found through analysis of standards containing alkanes, alkenes, alkylbenzenes, and alkylnaphthalenes; for species where standards were not available, their response factors were interpolated based on existing standards and their number of carbons. 3-Chlorothiophene was used as an external standard to improve the accuracy of quantification.

2.2.5. Overview of Computational Methods

The product distribution of the experiments is compared with model predictions from a model developed using the Reaction Mechanism Generator (RMG) software [17]. Important model parameters were identified using CHEMKIN-PRO's [26] sensitivity analysis, and improvements were made by performing quantum chemical calculations using Gaussian 03 [27].

2.2.6. Constructing Chemical Kinetics Simulations with RMG

The detailed algorithm of Reaction Mechanism Generator (RMG) has been discussed extensively in the literature [28] [29]. In short, the mechanism generation follows a flux-based algorithm to select important species and reactions that are important at the chosen reaction conditions, and omits reactions with much slower rates. Thermochemistry of species and rate coefficients of reactions are estimated using the RMG-database, which contains parameters from various sources of information, including experimental and calculated values from both the literature and the Green Group. Some of the parameters are accurately known, in those cases the known values are used rather than the RMG estimates. The RMG inputs for this chapter's models are referenced in

the supporting information of Lai et al. [19]. RMG was also used to calculate the species sensitivity towards thermochemistry.

RMG is an active open-source software project, so its database is constantly being improved, and the software is also frequently updated; to exactly reproduce an RMG model one should use exactly the same version of the database and the software. GitHub version commit strings of RMG-Py and RMG-database used for the generation of the different versions of the mechanisms shown in this work can be found in the RMG input files referenced in the supporting information of Lai et al. [19].

There are species in Lai Version 2 that were identified to have invalid structures. The version of RMG used over the course of this work does not enforce planarity of the benzene ring, and so allows bonds to be formed across the benzene ring. All reactions including these unreasonable species are manually removed after mechanism generation to ensure proper physical significance of the model; this change is reflected in the mechanism supplied in the supporting information. An example of one of the many invalid structures is the following species, where an intramolecular addition reaction of a radical formed a bond across the benzene ring.



2.2.7. CHEMKIN Simulations

The mechanisms generated using RMG were used in CHEMKIN-PRO 17.0 Release 15151 [26] to predict species concentration as a function of reaction time. The CHEMKIN input parameters include the batch reactor type, the RMG generated mechanism, a temperature profile $T(t)$ of the reactor determined from the experimental pressure profile, reactor volume of 22.6mL, and mole fractions of helium, and hexylbenzene in the feed. CHEMKIN-PRO requires the user to supply an initial pressure P_0 which is used to compute the total number of moles initially in the batch reactor via the ideal gas law. In our simulations, we used $P_0 = \frac{(n_{\text{Helium}} + n_{\text{Hexylbenzene}})RT_0}{V}$ so that the number of moles calculated by CHEMKIN was consistent with the actual number of initial moles in the experiments. The outputs of CHEMKIN includes the species concentration, rate of production of

species, and the sensitivity of species with respect to the Arrhenius A-factors, all of which were used in this investigation.

2.2.8. Gaussian 03 Calculations

Thermochemical and kinetic data were calculated using the Gaussian 03 quantum chemistry package [27]. Geometry, energy, and harmonic frequency, calculations were performed at the CBS-QB3 level of theory; hindered rotor calculations were performed in the B3LYP/CBSB7 level of theory. Hindered rotor calculations were made for each rotatable bond; these scans were stepped in 10° increments for the full 360° rotation with constrained optimizations at each step. The treatment of hindered rotors including the method of separating the large-amplitude and small-amplitude (harmonic oscillation) degrees of freedom is described in detail in Sharma et al. [30]

A thermochemistry calculation for hexylbenzene was performed at the M06-2X/cc-pVTZ level of theory to compare calculation methods.

2.2.9. RMG – Arkane (formerly known as Cantherm)

Partition functions were calculated using the rigid-rotor-harmonic-oscillator approximation with 1-D hindered rotor corrections. We assumed the 1-D rotors were separable (independent rotors approximation). The rotor moments of inertia were taken as $I^{(2,3)}$ at the equilibrium geometry. Eigenvalues for each rotor were computed in a basis set of 12 pairs of sine and cosine terms. The resulting thermodynamic parameters were fitted to NASA polynomials using the Arkane package of RMG [31]. This work uses a scaling factor of 0.99 for the harmonic frequency analysis, and the recommended bond additivity corrections [32].

2.3. Results and Discussion

2.3.1. New Experimental Results

In Carr's work, the hexylbenzene pyrolysis mechanism generated by RMG contained 137 species and 1706 reactions [18]; Carr's model's prediction of hexylbenzene conversion plotted in Figure 5 shows a close agreement with Carr's experiments, whereas other major species selectivity agrees within a factor of 3. Experimental conditions use 1mL of hexylbenzene, a heat up from 25°C to 450°C over ten minutes, 300 bar pressure, and reaction time from 15 to 40 minutes.

This present work replicates the experimental work of Carr et al, with an increased data point at 20 minutes of reaction time, and improved non-linear calibration factors for species at high concentration, yielding more accurate results. The experimental results from both studies are shown in Figure 5.

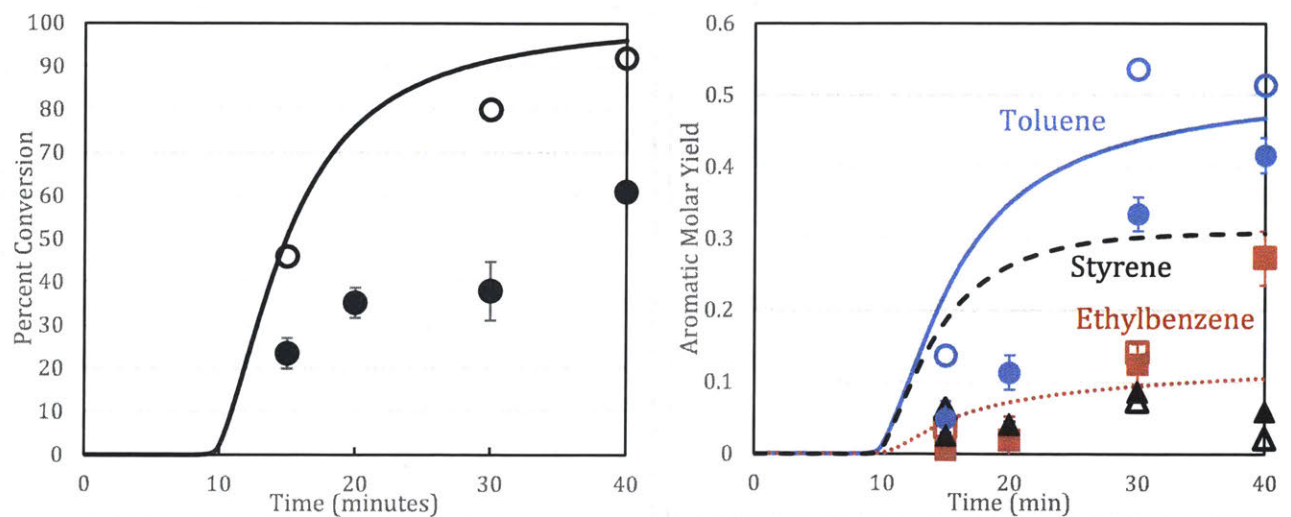
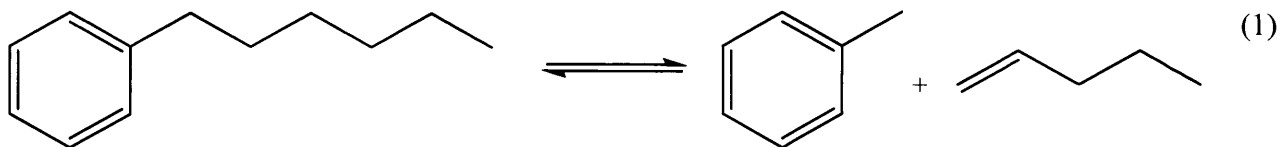


Figure 5 Carr et al. model (Lines) comparison with Carr et al. experiments (no fill symbols ○) and this work's experiments (filled symbols ●) for conversion of hexylbenzene (left) and molar yield of major aromatic products(right), including toluene (blue line/circles), styrene (black dashed line/triangles), and ethylbenzene (red dotted line/squares). Reaction conditions are at 22.6.mL volume, temperature ramp up to 450°C over 10 minutes based on experimental pressure profile (30-350 bar). Aromatic molar yield is defined here as moles aromatic compounds present in product divided by starting moles of hexylbenzene. Error bars denote the standard deviation of duplicated experiments. For instances where duplicates were not performed, error bars are averaged from other time points of the same study.

The inferred concentrations of the high concentration species hexylbenzene and toluene are significantly different due to the improved calibration. In contrast, the yield of ethylbenzene and styrene are extremely similar to Carr's experiments. The discrepancies between Carr et al's model and this work's experiments has motivated a re-examination of the hexylbenzene model.

2.3.2. Changes to Carr et al. Model

In the Carr et al. model, the main reaction consuming hexylbenzene is Reaction (1), a 4-membered-ring “retro-ene” reaction.



In the work of Carr et al. [18], reaction (1) was taken from Burklé-Vitzthum [33] who estimated the rate for the analogous reaction of butylbenzene forming toluene and propylene. The rate of this reaction is shown in Table 1.

For reaction (1) to take place, a strained 4-member ring transition state will be involved. It is not a typical “ene” reaction. Instead, the retroene reaction is described by Klein and Virk [34] to have a 6-membered ring transition state. The top half of Figure 6 depicts how reaction (1) would involve a strained 4-membered ring transition state for H-atom transfer, and the bottom half of the figure shows the 6-membered ring transition state and the resulting products of the retroene reaction.

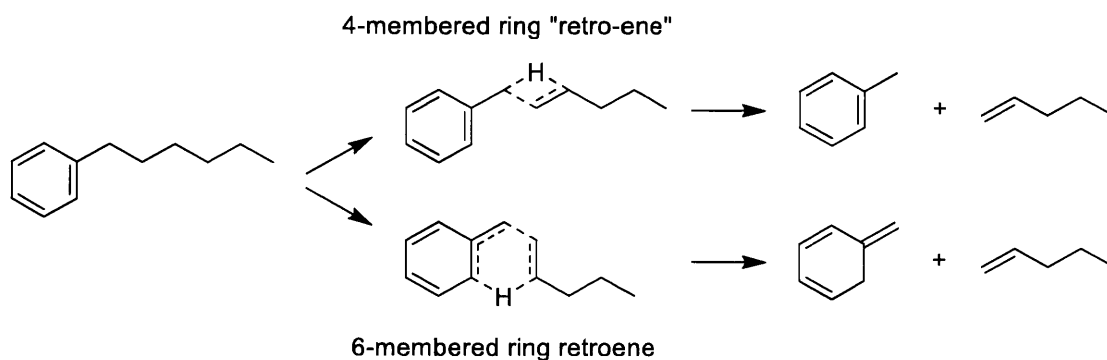


Figure 6 Schematic of 4-membered ring “retro-ene” described by Burklé-Vitzthum [33], and 6-membered ring retroene reaction described by Klein and Virk [34]. The 4-membered ring “retro-ene” reaction is used in Carr et al.’s model, and its rate is highly overestimated.

Our calculations at the CBS-QB3 level for 4-membered ring “retro-ene” reactions and for 6-membered ring retroene reactions are shown in Table 1. In both cases, the rate coefficients for both reactions are significantly slower than the rate proposed by Burklé-Vitzthum at 723K; 15

orders of magnitude slower for the 4-membered “retro-ene” reaction, and 6 orders of magnitude slower for the 6-membered retroene reaction. Furthermore, the activation energy of the 4-membered ring transition state reaction was found to be higher than the activation energy estimated by RMG for C-C scission rate, indicating the 4-member ring transition state would not feasibly take place since hexylbenzene would realistically go through C-C scission instead. We therefore removed the 4-membered-ring reaction; this is the most significant difference between newer versions of the hexylbenzene model from Carr’s version. The RMG model prediction of hexylbenzene conversion dropped significantly as a result.

Table 1. Rate of 4-membered ring “retro-ene” reaction by Burklé-Vitzthum [33] and this work, rate of 6-membered ring retroene reaction by this work, and RMG estimate of C-C scission rate. Calculations in this work done using the CBS-QB3 level of theory for propylbenzene.

	A (s ⁻¹)	N	E _a (kcal/mol)	Rate constant 723K (s ⁻¹)
Burklé-Vitzthum [33]	6.8 x 10 ¹²	0	54.4	2.44 x 10 ⁻⁴
This work (4-membered ring)	2.55 x 10 ¹⁴	-0.601	105	8.86 x 10 ⁻²⁰
This work (6-membered ring)	1.63 x 10 ⁷	1.686	73.9	4.93 x 10 ⁻¹¹
C-C Scission Rate	1.99 x 10 ¹³	-0.85	76.0	7.84E-13

Other changes were also introduced to the Carr model. These changes were due to the update of the RMG software, from its older Java version to the new RMG-Py [17]. These updates include many changes to the database on both thermochemistry and kinetic entries to reference more reliable sources. The cumulative changes are captured in the model named Lai Version 1 in Figure 7.

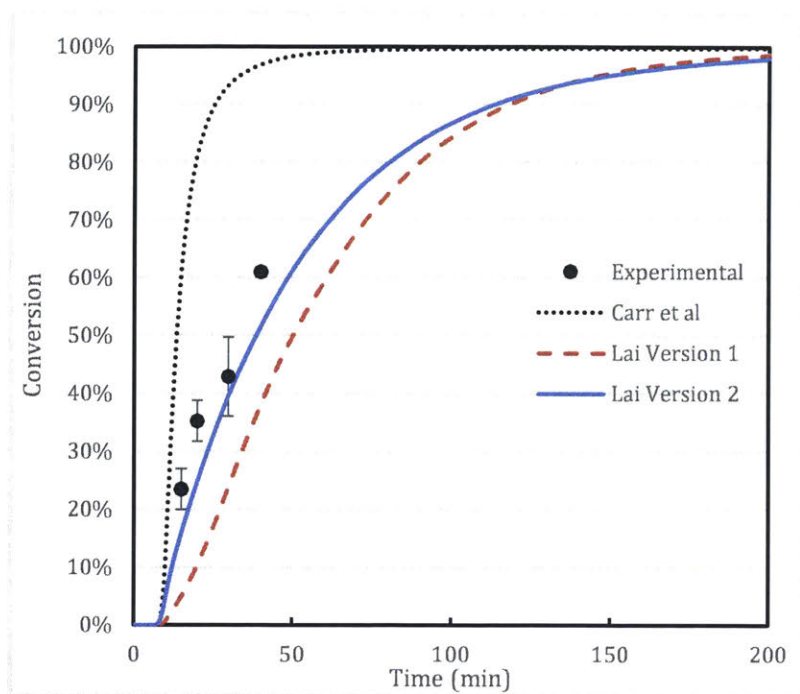


Figure 7 Conversion comparison between model by Carr et al (black dotted), Lai version 1 after removal of 4-membered ring “retro-ene” reaction and introduction of RMG-Py database (red dashed), and Lai version 2 (blue solid) after all revisions discussed in this article are applied. Experimental data points (circles) included for comparison. Reaction conditions are at 22.6.mL volume, temperature ramp up to 450°C over 10 minutes based on experimental pressure profile (30-350 bar).

Table 2. Model Version Description

Version Name	Description
Carr et al	RMG model outlined in Carr [18]
Lai version 1	Carr model, with 4-membered ring “retro-ene” reaction removed and use of RMG-Py database
Lai version 2	Lai version 1, after all revisions outlined in this work, including thermochemistry calculations of key species and kinetics recalculated for reaction (3)

Lai versions 1 and 2 of the hexylbenzene mechanism can be found in the supporting information in the format of RMG outputted CHEMKIN files.

2.3.3. Overview of new Reaction Pathway

The main pathways of the hexylbenzene pyrolysis mechanism differ significantly after removal of the “retro-ene” reaction. The reaction mechanisms generated throughout the bulk of this investigation follows pathway analysis outlined in Figure 8. Lai versions 1 and 2 mechanism are highly based on radical chemistry due to the elimination of the “retro-ene” reaction, unlike the Carr et al. mechanism, in which hexylbenzene consumption was driven by reaction (1), which bypasses the formation of radical species.

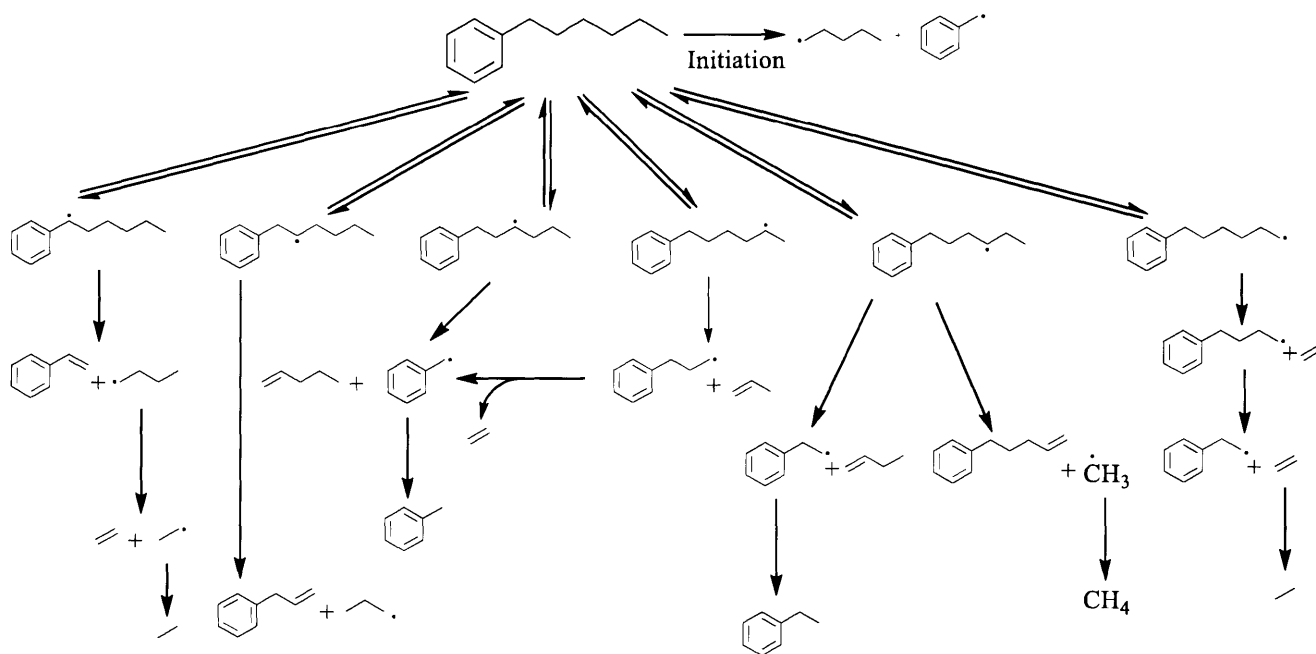


Figure 8 Overview of the chemical mechanism of the pyrolysis of Hexylbenzene in Lai Version 2 at short reaction times. The full chemical mechanism can be found in the supporting information and involves >200 reactions and >2500 reactions.

The pyrolysis of hexylbenzene starts with an initiation step to break down predominantly to benzyl and 1-pentyl radicals. With the generated radical pool, the radicals attack hexylbenzene at one of the six aliphatic carbons to form six isomeric radicals. The concentration of Rad 1 is at least an order of magnitude higher than all other aliphatic hexylbenzene radicals due its resonance stabilization with the aromatic ring shown in Figure 9.

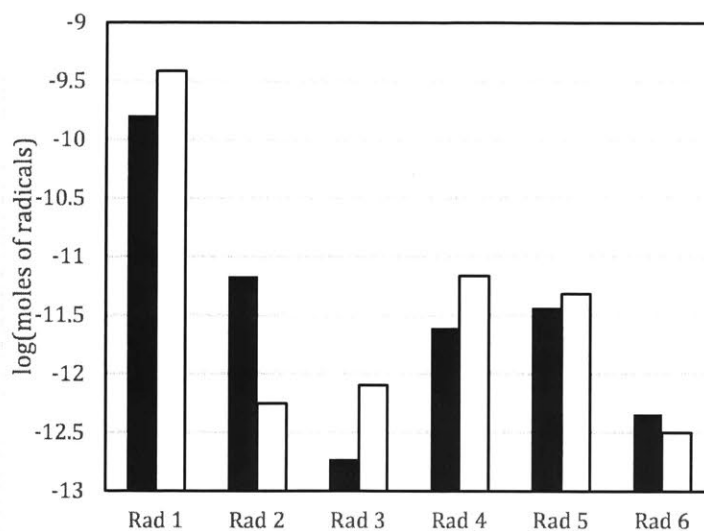
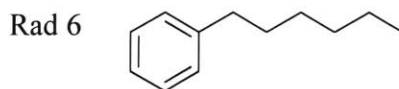
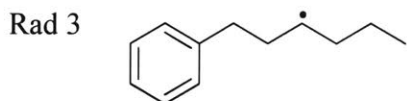
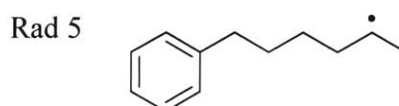
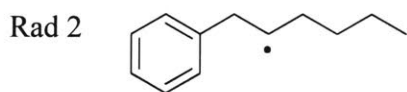
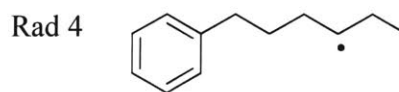
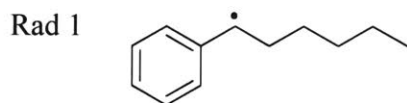


Figure 9 Moles of aliphatic hexylbenzene radicals in Lai Versions 1 (black) and 2 (white) at 16 minutes. Reaction conditions are at 22.6.mL volume, temperature ramp up to 450°C over 10 minutes based on experimental pressure profile, initial pressure of helium and hexylbenzene scaled to experimental feed, and mass fractions of 0.833 Helium and 0.167 hexylbenzene. Radical species are defined below:



These radicals are converted to other isomeric radicals through hydrogen abstraction reactions, or further react to form small products such as toluene, styrene, ethylbenzene, and other aliphatics through beta-scission.

The secondary paths involve radical termination of two alkylbenzyl radicals forming products with two aromatic rings, disproportionation of two radicals to produce species with multiple double bonds, and cyclization through intramolecular radical addition. Although the collection of all of the aforementioned reaction classes is important in predicting the formation of multi-ring

aromatics, the rate estimates and thermochemistry data related to these reaction classes is limited; as a result, they won't be discussed in great detail in this article. Regardless, all of the aforementioned classes included in the kinetic model using the best possible means of estimation at the time of generation of this model. The full kinetic model is attached in the supporting information.

2.3.4. Kinetic Sensitivity Analysis of Hexylbenzene

Matching the hexylbenzene conversion between the model and experiments is an important first step to improving the model, since errors in hexylbenzene conversion can cause extremely erratic differences in secondary chemistry.

We use the normalized sensitivity of hexylbenzene, defined by $s = d(\ln C_{\text{Hexylbenzene}})/d(\ln(k_i))$ (normalized rate of change of hexylbenzene concentration with respect to reaction rate constant for reaction i) as a metric to find reactions that highly impact the concentration of hexylbenzene. The reactions are reversible with fixed equilibrium constants, so increasing k_{forward} increases k_{backward} by the same factor. Figure 10 shows the sensitivity of hexylbenzene with respect to the seven reactions that have the highest sensitivity in the two models generated in this work.

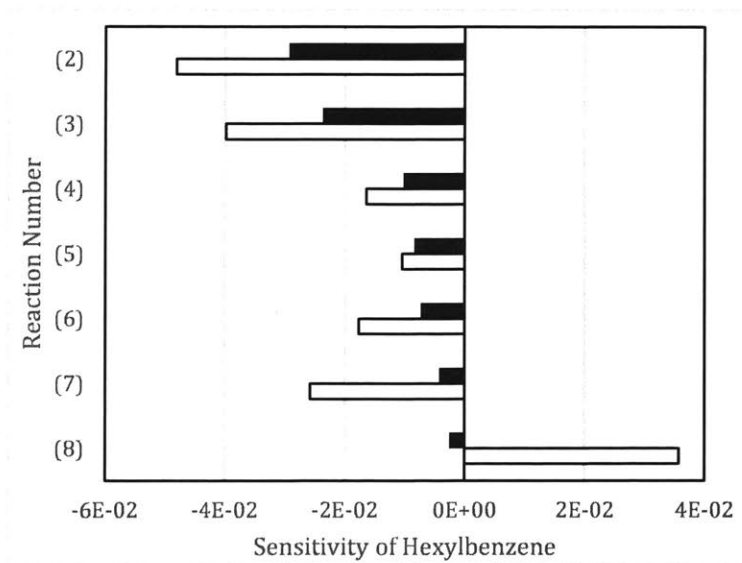
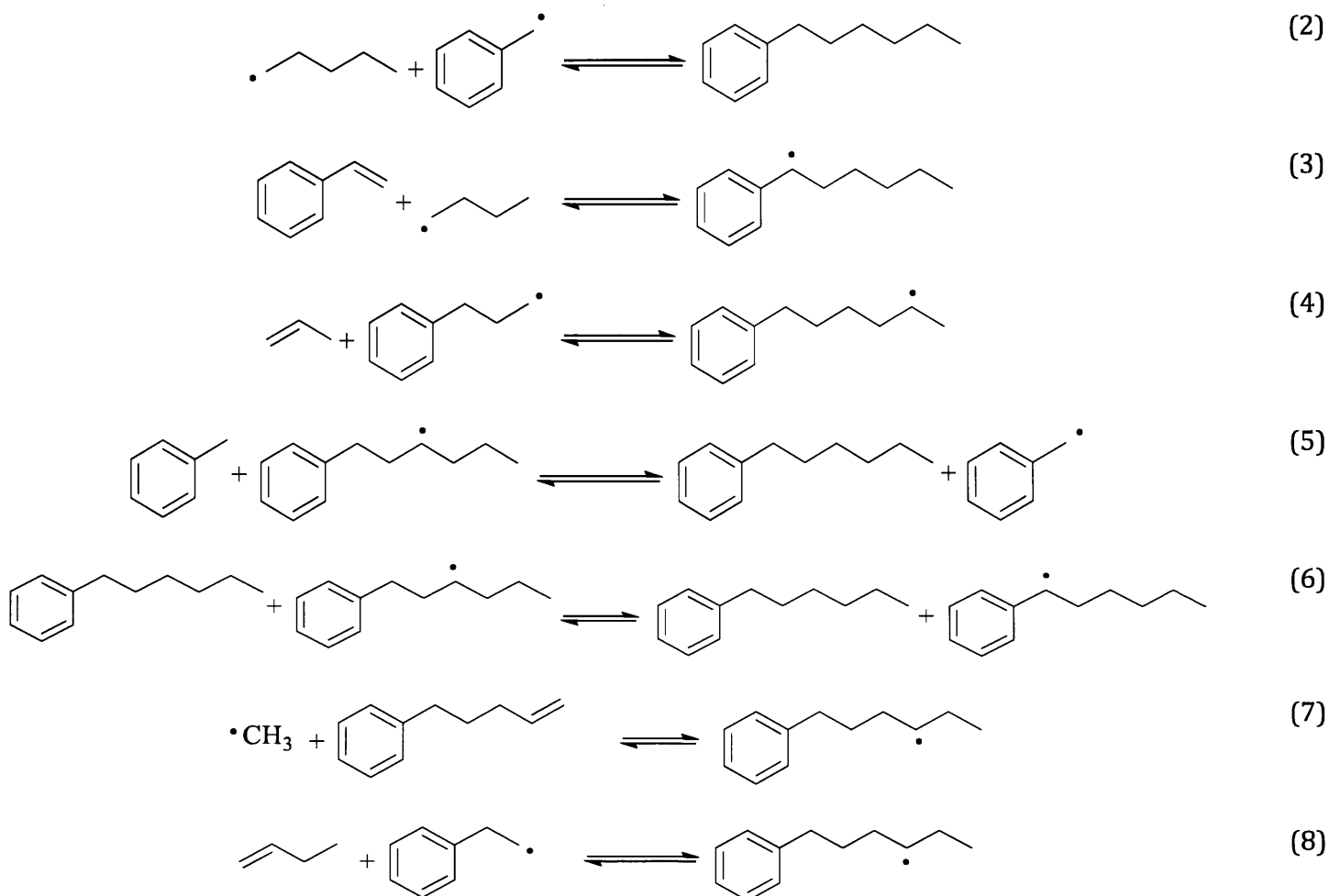


Figure 10 Sensitivity of hexylbenzene with respect to rate coefficients for Lai Versions 1 (black) and 2 (white) at 16 minutes. Reaction conditions identical to Figure 9. Reactions are listed in descending order of sensitivity in Lai Version 1.



Hexylbenzene conversion has a relatively high sensitivity to Reaction (2); this is the most sensitive reaction in Lai version 1, and second most sensitive reaction in Lai Version 2. The reason for the high sensitivity of reaction (2) is due to the reverse of reaction (2) being the main initiation step of hexylbenzene pyrolysis. Naturally, one would expect the reactant to be highly sensitive to the rate parameters of reaction (2), since no further reactions will take place in the absence of an initiation step. Other initiation steps that involve partitioning hexylbenzene to an alkylbenzyl radical and 1-alkyl radical are two orders of magnitude slower than reaction (2) in both Lai Versions 1 and 2, shown in Figure 11.

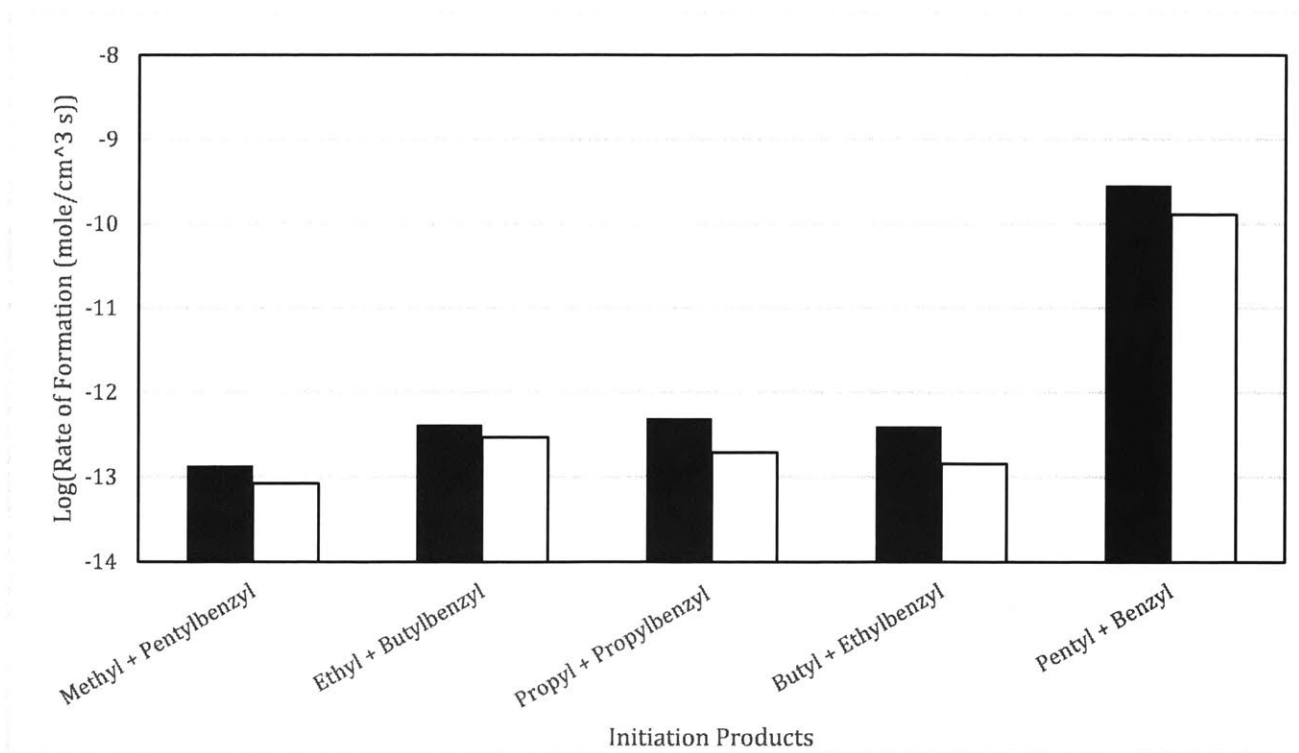


Figure 11 Log rate of formation of initiation reactions evaluated at 16 minutes reaction time for Lai Versions 1 (black) and 2 (white). Reaction conditions identical to Figure 9.

The reason that reaction (2) takes precedence over all other initiation steps is the benzylic stabilization of the benzyl radical; all other initiation steps that cleave a C-C bond on the alkyl chain of hexylbenzene do not feature any resonance stabilization, and therefore occur at a much slower rate because they are significantly more endothermic.

Hexylbenzene conversion is also relatively sensitive to Reaction (3) in Lai Version 1. The reverse of reaction (3) is a beta scission step that breaks the hexylbenzene carbon framework. The high sensitivity of this reaction compared with other beta-scission reactions can be attributed to the high concentration of Rad1 relative to all other hexylbenzene radicals shown in Figure 9.

Interestingly, reaction (3) is not the highest flux beta scission reaction. Figure 12 shows reaction 11 to have the highest flux due to the products of this reaction being resonantly stabilized.

Rad 3 (reactant of reaction (11)) is formed by Rad 1 (reactant of reaction (3)) through hydrogen abstraction reactions in both versions of the model; hexylbenzene concentration is highly sensitive towards reaction (3) as a result because it takes part in controlling the flux of other hexylbenzene beta scission reactions.

The other beta scission reactions share similar flux to reaction (3) despite the high concentration of Rad 1 since thermodynamically less stable radicals (Rad 2 – Rad 6) favors their beta scission. Figure 12 shows the relative fluxes of each beta scission reaction in the two versions of the model. Table 3 shows the rate rule estimate of these beta scission reactions made by RMG.

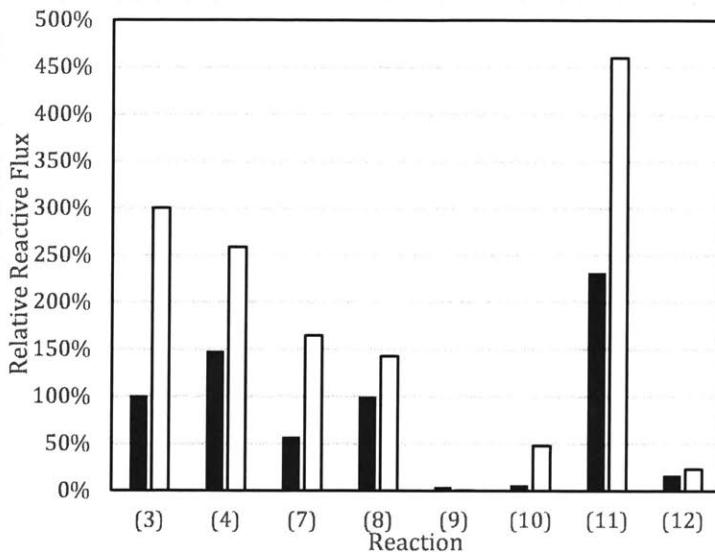
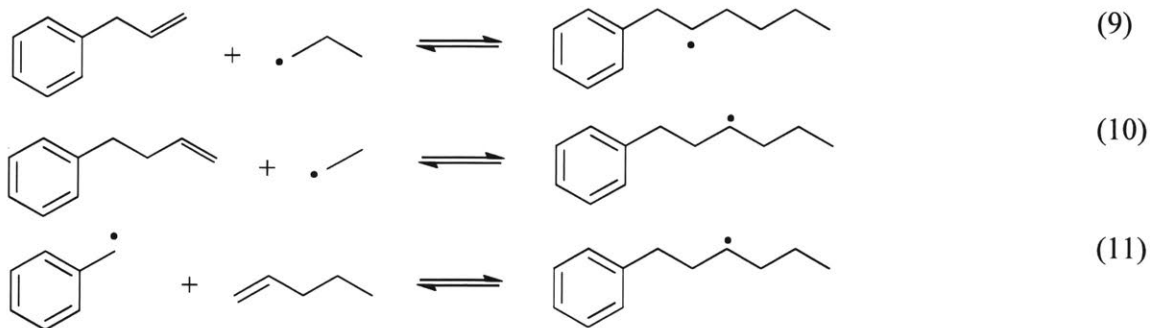


Figure 12. Relative reactive fluxes of beta scission of hexylbenzyl radicals evaluated at 16 minutes reaction time for Lai Versions 1 (black) and 2 (white). Reaction (3) in Lai Version 1 is set as 100% relative flux in this plot. Reaction conditions identical to Figure 9.



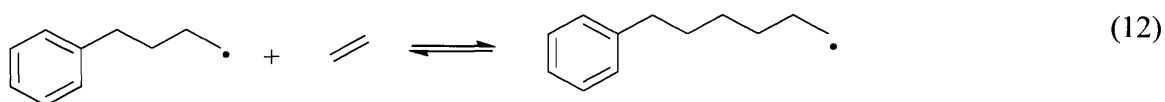


Table 3 RMG rate estimation for Beta-Scission Reactions

	A (cm ³ mol ⁻¹ s ⁻¹)	n	E _a (kcal/mol)
(3)	7.82 x 10 ²	2.41	3.71
(4)	2.13 x 10 ³	2.41	4.75
(7)	2.10 x 10 ⁴	2.41	5.32
(8)	2.13 x 10 ³	2.41	4.75
(9)	2.13 x 10 ³	2.41	4.75
(10)	2.13 x 10 ³	2.41	4.75
(11)	5.32 x 10 ⁴	2.10	10.0
(12)	3.98	2.44	5.37

In Lai Version 1, all other reactions appear to have a considerably lower sensitivity compared to these reactions (2) and (3) (the third most sensitive shown in Figure 10 has 43% the sensitivity of reaction (3)).

In Lai Version 2, the two most sensitive reactions are the same as Lai Version 1. However, two other beta-scission reactions (7) and (8) now have a higher sensitivity than the other reactions that showed a higher sensitivity in Lai Version 1. This is due to the higher flux of beta-scission reactions in general, shown in Figure 12, increasing their importance towards hexylbenzene conversion.

In Lai Version 1, the most sensitive reaction (2) has a remarkably low sensitivity of 2.4×10^{-2} at 16 minutes reaction time, meaning every percent increase in the system's most reactive rate constant will change the concentration of hexylbenzene by 0.024% only. It will therefore require a substantial change in the rate constants in this reaction mechanism in order for this model's conversion to match the experimental data. Interestingly enough, the magnitude of sensitivity values are higher in Lai Version 2, approximately 30% higher for reactions (2) and (3). This is due to the Lai Version 2 having a more reactive environment in general (hinted by the higher conversion).

To assess whether if any major errors exist in the rate constants of this system's most reactive reactions, the origin of the rate rule estimates must be considered. The thermochemistry of the species involved in these two reactions were estimated through Benson group additivity in RMG in Lai Version 1. The kinetics of reaction (2) was estimated using the rate coefficient for radical recombination of allyl and ethyl radicals from Tsang et al. [35], whereas the kinetics of reaction (3) was estimated using a CBS-QB3 calculation for the reaction between 1,3-butadiene and an ethyl radical to form the hexen-3-yl radical. The accuracy of these sources will be discussed in subsequent sections.

2.3.5. Kinetic Rates of Sensitive Reactions

Figure 13 and Figure 14 show the effect of applying various multipliers to the pre-exponential factors of reactions (2) and (3) on the overall hexylbenzene conversion.

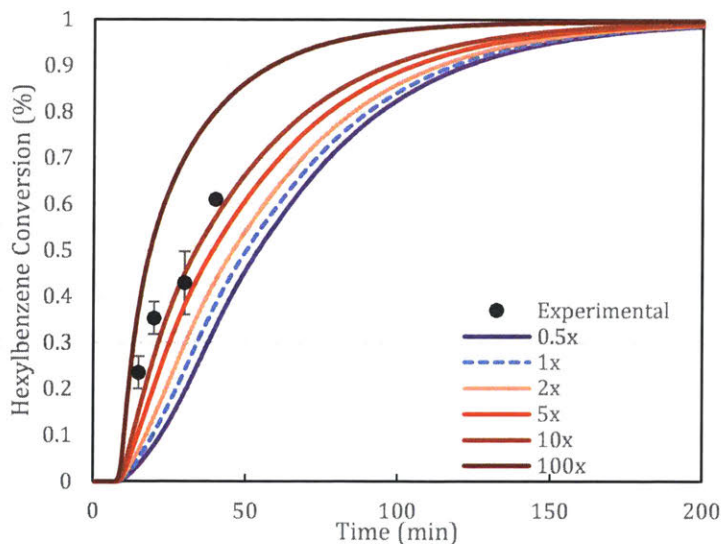


Figure 13. Conversion of Hexylbenzene in Lai Version 1 where the pre-exponential factor of reaction (2) is multiplied by 0.5, 1, 2, 5 10, and 100 times, denoted by the different colored curves. Reaction conditions identical to Figure 9.

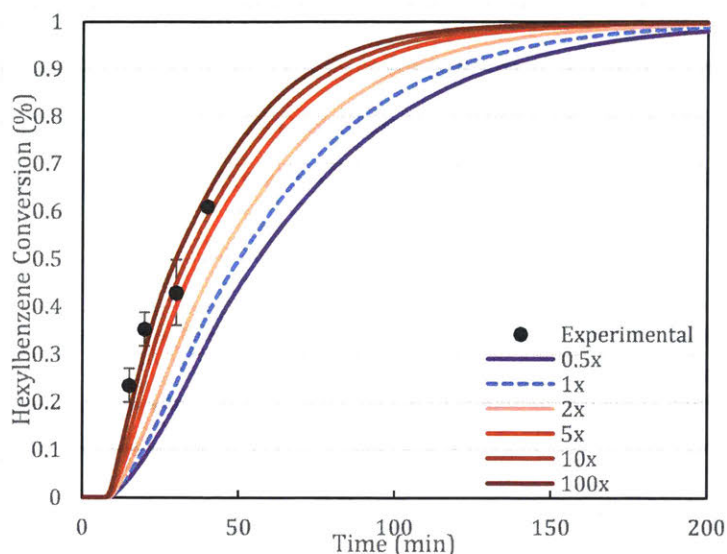


Figure 14. Conversion of Hexylbenzene in Lai Version 1 where the pre-exponential factor of reaction (3) is multiplied by 0.5, 1, 2, 5 10, and 100 times, denoted by the different colored curves. Reaction conditions identical to Figure 9.

Based on prior experience, we believe our rate estimates based on rate constants of analogous reactions found from the literature are accurate to about one order of magnitude; it would be very surprising if they differed by more than two orders of magnitude. The results show that a multiplier between 10-100x must be applied to the pre-exponential factors for either of the two of the most sensitive reactions in the system to bring the model predictions of Lai Version 1 in agreement with experimental results.

To try to resolve this discrepancy, we have computed a more accurate rate coefficient expression for reaction (3). Additional work was not done on reaction (2) because this reaction is barrierless, and therefore it can be expected to be comparable to other radical recombination reactions since there is little scope for the large errors that plague estimates for high barrier reactions such as the “retro-ene” reaction. Instead, the thermodynamics of reaction (2) determines the reverse rate of this reaction, and it will be further discussed in section 2.3.6.

The forward rate of reaction (3) was computed at the CBS-QB3 level, and an activation energy of 3.7 kcal/mol was found, which was identical to RMG’s estimate. The small change in pre-exponential factor leads to a factor of four increase at 723K in our updated rate constant. Given

the observation on Figure 14 where the rate of reaction (3) must be increased more than 100-fold to match the conversion of hexylbenzene between model and experiments, these calculations show that the error in rate of reaction (3) is an unlikely cause for the discrepancy in conversion. The rate constant parameters of reaction (3) using RMG's group estimates and CBQ-QB3 calculations are shown in Table 4.

Table 4 Rate constant parameters in modified Arrhenius format for reaction (3) estimated by RMG's group estimates and calculated by CBS-QB3 level of theory. Temperature range of 300-2500K.

	A (cm ³ mol ⁻¹ s ⁻¹)	n	E _a (kcal/mol)
RMG Group Estimate	780	2.4	3.7
CBS-QB3	240	2.8	3.7

The CBS-QB3 calculation has been added to the Reaction Mechanism Generator's training reaction database to improve the accuracy of future rate estimates for beta scission reactions.

Considering the reasonable sources of kinetic parameters for these two reactions and the very low sensitivity to the other reactions' pre-exponential factors, it is highly unlikely that the mismatch in conversion is due to poor rate rule estimations.

2.3.6. Thermochemistry Sensitivity of Hexylbenzene

Using process of elimination, we hypothesize that errors in the thermodynamic estimations of key species in the model could be the dominant source of the erroneous predicted conversion of hexylbenzene. We use the normalized sensitivity of hexylbenzene with respect to the Gibbs free energy of a species $d(\ln C_{\text{Hexylbenzene}})/d(G_i)$ to find out the effect of thermochemistry on the conversion of hexylbenzene. Figure 15 shows the sensitivity of hexylbenzene with respect to species that have the highest sensitivity in Lai Version 1.

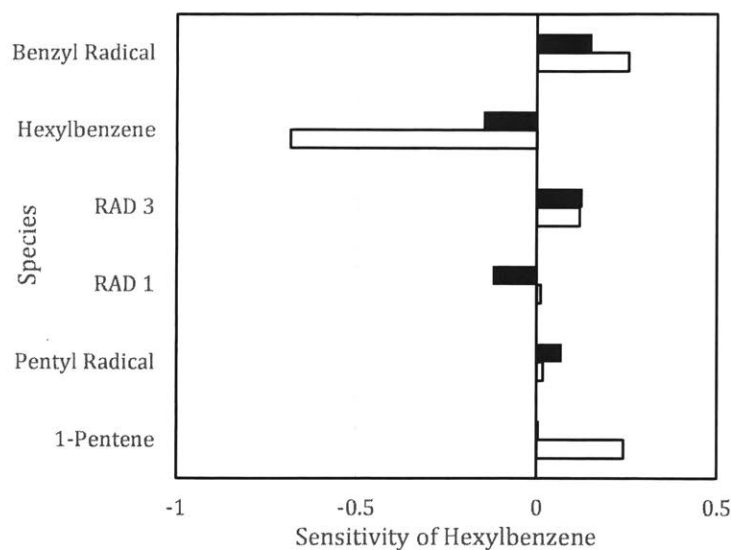


Figure 15 Sensitivity of hexylbenzene with respect to species Gibbs free energy for Lai Versions 1 (black) and 2 (white) at 15 minutes. Reaction conditions identical to Figure 9. Species are listed in descending order of sensitivity in Lai Version 1.

A comparison of Figure 15 to Figure 10 shows that the conversion of hexylbenzene is much more sensitive to species thermochemistry. Figure 10 suggests that the sensitivity of hexylbenzene concentration is less than 0.025 in Lai Version 1; i.e. that one would need to change rate coefficients by orders of magnitude to significantly change the hexylbenzene concentration, whereas Fig. 11 indicates that a change of 1-2 kcal/mole would have a significant effect.

In Lai Version 1, hexylbenzene conversion is most sensitive to the Gibbs Free Energy of the benzyl radical and hexylbenzene, both of which are involved in reaction (2); the pentyl radical also ranks highly in sensitivity, reinforcing the importance of the initiation reaction (2). Other hexylbenzene radicals also take an important role in the sensitivity of hexylbenzene concentration due to the importance of the size of radical pool in this mechanism.

To visualize this of sensitivity to thermochemistry, the enthalpy of hexylbenzene was modified by 0.5 to 10kcal/mol in Lai Version 1 to observe the effect on hexylbenzene conversion. Figure 16 shows the results of these modifications.

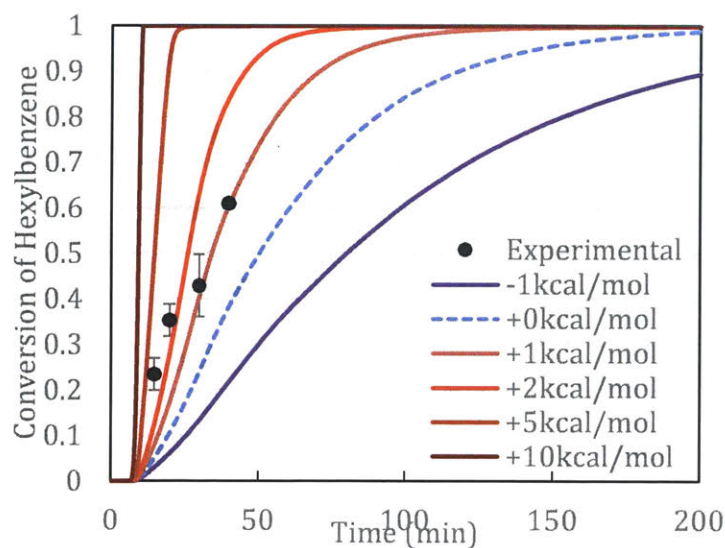


Figure 16. Model conversion of Hexylbenzene in Lai Version 1 with modified enthalpy of hexylbenzene (from -1kcal/mol to +10kcal/mol). It can be observed on this plot that a change as small as 1kcal/mol can significantly changes the conversion of hexylbenzene with respect to time. Reaction conditions identical to Figure 9.

From Figure 16, it can be seen that an error of 5kcal/mol in the Gibbs free energy of hexylbenzene is sufficient to account for the lack of agreement between the model and experimental conversion of Hexylbenzene.

In Lai Version 2, the most sensitive species are all involved in the initiation step, consistent with our understanding with the chemical mechanism, with Gibbs free energy of hexylbenzene being most sensitive, followed by the benzyl radical and 1-pentene.

Figure 15 shows an increase in the magnitude of species sensitivity in Lai Version 2. The sensitivity of hexylbenzene towards its own Gibbs Free Energy increases 4.5 times between Lai Version 1 and 2, whereas the sensitivity towards the free energy of benzyl radical sees a milder increase of 66%. Consistent with kinetic sensitivity, this is due to the higher reactivity of this mechanism at 16 minutes (indicated by higher conversion), causing any changes in the model's parameters to have a larger effect on hexylbenzene conversion. The stark increase in sensitivity towards the Gibbs Free Energy of hexylbenzene compared to the benzyl radical is due to hexylbenzene's (or its radicals) involvement in all of the most sensitive reactions, compared to

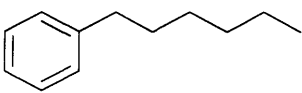
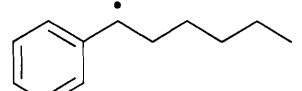
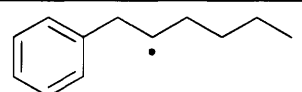
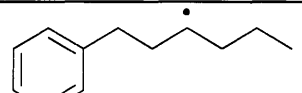
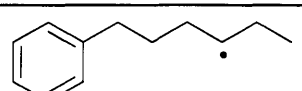
other species (such as the benzyl radical) that are only involved in a limited number of sensitive reactions.

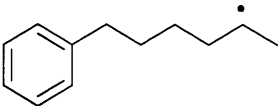
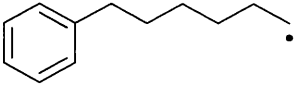
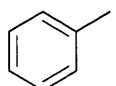
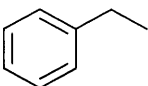
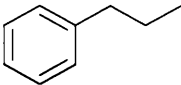
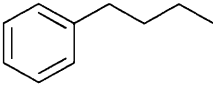
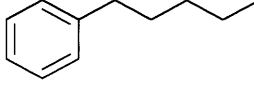
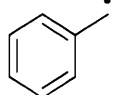
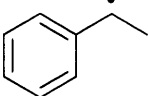
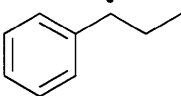
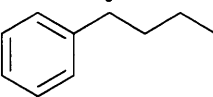
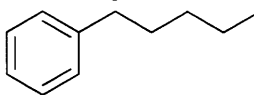
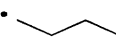
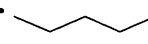
2.3.7. Thermodynamics of Key Species

In response to the discovery of the importance of accurate thermochemistry in this model, Gaussian 03 was used to compute the thermochemistry of many relevant species using the CBS-QB3 method. The thermochemistry of all the species involved in reactions (2) and (3) were computed. In addition, since alkylbenzenes and radicals of hexylbenzene are speculated to be an important component of this model, we expanded our calculated thermochemistry to include all aforementioned species.

The resulting thermochemistry of all considered species at 723K (reaction conditions) are shown in Table 5. Table 6 shows selected thermochemistry values from this work and the literature at 298.15K for comparison.

Table 5 Table of thermochemistry values for all species calculated in this work at 723K. Full NASA polynomials are available in the Supporting Information.

Species	Enthalpy of formation (723K) (kcal mol ⁻¹)	Entropy of formation (723K) (cal mol ⁻¹ K ⁻¹)
	21.5	193.6
	57.3	190.4
	67.1	195.4
	66.7	194.4
	66.7	195.7

	66.7	195.0
	70.2	194.4
	28.6	110.2
	27.3	126.7
	25.5	142.4
	24.1	159.9
	22.7	176.1
	67.6	109.1
	63.0	125.4
	61.6	141.0
	59.9	157.1
	58.8	173.4
	33.4	104.9
	31.9	124.7

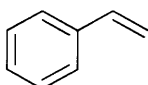
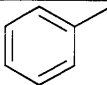
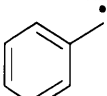
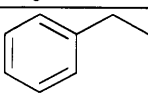
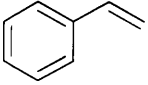
	54.7	119.7
---	------	-------

Table 6 Table of thermochemistry values at 298.15K, in comparison with literature values.

Species	Enthalpy of formation (298.15K) (kcal mol ⁻¹)		Entropy of formation (298.15K) (cal mol ⁻¹ K ⁻¹)	
	This work	Literature	This work	Literature
	11.6	12.0 [36]	76.5	76.92 [37]
	50.5	49.7 [38]	75.2	76.1 [38]
	6.94	7.12 [39]	85.7	86.2 [40]
	35.6	35.8 [39]	81.7	82.5 [41]

With the modified thermochemistry and updated rate rule calculated in section 2.3.5, the updated conversion of hexylbenzene and molar yield of major products predicted by our model is shown in Figure 7 (in Lai Version 2) and Figure 17 respectively. The updated model has 453 species and 3812 reactions.

It could be seen from Figure 7 that this updated model is much more accurate in quantitatively predicting the conversion of hexylbenzene, improving from a factor of 2 to a 30% difference. Similar to the previous iteration of the model, the aromatic selectivity of the three major species toluene, styrene and ethylbenzene match within a factor of 3, as shown in Figure 17.

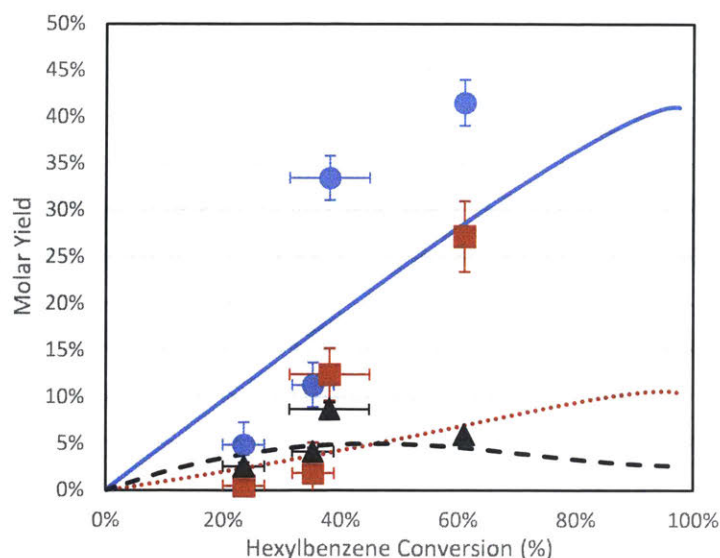


Figure 17 Model predicted (lines) and experimental measured (symbols) molar yield of major aromatic species for Lai Version 2, including toluene (blue), ethylbenzene (red), and styrene (black). Horizontal axis is set as conversion of hexylbenzene to allow better comparison of species selectivity between model and experiments. Reaction conditions identical to Figure 9.

In the Carr et al.'s model, the molar yield of styrene is highly over-predicted, whereas the molar yield of ethylbenzene is under-predicted. This issue is resolved in Lai Version 2 at low conversions, where styrene has a lower molar yield than ethylbenzene after 30% of hexylbenzene conversion, and the prediction for both species are in line with experimental results. This is caused by Lai Version 2 having a more radical oriented mechanism (as opposed to Carr et al. where most of the conversion is driven by the "retro-ene" reaction), which allows the conversion between styrene and ethylbenzene through hydrogen abstraction and disproportionation with surrounding radicals. The secondary chemistry at higher conversion more complicated, and this model currently does not capture the experimental behavior as a result.

It is worth noting that the sum of molar yield of major products in Figure 17 is higher than the conversion at the two highest conversion data points. This is an indication that the yield of these major products at longer reaction times are not exclusive to beta scission of hexylbenzene radicals, but are supplemented by the aromatization of the aliphatic carbon from hexylbenzene.

In this work, we focus on the molar yield of major species, since our model currently does not carry enough accuracy to predict the secondary products of this system. As a brief summary, other products that were formed are shown in the GCxGC chromatogram in Figure 18. Products can be found throughout aliphatic groups to aromatic species that have more than three rings. The experiments suggest the formation of aromatic rings with three or more rings, indicating that there are addition pathways that RMG does not currently predict, as the current RMG-generated mechanism does not include any 3 ring aromatic species.

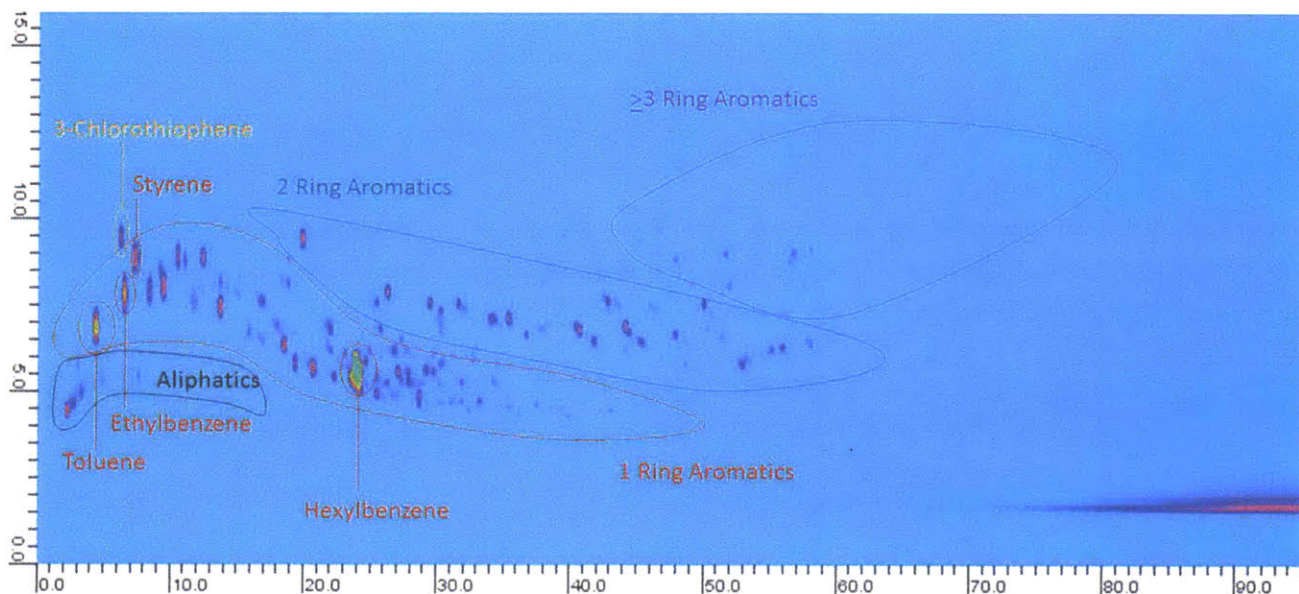


Figure 18 GCxGC chromatogram of hexylbenzene pyrolysis products at 450°C, 40 minutes. Chromatogram shows many peaks in regions with two or more aromatic rings.

2.3.8. Uncertainty of species thermochemistry

In Figure 7, it can be seen that the model conversion of hexylbenzene matches the experimental conversion due to the significant improvement of thermochemistry estimates. To understand the precision of the model, the error bounds of hexylbenzene conversion for Lai Version 2 were estimated by adding or subtracting the CBS-QB3 uncertainty (2.4 kcal/mol [42]) to the Gibbs free energy of hexylbenzene (Figure 19).

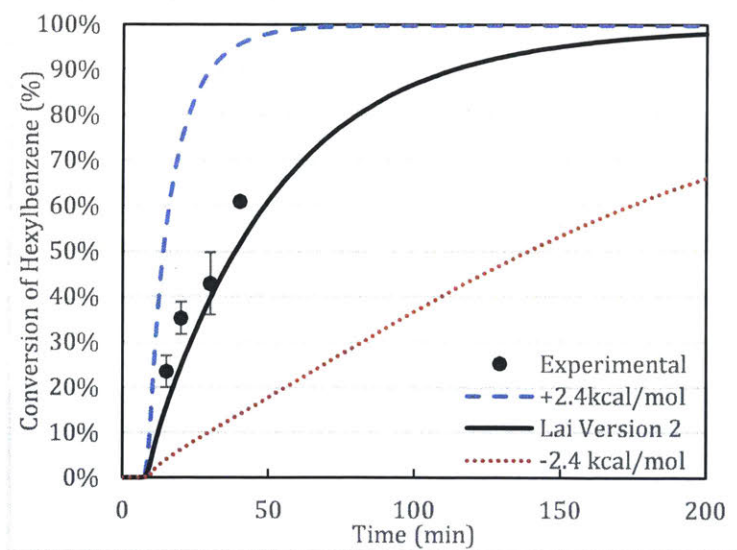


Figure 19. Error bounds of hexylbenzene conversion in Lai Version 2, computed by adding/subtracting the root mean square deviation of enthalpy for the CBS-QB3 level of theory to Hexylbenzene's Gibbs free energy in Lai Version 2.

It can be seen that the error bounds envelop the experimental data points by a large margin, showing that the uncertainty in the CBS-QB3 method can influence the predictions of the mechanism for a wide range of hexylbenzene conversions.

The CBS-QB3 level of theory is not sufficiently precise for predicting hexylbenzene conversion due to the high sensitivity of conversion to thermochemistry of species in the model as shown in this work. Future work directed at more accurately determining the thermochemistry of alkylaromatics and their radicals could significantly improve the accuracy of chemical mechanisms that include alkylaromatics.

Many recent calculations of rates and thermochemistry have used the M06-2X/cc-pVTZ method which is one of the best DFT functionals for this purpose [43]. A calculation of hexylbenzene's thermochemistry was performed using the M062x/cc-pVTZ method to quantify the variability of a species' Gibbs free energy when calculated using different quantum chemistry methods. The results are shown in Figure 20.

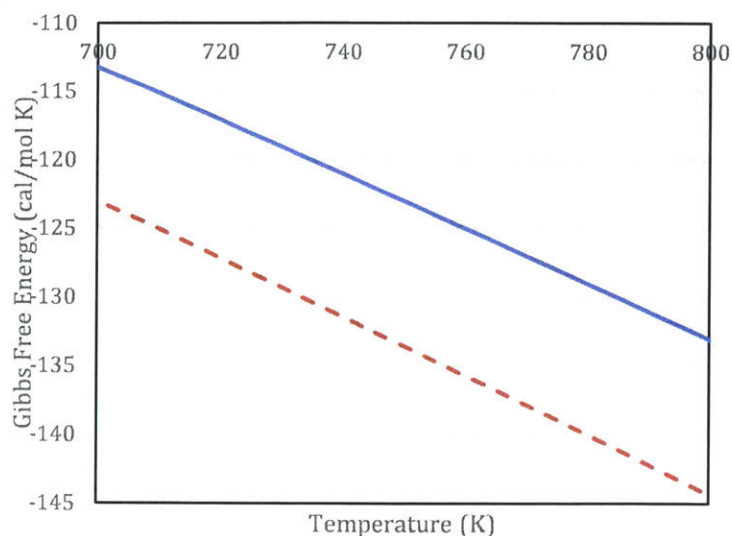


Figure 20 Gibbs free energy comparison of Hexylbenzene using CBS-QB3 method (blue solid line) and M06-2x/cc-pVTZ method (red dashed line). At the temperature of interest (723K), there is a 10.1 kcal/mol difference.

The difference in Gibbs free energy between the two calculations is 10.1 kcal/mol at 723K, a huge discrepancy. As expected, the CBS-QB3 value is closer to the experimental data. This highlights potential problems with relying on DFT for thermochemistry, and how mixing calculations done at different levels of theory can introduce large errors in chemical mechanisms. Clearly, more reliably accurate methods are needed, but this remains challenging for molecules and radicals with 12 carbons, because CBS-QB3 and other high accuracy methods such as G3 scale very poorly with the size of the molecule. In this investigation, calculations for hexylbenzene using the G3 and CCSD(T)-F12 methods were attempted, but were impossible with our computational resources.

2.4. Conclusions

Through the use of sensitivity and quantum calculations done at the CBS-QB3 level, this work was able to (1) identify the key reactions that play a role in the conversion of hexylbenzene and to rule out the “retro-ene” reaction assumed in other works [33], (2) identify the importance of thermodynamic parameters of various species in the prediction of hexylbenzene conversion, and (3) update the model with more accurate thermodynamic and kinetic parameters. Although quantitative agreement in conversion was achieved between model and experiments, agreement

for species selectivity was not achieved with rather large discrepancies at high conversion. Part of this may be due to the high sensitivity of species yield with respect to thermochemistry, which is still not known to sufficient accuracy; it is also certain that the model is missing some secondary products and reactions which are important at high conversions. Further investigation showed that different methods for computing thermochemistry can cause erratic differences in the predicted conversion of hexylbenzene, emphasizing the importance of developing high-accuracy methods for predicting the thermochemistry of relatively large alkylaromatic reaction intermediates.

3. Chapter 3

Thermochemistry and Group Additivity Values for Fused Two Ring Species and Radicals

This chapter is closely related to Lai, Khanniche, and Green, “Thermochemistry and Group Additivity Values for Fused Two-Ring Species and Radicals” [44]. The thermochemistry of many spirocyclic species reported in this chapter were computed not by me, but by my collaborator Dr. Sarah Khanniche, who was a co-author of the journal publication reporting this work. They are included here as a unified set with the computations I performed for clarity of presentation.

Chapter Abstract

Motivated by the lack of understanding in the chemical mechanisms of alkylaromatic pyrolysis, the thermochemistry of fused two ring aromatic molecules and radicals were calculated in this work using the CBS-QB3 level of theory. The enthalpies of formation of some fused ring species differ by as much as 13 kcal/mol from previous estimates. New group values were defined to facilitate better thermochemistry estimates in the future, and were found to match the CBS-QB3 calculated values with an average deviation of 0.4 kcal/mol and a standard deviation of 0.9 kcal/mol, a substantial improvement from previous estimation methods. We discuss the thermochemical characteristics of the various polycyclic and radical groups developed in this work.

3.1. Introduction

The accurate evaluation of thermochemical properties is extremely important for the purposes of constructing kinetic models for alkylaromatic pyrolysis systems, an extensively studied area of high relevance to crude oil upgrading [19] [18] [25] and production of chemicals [45] [46]. One particular tool for constructing kinetic models is the Reaction Mechanism Generator (RMG) [16] which requires reliable fast estimates of thermochemical properties in order to generate useful chemical mechanisms. Previous work in Chapter 2 has shown the effects of thermochemistry on

product distribution [19], where changes as small as 2 kcal/mol in the Gibbs free energy of a few key species could significantly alter the yield of relevant products.

This work is motivated by attempts to accurately model formation of fused two ring aromatic species, likely precursors of coke formation in alkylaromatic pyrolysis. While the thermochemical databases carry a high volume of information, the information specifically describing the thermochemistry of fused two ring species at the industrially relevant pyrolysis temperature of 450°C is sparse, and scattered throughout different sources, with many different methods of estimation or levels of theory. These thermochemical databases include the NIST thermochemical tables [47], the Third Millennium Ideal Gas and Condensed Phase Thermochemical Database [48], Active Thermochemical Tables [49], Pedley et al. [50], and Goldsmith et al. [51]. Table 7 summarizes the thermochemical databases and their characteristics

Table 7 Summary of thermochemical databases and their various characteristics

Database	Source	Type of species
NIST Thermochemical Tables [47]	Experimental and theoretical	Enthalpy, entropy, and tabulated heat capacities for stable species, radicals, and ions
Third Millennium Ideal Gas and Condensed Phase Thermochemical Database [48]	Experimental and theoretical	Full NASA polynomials for stable species and radicals
Active Thermochemical Tables [49]	Experimental and theoretical	Enthalpy only for stable species, radicals, and ions
Pedley et al. [50]	Experimental and theoretical	Enthalpy only for organic species
Goldsmith et al. [51]	Theoretical only	Enthalpy, entropy, and tabulated heat capacities for small carbon containing species and radicals only

This work calculates the thermochemistry of relevant reaction intermediates starting from long chain alkylaromatic radicals leading up to fused two ring aromatics (naphthalene and indene) and spiro compounds (phenyl migration intermediates). The energies were calculated using the CBS-QB3 level of theory. Group additivity values (GAVs) were developed to aid the future estimation of thermochemistry for similar compounds at high accuracy to avoid repeatedly running costly quantum calculations.

The group additivity value (GAV) method was developed by Benson [52] [53] and further refined by Ritter and Bozzelli [54]; this method is a simple and convenient means to estimate the thermochemical properties of molecules, including the enthalpy of formation, entropy, and heat capacities given the known group values that constitute molecules of interest. This GAV method was further developed by Lay et al. [55] to describe the energy of radical species through hydrogen bond increments (HBI) under the following scheme:

$$\Delta H_{f,298 K}^{\circ}(R \cdot) = \Delta H_{f,298 K}^{\circ}(RH) + H_{HBI} - \Delta H_{f,298 K}^{\circ}(H)$$

Where H_{HBI} is the hydrogen bond increment of a radical type

$\Delta H_{f,298 K}^{\circ}(R \cdot)$ is the enthalpy of formation of the radical

$\Delta H_{f,298 K}^{\circ}(RH)$ is the enthalpy of formation of the corresponding hydrogenated stable species

and $\Delta H_{f,298 K}^{\circ}(H)$ is the enthalpy of formation of the hydrogen atom, 52.1 kcal/mol.

HBI values have also been described for entropy and heat capacity:

$$\Delta S_{f,298 K}^{\circ}(R \cdot) = \Delta S_{f,298 K}^{\circ}(RH) + S_{HBI}$$

$$C_{p,T}(R \cdot) = C_{p,T}(RH) + C_{p,T,HBI}$$

This method is currently used by THERM [54] and RMG [16] to estimate the thermochemistry of unknown species.

Existing GAVs for polycyclic groups were described in Benson et al. [52], Yu et al. [56], and Han et al. [57], citing data from calorimetry experiments and computational calculations using various levels of theory (such as B3LYP//6-31G(d) or M06-2X//cc-pVTZ). Some previous GAVs were developed under different schemes; for example, Benson describes polycyclic aromatics using

atom centered groups, Yu et al. used bond-centered groups, and Han et al. treats an entire 2-ring structure as a group to better account for ring strain effects. These different methods give different estimates of the molecule's thermochemistry, and it is often hard to know which of the estimates are accurate.

Lay et al. [55] and Li and Curran [58] reported HBI values for many radical groups such as secondary and tertiary benzyl radicals, allyl radicals, and super allylic radicals, but these group structures may not be sufficiently specific to describe aromatic related radicals described in this work. Some of Lay et al.'s HBI values are derived from experimental data and are likely accurate, but other values are derived from semi-empirical calculations and are more doubtful.

In response to the aforementioned shortcomings, this work updates polycyclic and radical groups encountered in our mechanisms of interest using the CBS-QB3 level of theory, Han's [57] method for estimating polycyclic species, and retains the HBI format of Lay for radicals to maintain internal consistency with RMG's database.

Another method of rapid estimation for thermochemistry of unknown species is through machine learning algorithms, suggested by Li et al. [59], where a molecular graph convolutional neural network is used with a dropout training strategy to achieve the extrapolation of thermochemistry from a large database of training species. There are currently advantages and disadvantages for using Li et al.'s method; some of the advantages include (1) the lack of user interference in designing new group values, (2) the incorporation of features that may not be possible in the GAV method, and (3), the easy of retraining an estimation model. However, these advantages are met by drawbacks such as (1) the lack of user transparency, since users will no longer know the contributions towards a thermochemistry estimate, and (2) a large quantity of data is required for this method of estimation to be effective. Considering the potential benefits of both methods, these two methods should be developed in parallel until the available training data for Li et al. allows its benefits to outweigh its disadvantages.

3.2. Computational Details

In this work, quantum mechanical calculations are performed using Gaussian 03 [27], followed by the calculation of partition functions and fitting to NASA polynomials using the Cantherm software package that is part of RMG. Finally, group additivity estimates are derived through least-squares, solving the associated system of linear algebra equations using Python's numpy module.

Description of this work's methodology on Gaussian 03 calculations can be found in section 2.2.8.

3.2.1. RMG – Cantherm

In addition to the methodology outlined in 2.2.9, for cases where there are optical isomers and/or internally symmetric hindered rotors, $R \cdot \ln(\text{Symmetry number})$ is subtracted from the entropy of the molecule, where R is the gas constant. This subtraction assumes the species of interest is a homogenous mixture of all different optical isomers in all conformations. The S_{GAV} and S_{HBI} values reported here do not include the symmetry correction, it is assumed the user will apply the symmetry number correction for their particular molecule of interest.

RMG is an active open-source software project; as a result, the methods are constantly being improved. To facilitate replication of this work, the exact version of Cantherm used in this work can be found in the GitHub version commit string found in the supporting information of Lai et al. [44]. Cantherm has been renamed to Arkane as of the publication of this article; but due to the version of RMG used, this article will continue to refer to the software package as Cantherm.

3.2.2. Group Additivity Estimates

A script was written utilizing python's numpy module to convert thermochemistry values to hydrogen bond increments or group additivity values that minimize the error in the following linear system of equations:

$$(A)(B) + (C)(D) = (E)$$

Matrix operations were carried out to solve for the unknown **matrix B**, each row of which carries the unknown GAV and HBI values (including enthalpy, entropy, and heat capacity at various temperatures).

Each row of **matrix A** carries the number of occurrences of each unknown group in one of the compounds in the training set.

Each row of **matrix C** carries the number of occurrences of each known group in one of the molecules in the training set.

Each row of **matrix D** carries the known group values for one of the groups found in **matrix C**. Same format as **matrix B**.

Matrix E is a matrix of thermochemistry data for the compounds in our training set. Same format as **Matrix B**.

The weighted least-squares equation for B is

$$B = Wz$$

Where

$$W = (Q^T Q)^{-1} Q^T$$

$$Q_{ij} = A_{ij}/\sigma_i$$

$$\sigma_i = \sigma_{E_i}^2 + \sum_j c_{ij}^2 \sigma_{D_j}^2$$

$$z_i = \frac{E_i - \sum_j c_{ij} D_j}{\sigma_i}$$

σ_{E_i} denotes the uncertainty for thermochemistry data of species i

σ_{D_j} denotes the uncertainty for the thermochemistry data of the known group j

The sensitivities of the inferred group values B_i to errors in E or D is given by

$$\frac{\partial B_j}{\partial E_i} = W_{ij}$$

$$\frac{\partial B_j}{\partial D_l} = - \sum_l W_{ij} c_{jl}$$

In the development of group additivity values, **Matrix E** does not contain any entropy modifications due to symmetry, since symmetry is not an inherent part of the group additivity estimation method. Instead, RMG's group additivity evaluation method evaluates external rotational symmetry, internal symmetry due to hindered rotors, and optical isomers of a molecule and accounts for entropy changes due to symmetry after all group additivity contributions are made.

3.2.3. Uncertainty Analysis

The uncertainty associated to each GAV developed in this work was derived through uncertainty propagation [60], which uses the following equation:

$$s_{GAV} = \sqrt{\sum_i \left(\frac{d GAV}{di}\right)^2 s_i^2}$$

Where s_{GAV} is the standard deviation of a group additivity value
 i is a component that contributes to the development of the GAV, including the CBS-QB3 method [61], and the uncertainty of other GAVs that belong to the model species
 s_i is the uncertainty associated to component i

The standard deviation of the group additivity value s_{GAV} is divided by the square root of number of points used to generate the value to give the standard error. This work finds the uncertainty of the enthalpy of published GAVs to be 0.5-5.3 kcal/mol, and uncertainty of entropy to be 0.2-2.5 cal/mol K.

This work presents reliable GAV for many functional groups that will be helpful in kinetic modeling. In particular, further work on spiro radicals will be helpful to reduce the uncertainty in the associated group values, and so more accurate estimates of other molecules containing those groups.

More details for the computation of uncertainties, and the uncertainties of all GAVs are published in the supporting information of Lai et al. [44].

3.3. Results and Discussion

3.3.1. Fused Two Ring Aromatic Formation Mechanism

The selection of fused two ring species investigated in this work is motivated by our observation of ethyltetralin and propylindane products of hexylbenzene pyrolysis [19]. This work further investigates the thermochemistry of the formation of these compounds, and proposes the reaction mechanisms in Figure 21 and Figure 22 for the formation of fused two ring aromatic compounds in hexylbenzene pyrolysis:

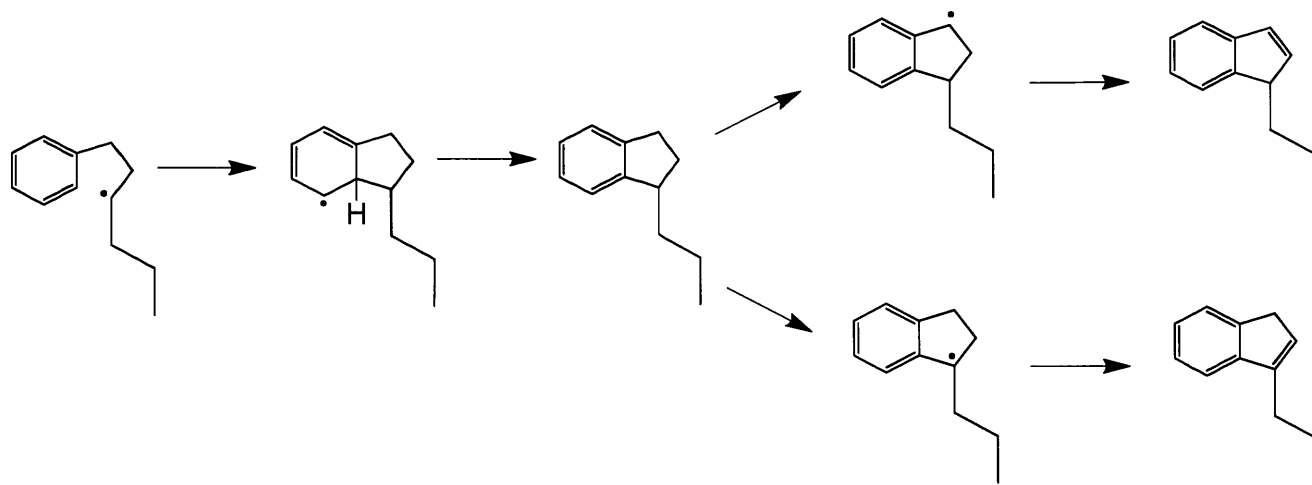


Figure 21 Proposed formation mechanism for propylindene from the third hexylbenzene radical

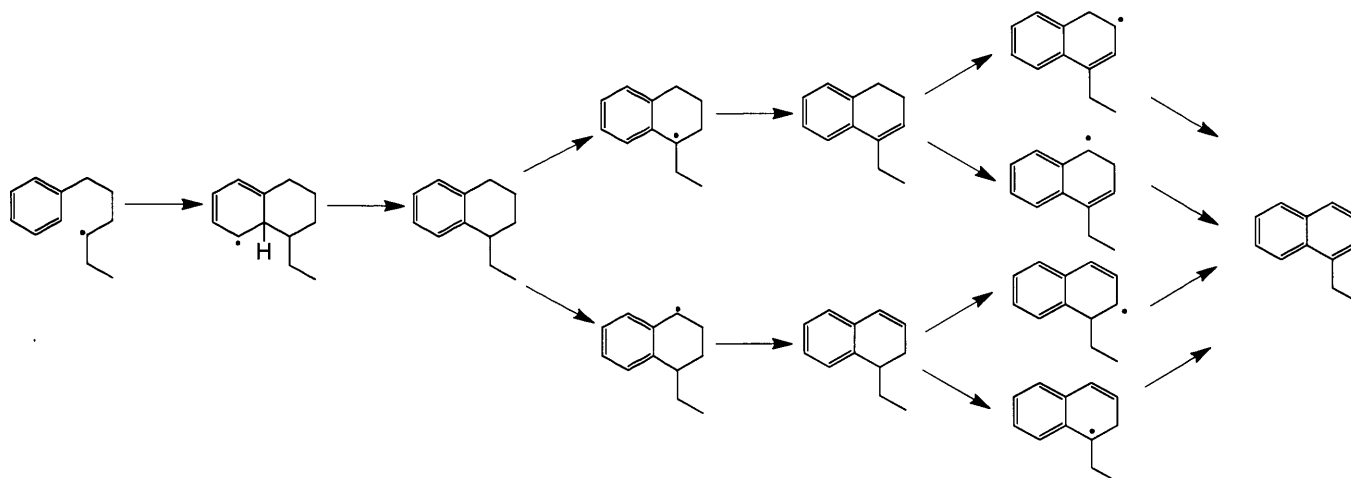


Figure 22 Proposed formation mechanism of ethylnaphthalene from the fourth hexylbenzene radical

In the two proposed mechanisms, a hexylbenzene radical on the third/fourth carbon off the alkyl chain undergoes intramolecular addition to form a fused two ring structure, forming a radical precursor of propylindane/ethyltetralin. This precursor loses a hydrogen either through hydrogen beta-scission or disproportionation to form the stable species propylindane and ethyltetralin. Throughout the pathway, stable species may further lose hydrogen in allylic/benzylic positions through hydrogen abstraction, and radical species may lose hydrogen adjacent to radical carbons to through hydrogen beta-scission and disproportionation until the fused species becomes fully aromatized into propylindene and ethylnaphthalene. This work calculates the thermochemistry of

all the polycyclic compounds in Figure 21 and Figure 22 (for thermochemistry of hexylbenzene radicals see Lai et al. [19]).

In addition, this work also investigates the thermochemistry of the competing phenyl migration pathways, a competing class of intramolecular addition pathways with only one shared carbon atom. Figure 23 shows the phenyl migration pathways of interest.

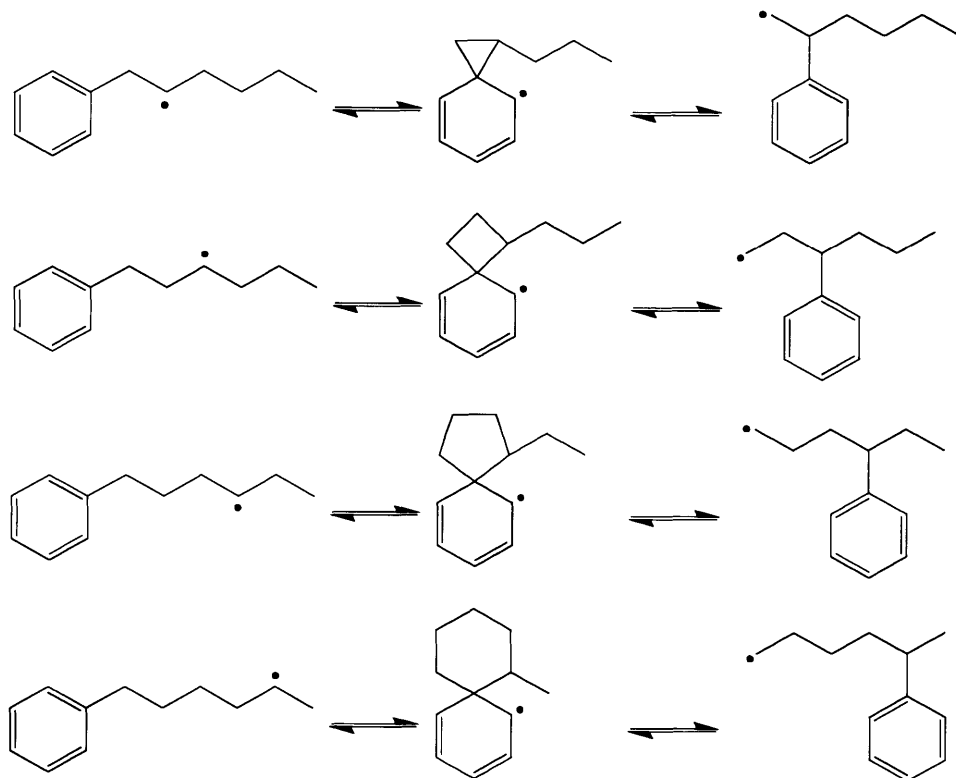


Figure 23. Proposed phenyl migration pathways from hexylbenzene to x-phenyl-1-hexyl radicals.

Here we focus on the thermochemistry of the fused ring radical. Due to the confounding unknowns of the polycyclic correction and the radical correction in this class of compound, the thermochemistry of both the radicals and their stable species counterparts were calculated. The thermochemistry of the x-phenyl-1-hexyl radicals are reported in the supporting information of Lai et al. [44]. Note the spiro radical intermediates have different resonance forms which of course have the same energy. However, in the GAV/HBI method, one needs to supply different HBI values for each resonance form, since each R is derived from a different RH.

This work is primarily focused on the thermochemistry of the aforementioned reaction pathways, and derivation of GAV's so that other similar pathways could be accurately estimated. A detailed study of the transition states of the same reactions was recently reported by Khanniche et al. [62]

3.3.2. Thermochemistry of Fused Two Ring Aromatic Species

As found in previous work [19], accurate thermochemistry is needed to make correct predictions for product yield. The thermochemistry of all polycyclic species shown in Figure 21-Figure 23. In Figure 23, hydrogenated counterparts of the calculated species in the 1,3 and 1,4-cyclohexadiene resonance structures were also calculated to determine the unknown radical and polycyclic thermochemical groups. In addition, all variants of species in the three figures with varying chain lengths up to 12 carbons were also calculated; for example, indene, methyindene, and ethylindene were calculated alongside propylindene. This resulted in the calculation of 83 species at the CBS-QB3 level of theory. Thermochemical data calculated are gathered in Table 8. Full NASA Polynomials can be found in the supporting information of Lai et al. [44]. A few of these species have been studied previously, and comparisons to prior works for those species are listed in Table 9.

Table 8 Thermochemical data of species calculated in this work.

SMILES String	Enthalpy of formation (298 K) (kcal/mol)	Entropy (298 K) (cal/mol K)
Aromatic Pi Radicals of Indane		
<chem>C1=CC=C2CCCC2[CH]1</chem>	44.7	87.7
<chem>CC1CCC2=CC=C[CH]C21</chem>	36.7	96.0
<chem>CCC1CCC2=CC=C[CH]C21</chem>	31.7	104.1
<chem>CCCC1CCC2=CC=C[CH]C21</chem>	26.8	112.4
Alkylated Indanes		
<chem>C1=CC=C2CCCC2=C1</chem>	13.2	82.1
<chem>CC1CCC2=CC=CC=C21</chem>	5.6	90.5
<chem>CCC1CCC2=CC=CC=C21</chem>	0.6	98.3
<chem>CCCC1CCC2=CC=CC=C21</chem>	-4.5	107.0
Benzylic Radicals of Indane		
<chem>C1=CC=C2CC[CH]C2=C1</chem>	49.5	84.7

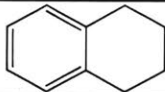
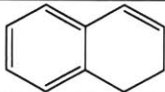
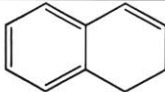
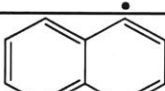

CC1C[CH]C2=CC=CC=C21	42.2	93.4
C[C]1CCCC2=CC=CC=C21	39.4	93.7
CCC1C[CH]C2=CC=CC=C21	37.0	100.7
CC[C]1CCCC2=CC=CC=C21	34.6	101.2
CCCC1C[CH]C2=CC=CC=C21	32.0	109.5
CCC[C]1CCCC2=CC=CC=C21	29.2	108.7
Alkylated Indenes		
C1=CC=C2CC=CC2=C1	38.0	79.8
CC1C=CC2=CC=CC=C21	31.3	88.5
CC1=CCC2=CC=CC=C21	28.3	87.9
CCC1C=CC2=CC=CC=C21	26.3	96.9
CCC1=CCC2=CC=CC=C21	23.3	96.3
CCCC1C=CC2=CC=CC=C21	21.2	105.9
CCCC1=CCC2=CC=CC=C21	18.1	106.0
Aromatic Pi Radicals of Tetralin		
C1=CC=C2CCCCC2[CH]1	32.3	89.8
CC1CCCC2=CC=C[CH]C21	25.1	98.2
CCC1CCCC2=CC=C[CH]C21	21.2	106.5
Alkylated Tetralins		
C1=CC=C2CCCCC2=C1	4.6	97.4
CC1CCCC2=CC=CC=C21	-2.1	95.3
CCC1CCCC2=CC=CC=C21	-6.8	103.0
Benzylic Radicals of Tetralin		
C1=CC=C2CCC[CH]C2=C1	39.2	88.2
C[C]1CCCC2=CC=CC=C21	30.8	96.8
CC1CC[CH]C2=CC=CC=C21	32.8	96.3
CC[C]1CCCC2=CC=CC=C21	25.7	102.5
CCC1CC[CH]C2=CC=CC=C21	28.3	102.9
Alkylated Dihydronaphthalenes		
C1=CC=C2CCC=CC2=C1	29.4	85.2
CC1=CCCC2=CC=CC=C21	21.0	92.3
CC1CC=CC2=CC=CC=C21	22.8	93.2
CCC1=CCCC2=CC=CC=C21	16.0	98.9

CCC1CC=CC2=CC=CC=C21	16.9	102.1
Allylic and Benzylic Radicals of Dihydronaphthalene		
C1=CC=C2C=C[CH]CC2=C1	57.4	87.1
C1=CC=C2C=CC[CH]C2=C1	62.0	86.5
CC1[CH]C=CC2=CC=CC=C12	50.8	93.6
C[C]1CC=CC2=CC=CC=C12	53.7	93.5
CC1=C[CH]CC2=CC=CC=C12	49.2	96.3
CC1=CC[CH]C2=CC=CC=C12	53.6	95.1
CCC1[CH]C=CC2=CC=CC=C12	44.2	101.9
CC[C]1CC=CC2=CC=CC=C12	49.3	102.8
CCC1=C[CH]CC2=CC=CC=C12	44.7	103.5
CCC1=CC[CH]C2=CC=CC=C12	48.7	102.9
Naphthalenes		
C1=CC=C2C=CC=CC2=C1	35.1	82.3
CC1=CC=CC2=CC=CC=C12	27.0	89.9
CCC1=CC=CC2=CC=CC=C12	22.1	96.6
Phenyl Migration Radicals		
CCCCC1CC12C=CC=CC2	43.3	118.6
CCCC1CCC12C=CC=CC2	43.0	118.4
CCC1CCCC12C=CC=CC2	25.8	108.1
CC1CCCCC12C=CC=CC2	21.5	103.4
Rad 2 Phenyl Migration 1_4		
CCCCC1CC12C=CCC=C2	24.5	117.2
CCCC1CC12C=CCC=C2	29.3	106.3
CCC1CC12C=CCC=C2	34.3	97.5
CC1CC12C=CCC=C2	40.2	89.4
C1CC12C=CCC=C2	46.8	81.6
Rad 2 Phenyl Migration 1_3		
CCCCC1CC12C=CC=CC2	25.2	117.5
CCCC1CC12C=CC=CC2	30.1	107.2
CCC1CC12C=CC=CC2	35.2	98.3
CC1CC12C=CC=CC2	41.3	90.5
C1CC12C=CC=CC2	47.8	82.7

Rad 3 Phenyl Migration 1_4		
CCCC1CCC12C=CCC=C2	21.3	110.5
CCC1CCC12C=CCC=C2	26.6	101.8
CC1CCC12C=CCC=C2	32.5	93.7
C1CCC12C=CCC=C2	40.9	87.2
Rad 3 Phenyl Migration 1_3		
CCCC1CCC12C=CC=CC2	21.8	111.3
CCC1CCC12C=CC=CC2	27.0	102.6
CC1CCC12C=CC=CC2	32.6	95.0
C1CCC12C=CC=CC2	40.9	87.9
Rad 4 Phenyl Migration 1_4		
CCC1CCCC12C=CCC=C2	3.7	106.2
CC1CCCC12C=CCC=C2	9.0	98.8
C1CCCC12C=CCC=C2	17.2	92.3
Rad 4 Phenyl Migration 1_3		
CCC1CCCC12C=CC=CC2	5.9	108.3
CC1CCCC12C=CC=CC2	9.6	98.6
C1CCCC12C=CC=CC2	16.8	92.6
Rad 5 Phenyl Migration 1_4		
CC1CCCCC12C=CCC=C2	-0.8	101.6
C1CCCCC12C=CCC=C2	6.9	95.4
Rad 5 Phenyl Migration 1_3		
CC1CCCCC12C=CC=CC2	0.0	106.3
C1CCCCC12C=CC=CC2	6.2	95.6

Table 9 Thermochemical data comparison between this work and other literature sources (all data available).

Molecular Structure	Enthalpy of formation (298 K) (kcal/mol)		Entropy (298 K) (cal/mol K)	
	This Work	Literature	This Work	Literature
	13.2	14.5 [50]	82.1	
	38.0	39.2 [48] 39.1 [50]	79.8	80.3 [48]

	4.6	6.4 [50]	97.4	
	29.4	28.0 [48]	85.2	85.9 [48]
	62.0	54.9 [48]	86.5	86.9 [48]
	35.1	28.2 [48] 35.9 [50]	82.3	80.2 [56]
	27.0	28.3 [37]	89.9	89.8 [37]

The literature values shown in Table 9 are lacking in entropy values. While many of the calculations from our group are valuable, it is important to note that the computational methods used in this work are not perfect calculations, and caution in using these values should be taken without accurate benchmarking. This matter is particularly prominent since ring puckering effects that may exist in this work's species calculations might not be treatable using the 1-D hindered rotor harmonic oscillator approximation.

A comparison of these calculated values was made with RMG's estimates. Figure 24 shows the distribution of Gibbs free energy difference between RMG's estimates and this work's calculations at 298 K. On average, RMG overestimates the Gibbs free energy of the fused polycyclic species by 7.3 kcal/mol, with a standard deviation of 4.1 kcal/mol. The deviations range from -3 to +13 kcal/mol.

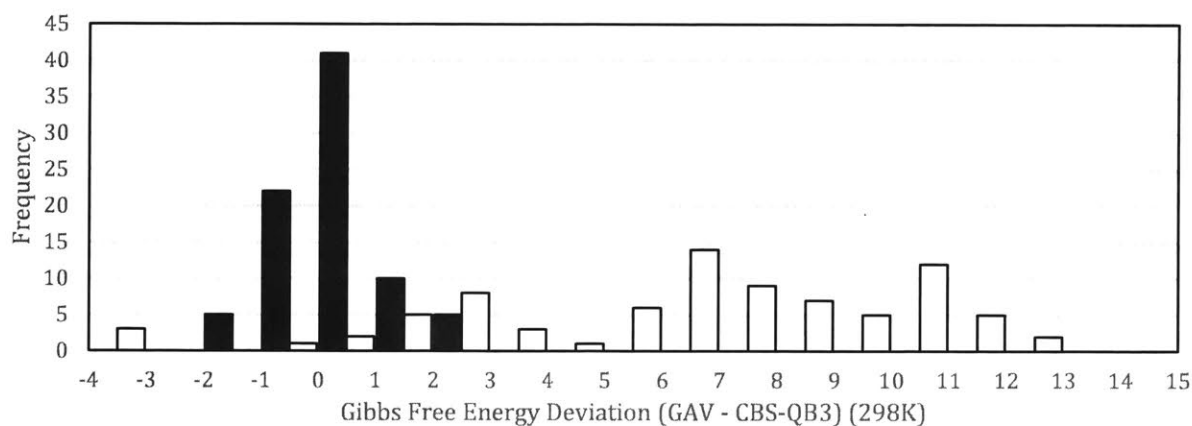


Figure 24 Distribution of Gibbs free energy deviation (kcal/mol) for 83 calculated fused two ring species up to 12 carbon atoms. Distribution for previous RMG estimates (white) and with updated group values (black) are shown.

As demonstrated in our previous work [19], this difference in Gibbs free energy is significant to adversely affect product distribution predictions. To facilitate better estimations of similar molecules and radicals in the future, we have updated RMG's group values used to describe the polycyclic species of interest.

Figure 24 shows the updated energy deviations from the new group values derived from our thermochemistry calculations. The average deviation of Gibbs free energy has been dropped to 0.4 kcal/mol, with a standard deviation of 0.9 kcal/mol; it can also be seen that the deviations follow a more normal distribution. The specific differences that led to this decrease are discussed in the following sections.

3.3.3. Derived Group Values

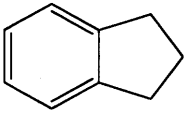
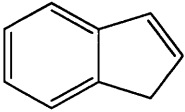
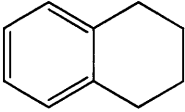
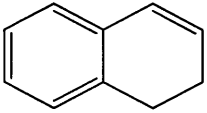
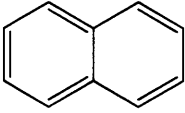
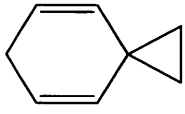
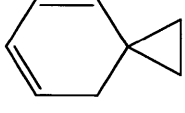
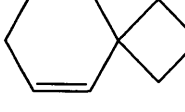
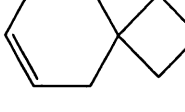
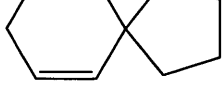
RMG's thermochemistry estimation is based off Benson's thermochemical group additivity [63], Lay et al.'s radical hydrogen bond increments [55], and Han et al.'s calculations for polycyclic compounds [57]. These values were evaluated from various calorimetry experiments, literature sources, and calculations at various levels of theory.



The thermochemistry groups in question for this work are polycyclic groups which were derived using limited training data by Han et al. [57], and hydrogen bond increments where the radical descriptors from Lay et al. (derived for simple radicals) were not specific enough to describe the resonance behavior of the more complicated radicals considered here. The groups that were in question in this work are summarized in Table 10 and Table 11.

3.3.3.1. Polycyclic Group Values

The thirteen polycyclic groups involve structures of indane, indene, tetralin, dihydronaphthalene, naphthalene, and several spiro compounds. Table 10 shows the original and updated values for enthalpy and entropy, as well as the sources of the original values. Group values for c_p can be found in the supporting information of Lai et al. [44].

Table 10. Original and updated values of polycyclic groups and the sources of RMG's original group values.

Polycyclic Group	H(298K) Kcal/mol		S(298K) cal/mol K		Source of Original RMG Value
	Original	Updated	Original	Updated	
	3.7	2.7	23.2	22.3	CBS-QB3 calculation for indane
	2.1	2.2	33.1	28.7	Verevkin (2011), experimental H, PM7 level of theory S and Cp [64]
	-0.2	-0.2	15.0	18.6	CBS-QB3 calculation for tetralin
	4.3	-1.1	20.9	20.5	Han et al. (2018) M06-2X/cc-pVTZ calculations for shown species [57]
	0	-1.0	-2.8	-2.0	Long et al. (2018), CBS-QB3 calculations for Naphthalene [65]
	26.7	24.8	53.7	55.6	Han et al. (2018) M06-2X/cc-pVTZ calculations for shown species [57]
	32.1	30.4	58.5	58.8	Han et al. (2018) M06-2X/cc-pVTZ calculations for shown species [57]
	30.0	22.6	51.0	50.9	Han et al. (2018) M06-2X/cc-pVTZ calculations for shown species [57]
	34.4	27.0	53.3	54.0	Han et al. (2018) M06-2X/cc-pVTZ calculations for shown species [57]
	14.2	4.5	47.8	46.6	Han et al. (2018) M06-2X/cc-pVTZ calculations for shown species [57]

	17.4	9.2	48.9	49.4	Han et al. (2018) M06-2X/cc-pVTZ calculations for shown species [57]
	9.4	-0.4	40.5	39.6	Han et al. (2018) M06-2X/cc-pVTZ calculations for shown species [57]
	12.7	3.6	42.7	45.3	Han et al. (2018) M06-2X/cc-pVTZ calculations for shown species [57]

Indane, tetralin, and naphthalene previously had group values based off the same level of theory, albeit a narrower selection of model compounds. As a result, the thermochemistry corrections of these groups are relatively small. The original and updated group values differ by < 1 kcal/mol for enthalpy of formation, and < 6 cal/mol K for entropy. These differences account for less than 2 kcal/mol difference in the Gibbs free energy at 298 K.

The original RMG values for the indene polycyclic group were taken from work by Verevkin et al. [64], where the enthalpy of formation of indene was experimentally determined, and the entropy and heat capacity values were calculated using the PM7 level of theory. Based on our assessment, it is inconclusive whether Verevkin's estimation is more accurate than our work's results. Our CBS-QB3 calculations finds the same enthalpy of formation as Verevkin's experimental work, which is reassuring. For the entropy of this polycyclic group, a 6 cal/mol K difference was observed due to the difference in calculation method and the smaller set of model compounds used in the old estimation. The PM7 method has a 1.86 kcal/mol root mean square error in enthalpy of stable molecules [66] and 5 cal/mol K in entropy [67]; this can be compared to the accuracy of CBS-QB3 documented by Somers and Simmie [42], with a mean signed error of -2.78 kcal/mol in ΔH_f^{298K} for closed shell species. Unfortunately, the accuracy of CBS-QB3 entropies for a broad range of molecules has not been documented in the literature, but previous calculation examples from our work have been in close agreement with the literature [19] [56]. Between this work (Table 9) and [19], entropy values calculated by CBS-QB3 differ by no more than 2 cal/mol K to found literature sources.

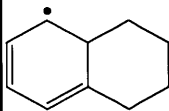
The dihydronaphthalene polycyclic correction has a 5 kcal/mol difference in enthalpy, a relatively stark disagreement with our previous source of thermochemistry estimation. This difference brings ~5 kcal/mol difference in the Gibbs free energy of a species at 298K, and is an important correction to RMG's thermochemistry group values. The original source of this polycyclic correction came from the M06-2X/cc-pVTZ level of theory. Differences larger than 5 kcal/mol in enthalpy of formation between this level of theory and CBS-QB3 has been observed in the past in our group's work for calculations on hexylbenzene [19], and this change is an important correction to the polycyclic group value of dihydronaphthalene.

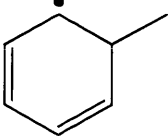
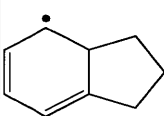
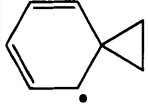
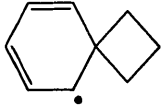
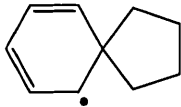
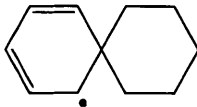
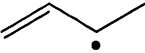
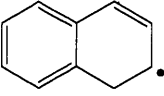
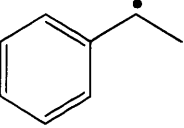
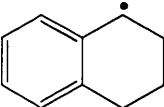
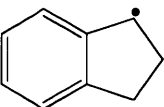
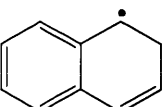
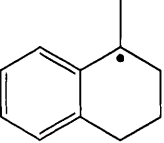
The polycyclic groups for spiro compounds differ from previous estimates by up to 13 kcal/mol in enthalpy of formation, and up to 2 cal/mol K in entropy. The large discrepancies in the enthalpy of formation are due to the differences between M06-2X/cc-pVTZ and the more accurate CBS-QB3 (with BAC) method used here. Consistent with common chemical intuition, polycyclic groups featuring three or four membered rings exhibit a much higher enthalpy correction than groups with five or six membered secondary rings, as small rings exhibit ring strain. It can be seen that 1,4-cyclohexadienes have a lower enthalpy of formation than 1,3-cyclohexadiene isomers.

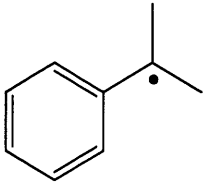
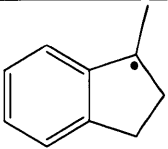
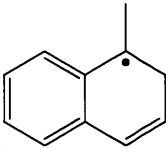
3.3.3.2. Hydrogen Bond Increments for Radicals

Four HBI values were originally used by RMG to estimate the thermochemistry of our fused polycyclic species. These groups lacked sufficient specificity towards our radicals of interest; therefore Table 11 shows our newly developed HBI groups (13 total), their hydrogen bond increment values, as well as the sources of the original HBI values. Group values for C_P can be found in the supporting information of Lai et al. [44].

Table 11. Original and updated HBI groups for radicals, with their respective enthalpy/entropy values and the source of RMG's original value. Enthalpy values in kcal/mol, and entropy values in cal/mol K.

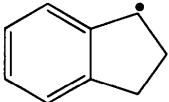
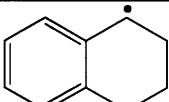
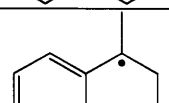
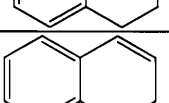
Old Group	H 298K	S 298K	Structure Label	New Group	H 298K	S 298K	Source of Original RMG Value
	75.0	1.3	A		73.7	0.8	CBS-QB3 calculations for methylcyclohexadienyl and hexylcyclohexadienyl radicals

			B		74.5	0.4	
			C		70.7	-1.8	
			D		72.5	2.7	
			E		73.5	-3.3	
			F		74.0	-1.2	
	85.6	-3.8	G		80.1	1.9	Roth et al. [68] experimental enthalpy, Lay et al. [55] MNDO/PM3 calculations for entropy. Model compound is 1-buten-3-yl radical
	88.1	-4.9	H		86.4	1.3	Lai et al. [19] CBS-QB3 calculations Model compounds include benzyl, ethylbenzyl, propylbenzyl, butylbenzyl, pentylbenzyl, and hexylbenzyl radicals
			I		88.5	3.1	
			J		83.7	1.4	
	83.8	-5.3	K		84.7	1.7	Robaugh et al. [69] and Hippler et al. [70] experimental enthalpy, Lay et al. [55] MNDO/PM3 calculations for entropy.

			L		85.4	4.4	Model compound is 2-Phenyl-2-propyl radical
				M		83.3	

Several HBI groups can be found in the Handbook of Bond Dissociation Energies in Organic Compounds by Luo [71]. The cited groups are shown in Table 12 for comparison. It was found that the CBS-QB3 fitted values are typically > 2 kcal/mol higher than the various literature sources found with the exception of the dihydronaphthalene radical. The methods of determining BDE's cited in Table 12 include correlation between BDEs and rate constants/activation energies [72] [73] [74], photoacoustic calorimetry [75], and pyrolysis kinetics [76]; it is reasonable to believe that the CBS-QB3 method can generate more accurate thermochemistry results than some of the methods used (particularly the correlation based rate constants/activation energies).

Table 12 All available comparisons between this work's hydrogen bond increments compared to Handbook of Bond Dissociation Energies in Organic Compounds [71].

	This Work	Luo [71]
	88.5	85.9 [72]
	86.4	82.9 [75] 83.6 [72] 82.6 [73]
	84.7	79.3 [74]
	80.1	86.0 [76] 80.4 [73]

The four spiro radicals (C through F) differ noticeably from the original source, with a < 5 kcal/mol difference in enthalpy and < 4 cal/mol K difference in entropy. This indicates that these fused cyclohexadienyl radicals differ modestly in energy from analogous radicals which don't have

fused rings. The only exception is the enthalpy correction of group **C**, where this difference originates from the high ring strain geometry of this species, and the introduction of a radical greatly alters this ring strain.

The addition of a fused ring to secondary and tertiary benzylic radicals does not cause the enthalpy HBI correction for the radical to change very much in the case of **H** and **I** structures (within 2 kcal/mol), but causes a large difference in entropy correction up to 8.5 cal/mol K. This difference in entropy is due to hindered rotor difference between a free benzyl radical and a fused benzyl radical; particularly, non-fused benzyl radicals lose a hindered rotor with the introduction of the radical (due to resonance with the aromatic pi bonds), whereas fused benzyl radicals do not experience changes in hindered rotors with the introduction of a radical.

The enthalpy and entropy of formation of **G** and **J** differ from its original source by 5 kcal/mol and 5 cal/mol K respectively, missing the extra stabilization due to resonance with the aromatic ring as well as the difference in entropy associated with rotor loss. This resonance stabilization is not fully reflected in the HBI group, since part of it is attached to the polycyclic group value.

This work finds that there is little difference in enthalpy correction between radicals found on five membered secondary ring structures (e.g. indane) versus radicals found on six membered secondary ring structures (e.g. tetralin), with enthalpy differences lower than 2 kcal/mol. The same is found for entropy, where this difference is found to be less than 3 cal/mol K.

3.4. Conclusions

This study was motivated by the lack of data on thermochemistry of fused two ring aromatics relevant to intramolecular addition and phenyl migration reactions, classes of reactions that are of great interest in understanding the chemistry of alkylaromatics. This work provides thermochemistry values for 83 alkylated fused two ring species. Group additivity values are derived from the aforementioned thermochemistry values; these groups include polycyclic structures for fused two ring aromatics, and hydrogen bond increment values for radicals that

were previously lacked sufficient specificity. These new group values agree with the Gibbs free energy found from CBS-QB3 calculations within 0.4 kcal/mol, with a standard deviation of 0.9 kcal/mol. Discussion was provided, highlighting differences between old sources and our current work, and rationalizing differences based on the molecular features such as hindered rotor effects and resonance stabilization. The newly developed groups can be used in the future to estimate the thermochemistry of species that carry similar structures, and will aid the prediction of the formation of fused two ring aromatics.

4. Chapter 4

Thermochemistry and Kinetics of Intermolecular Addition of Radicals to Toluene and Alkylaromatics

This work is closely related to the article by Lai and Green, "Thermochemistry and Kinetics of Intermolecular Addition of Radicals to Toluene and Alkylaromatics" [77].

Chapter Abstract

To better understand intermolecular radical additions to aromatic rings that take place in the pyrolysis of alkylaromatics at low to moderate temperatures (~450°C), the thermochemistry and kinetics of several reactions of this type are investigated using the CBS-QB3 level of theory. The calculated thermochemistry of the adduct radicals is significantly different from previous estimates; the average discrepancy in Gibbs free energy at 298 K is 5.3 kcal/mol. A group additivity value for aromatic pi radicals was developed to facilitate rapid accurate estimates for other molecules containing this functional group; average discrepancy in Gibbs free energy using the updated group additivity value is improved to 0.5 kcal/mol. Previous estimations of the rate coefficients of these reactions were found to be inaccurate due to the lack of important features such as loss of aromaticity in the compounds used as the training set for the estimation. Rate coefficients for addition of several different radicals to aromatic rings are reported. The reaction rates are comparable for ortho, meta, and para additions, slowest for addition to the substituted position, and insensitive to the length of alkyl chains attached to the aromatic reactant.

4.1. Introduction

The pyrolysis of alkylaromatics is important in oil refining [18] [19] [25] [78], coal pyrolysis [79], studies relevant to organic geochemistry [15], and production of chemicals [45] [46]. In the past, many reaction types relevant to alkylaromatic pyrolysis have been studied, such as unimolecular initiation and radical recombination [15] [80] [81], disproportionation [82] [83] [84] [85],

hydrogen abstraction [15] [86] [87], beta scission [19] [81] [88], and intramolecular addition [15] [81].

As part of the beta scission/intermolecular addition family, intermolecular addition to aromatic rings has not been studied extensively. Initiation, radical recombination [15] [33], and disproportionation [85] reactions carry high relevance due to their production/elimination of two radicals, dramatically changing the reactivity of the pyrolysis system. Aliphatic beta scission directly reduces molecular weight and forms desired alkene products, while aromatic intermolecular addition (and its reverse, beta-scission of aromatic pi radicals) have more subtle effects. The chemistry of alkylaromatics is dominated by resonantly stabilized benzylic radicals [19] [89], whereas aromatic pi radicals are relatively difficult to form since they require loss of aromaticity [90]. Aromatic intramolecular addition reactions are more frequently studied than the intermolecular reactions, because they form fused ring aromatic species, associated with coke formation [15] [81].

Despite the relative lack of prior work in aromatic intermolecular addition, there have been some relevant studies. Previous moderate-temperature experimental work from this group [19] and Lannuzel et al. [85] reports products such as 1-methyl-2-(phenylmethyl) benzene from alkylaromatic pyrolysis, which are likely products formed by the addition of benzylic radicals to aromatic rings. At very high temperature, addition of OH, H, and O to benzene rings is known to occur [91] [92] [93]. Shukla et al. observed addition of phenyl radical to benzene, and proposed this was important in polyaromatic hydrocarbon (PAH) formation [94]. Computationally, our previous work [19] generated a reaction mechanism for the pyrolysis of hexylbenzene using the Reaction Mechanism Generator (RMG) [16]. The resulting mechanism contains a substantial number of products formed through radicals adding to the aromatic bonds of hexylbenzene and other alkylaromatics, very few of which match our experiments, suggesting significant flaws in the model.

In the interest of gaining a better understanding of this class of reactions and to be able to generate more accurate chemical mechanisms, this work studies the addition of aliphatic and

aromatic radicals to aromatic pi bonds. This reaction class has the potential to form multi ring aromatics connected by alkyl bridges, allowing for the possibility of further aromatic and coke formation, an active area of interest [78] [4] [95] [96]. Aromatics connected by alkyl bridges are thought to be key structures in coal, petroleum, and heavy oil fractionations [97] [98] [99].

4.2. Methods

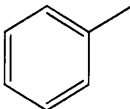
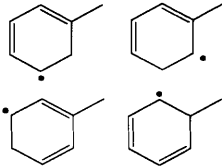
In this work, quantum calculations are performed using Gaussian 03 [27], followed by the calculation of partition functions and fitting to NASA polynomials using the Cantherm software that is part of the RMG package [16]. Finally, group additivity estimates are derived through solving a least squares system of linear equations, based on previous group additivity values in the RMG database by Benson et al. [53] and Lay et al. [55]. A detailed description of the methodology for Gaussian 03 calculations, RMG Cantherm, and generating group additivity values can be found in sections 2.2.8, 3.2.1, and 3.2.2.

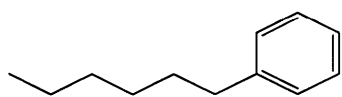
4.3. Results and Discussion

4.3.1. Aromatic Intermolecular Addition Reactions of Interest

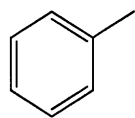
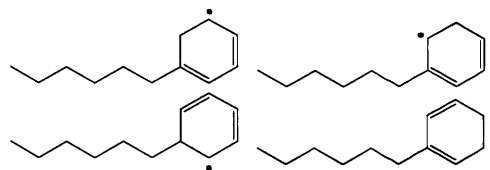
In this work, the aromatic intermolecular addition reactions between toluene/hexylbenzene and various radicals were studied. The radicals are the hydrogen atom, methyl radical, ethyl radical, benzyl radical, and 1-phenyl-1-ethyl radical; the selection of radicals is based on the relative radical concentrations in our system of interest found in previous work [19]. The products considered are shown in Table 13.

Table 13 Aromatic intermolecular addition pairings considered for this work; possible resulting species are listed.

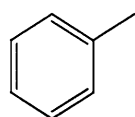
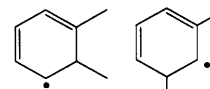
Aromatic Species	Radical Species	Resulting Species
	$\text{H}\cdot$	



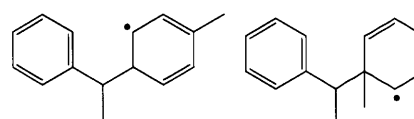
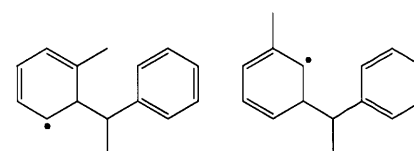
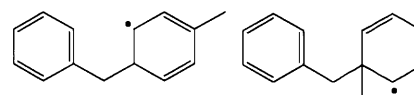
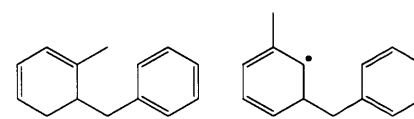
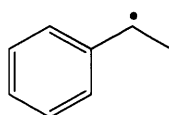
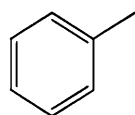
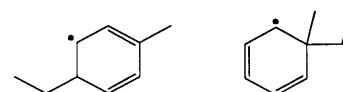
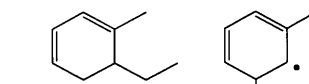
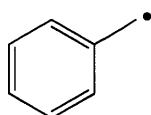
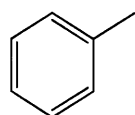
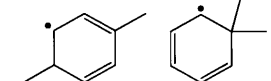
H•



•CH₃



•C₂H₅



The purpose for the various types of pairings between aromatics and radicals is to gain an understanding of the effects of different types of aromatic side chains and radicals on the rate of aromatic intermolecular addition.

4.3.2. Thermochemistry of Intermolecular Addition Products

The thermochemistry of all the resulting radicals shown in Table 13 (total of 24) were calculated at the CBS-QB3 rigid-rotor-harmonic-oscillator approximation + 1-D rotors level of theory. In addition, thermochemistry for recombination products with hydrogen for adducts of Toluene + H, CH₃, and C₂H₅ were also calculated. This data is shown in Table 14; full NASA polynomials and heat capacity data can be found in the supporting information of Lai and Green [77]. This work finds limited matches between species reported here and species in the NIST Thermochemical Database [47] or Burcat's Third Millennium Database [100]; benchmarking was unavailable for this section due to the lack of thermochemistry data related to this work.

Table 14 Thermochemical data of species calculated in this work. Heat capacities given in supporting information.

Species	SMILES String	Enthalpy of formation (298 K) (kcal/mol)	Entropy (298 K) (cal/mol K)
Toluene + H•			
Ortho	<chem>CC1=CC=C[CH]C1</chem>	39.2	81.5
Meta	<chem>CC1[CH]CC=CC=1</chem>	40.4	81.9
Para	<chem>CC1C=CC[CH]C=1</chem>	40.3	82.4
Substituted	<chem>CC1[CH]C=CC=C1</chem>	42.2	80.8
Hexylbenzene + H•			
Ortho	<chem>CCCCCCC1=C[CH]C=CC1</chem>	14.8	129.5
Meta	<chem>CCCCCCC1[CH]C=CCC=1</chem>	15.6	129.6
Para	<chem>CCCCCCC1C=CC[CH]C=1</chem>	15.4	128.6
Substituted	<chem>CCCCCCC1C=C[CH]C=C1</chem>	16.7	129.2
Toluene + •CH₃			
Ortho	<chem>CC1=CC=C[CH]C1C</chem>	33.1	90.2
Meta	<chem>CC1[CH]C(C)C=CC=1</chem>	33.6	90.6
Para	<chem>CC1C=CC(C)[CH]C=1</chem>	33.5	89.7
Substituted	<chem>CC1(C)[CH]C=CC=C1</chem>	34.0	87.2
Toluene + •C₂H₅			
Ortho	<chem>CCC1[CH]C=CC=C1C</chem>	27.4	98.0
Meta	<chem>CCC1[CH]C(C)=CC=C1</chem>	28.1	99.7
Para	<chem>CCC1[CH]C=C(C)C=C1</chem>	28.3	98.2

Substituted	CCC1(C)[CH]C=CC=C1	28.3	95.4
-------------	--------------------	------	------

Toluene + Benzyl Radical

Ortho	CC1=CC=C[CH]C1Cc1ccccc1	58.9	115.5
Meta	CC1[CH]C(C=CC=1)Cc1ccccc1	59.6	118.8
Para	CC1C=CC([CH]C=1)Cc1ccccc1	59.3	117.0
Substituted	CC1([CH]C=CC=C1)Cc1ccccc1	60.1	113.3

Toluene + 1-Phenyl-1-Ethyl Radical

Ortho	CC1=CC=C[CH]C1C(C)c1ccccc1	53.2	121.5
Meta	CC1[CH]C(C=CC=1)C(C)c1ccccc1	53.4	130.3
Para	CC1C=CC([CH]C=1)C(C)c1ccccc1	53.0	126.5
Substituted	CC(c1ccccc1)C1(C)[CH]C=CC=C1	53.8	119.1

Toluene + C₂H₅ + H Stable

Ortho	CCC1CC=CC=C1C	4.9	96.5
Ortho	CCC1C=CC=CC1C	5.6	97.2
Ortho	CCC1C=CCC=C1C	5.0	98.5
Meta	CCC1CC(C)=CC=C1	5.5	97.4
Meta	CCC1C=C(C)C=CC1	7.2	97.5
Meta	CCC1C=C(C)CC=C1	5.5	97.4
Para	CCC1CC=C(C)C=C1	5.6	98.1
Para	CCC1C=CC(C)C=C1	7.4	96.7
Substituted	CCC1(C)CC=CC=C1	6.3	96.1
Substituted	CCC1(C)C=CCC=C1	5.8	94.7

Toluene + CH₃ + H Stable

Ortho	CC1=CC=CCC1C	10.5	88.7
Ortho	CC1C=CC=CC1C	9.7	88.8
Ortho	CC1=CCC=CC1C	10.3	89.4
Meta	CC1=CC(C)CC=C1	9.8	88.3
Meta	CC1CC(C)C=CC=1	12.8	89.7
Meta	CC1=CC(C)C=CC1	11.1	89.4
Para	CC1C=CC(C)CC=1	10.4	89.0
Para	CC1C=CC(C)C=C1	12.8	87.6
Substituted	CC1(C)CC=CC=C1	11.0	87.0
Substituted	CC1(C)C=CCC=C1	11.3	86.6

Toluene + H + H Stable			
Ortho/Meta	CC1=CC=CCC1	17.6	80.5
Ortho/Meta	CC1=CCC=CC1	17.0	80.3
Ortho/Sub	CC1C=CC=CC1	17.3	81.1
Meta/Para	CC1C=CCCC=1	19.3	79.6
Para/Sub	CC1C=CCC=C1	19.7	80.4

4.3.3. Derived Thermochemistry Group Values for Intermolecular Addition Products

The calculated thermochemistry values in Table 14 were compared to the previous RMG's estimates in Figure 25 which uses a group additivity estimation method outlined by Benson [53], and further refined by Lay et al. [55] for radical species; some of these groups used include aromatic C-H, aromatic C-C, and primary C-C, etc. In this comparison, the Gibbs free energy deviation between RMG's estimate and this work's calculations differ by 5.3 kcal/mol on average, with a standard deviation of 4.5 kcal/mol at 298K.

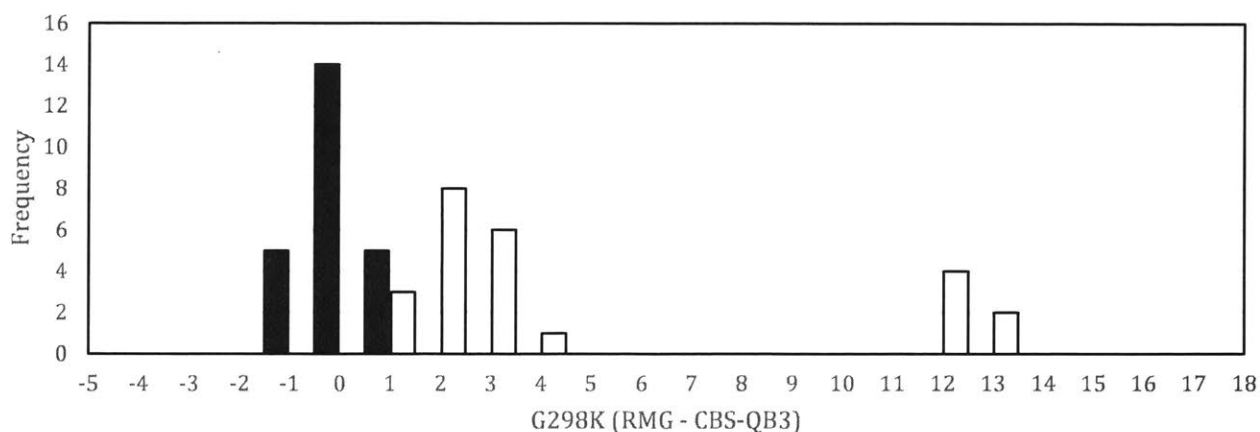
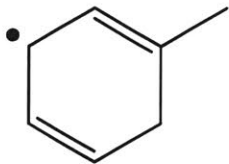
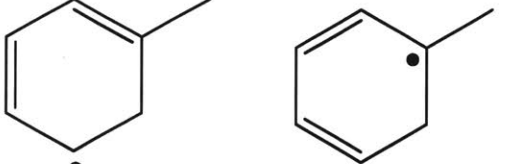
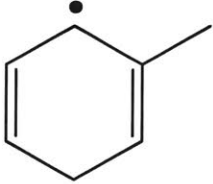
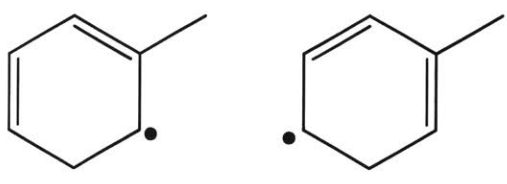
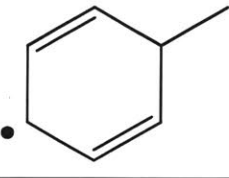
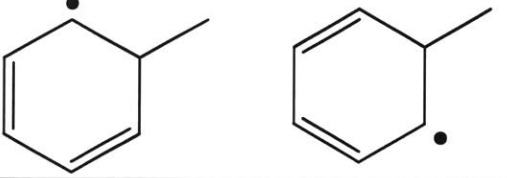
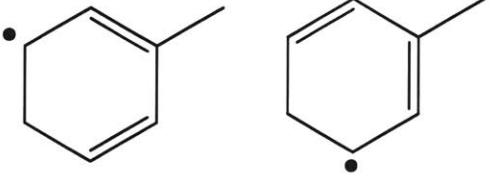
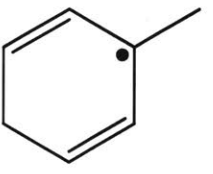


Figure 25 Distribution of Gibbs free energy deviation (kcal/mol) for 24 calculated aromatic intermolecular addition products. Distribution for RMG estimates previously (white) and after adding the aromatic pi radical group (black) are shown.

Figure 25 suggests that there is a systematic error in RMG's group additivity estimate, where RMG overestimates the single Gibbs free energy when compared to CBS-QB3 calculation, by a range of 1 to 14 kcal/mol, a significant difference that could yield dramatically different product distributions in kinetic models [19].

This work identifies that all estimations with a Gibbs free energy deviation > 10 kcal/mol from Figure 1 belong to products of aromatic intermolecular addition to the para position. This origin of the large discrepancy is due to RMG's thermochemistry estimation algorithm, which uses the lowest energy resonance structure as a molecule's thermochemistry. In the cases of addition to the ortho, meta, and substituted position, RMG identifies that the lowest energy resonance structures corresponds to the radical group that describes "secondary radicals between two pi bonds". However, for addition to the para position, RMG incorrectly identified the lowest energy resonance structure as corresponding to the radical group that describes "secondary allyl radicals". RMG mistakenly identified the resonance structure containing a tertiary radical between two pi bonds as a tertiary alkyl radical without any resonance stabilization for the para addition product. The geometries described in this discussion can be found referenced in Table 15.

Table 15 Various resonance structures estimated by RMG for Toluene + H products and how RMG classified them due to the lack of specify in radical groups. On the top, products of addition in the ortho, meta, and substituted position all feature the “bisallylic radical between pi bonds” as the lowest energy resonance structure. On the bottom, the product of Toluene + H in the para position, RMG identifies this radical as either a “secondary allyl radical” or “tertiary alkyl radical” depending on the resonance structure, and therefore mispredicts the energy of this species by a greater deviation.

Addition Site	Low Energy Resonance Structures (Secondary Radical Between Pi Bonds)	High Energy Resonance Structures (Classified as Allyl Radicals)
Ortho		
Meta		
Substituted		
	<p align="center">“Low Energy” Resonance Structures (Classified as Allyl Radicals)</p>	<p align="center">“High Energy” Resonance Structure (Misidentified as Tertiary Alkyl Radical)</p>
Para		

The thermochemistry estimation outlined in Table 15 identifies a twofold problem. First, this example highlights that the same species will lead to different outcomes of energy estimation when presented in different resonance structures where the radical is placed differently. A proper thermochemistry estimation across these different resonance structures should not result in a significant energy difference (they are really the same species). Second, the radical classification scheme used by RMG was not sufficiently specific towards the aromatic pi radical that is of particular interest in aromatic intermolecular addition reactions. While the “secondary radical between two pi bonds” group successfully captures the resonance stabilization with the two pi

bond system, the group value was derived not from a cyclic molecule; but from aliphatics where changes in the rotors has a large effect on entropy, and the near aromatic behavior isn't captured accurately either. The secondary allyl radical and tertiary alkyl radical descriptions are even further from reality, causing RMG to make poor estimations of the thermochemistry of aromatic pi radicals in the past.

In response to the large Gibbs free energy deviations, a new aromatic pi radical hydrogen bond increment (HBI) group [55] was developed using the methodology outlined in the methods section, where 19 out of 24 thermochemistry calculations made in this work are used as training data. In this work, only one new radical group (named the aromatic pi radical in Table 16) was derived. The error of estimation for the test set (5 out of 24 species, mutually exclusive from the training set) was decreased from 6.9 kcal/mol using old estimates to 0.7 kcal/mol using the updated aromatic pi radical. The enthalpy and entropy correction of this group is compared to other radical groups that were previously used to describe these species in Table 16.

Table 16 Comparison of enthalpy and entropy for the hydrogen bond increments for the aromatic pi radical (this work), secondary radical between two pi bonds, secondary allyl radical, and tertiary alkyl radical³⁴

	Enthalpy 298K (kcal/mol)	Entropy 298K (cal/mol K)
Aromatic Pi Radical	75.3	1.6
Secondary radical between two pi bonds	76.0	-4.1
Secondary Allyl radical	85.6	-3.8
Tertiary alkyl radical	96.5	5.2

In addition to the numerical group value, the substructure corresponding to this group must be defined. We require the hydrocarbon parent of aromatic pi radicals to contain a 1,3-cyclohexadiene or 1,4-cyclohexadiene structure, both of which will receive an identical hydrogen bond increment correction. The H removed to form the radical must be on a tetrahedral carbon adjacent to at least one double bonded carbon, and the carbon must be member of the cyclohexadiene ring. Additionally, tertiary aromatic pi radicals are treated identically to secondary aromatic pi radicals.

The performance of the updated group values can be observed in Figure 25, where the Gibbs free energy deviation is centered much closer to zero, with an average of 0.5 kcal/mol and a standard deviation of 0.6 kcal/mol.

Since the heat of formation of aromatic intermolecular additions are only slightly negative, the reverse of these reactions are fast, and aromatic pi radicals have a short lifetime as a result. These reactions are important if the radical has other fast decomposition pathways; for example, $\text{H} + \text{Toluene} \rightarrow \text{Aromatic Pi radical} \rightarrow \text{CH}_3 + \text{Benzene}$. Note that if there is no other fast decomposition channel, the aromatic intermolecular addition reaction will rapidly equilibrate. In this case, the addition reactions are important if the concentration of aromatics are high enough, at sufficiently low temperatures that the equilibrium constant is large, such that the product $K_c^*[\text{aromatics}] > 1$, since in that case a large fraction of the radicals in the system will be aromatic pi radicals.

4.3.4. Future work for thermochemistry estimations in intermolecular addition

While the developed HBI values in this work are developed with sufficient depth for RMG to estimate the thermochemistry of species that may arise in alkylaromatic pyrolysis systems, the degree to which these group values can be extrapolated to other unknown aromatic pi radicals is also not well understood, and other methods of thermochemistry estimation should be considered.

One of the other methods developed in this group by Li et al. [59] employs the use of machine learning to allow for the machine to identify characteristics that users might not be able to easily identify. One of the drawbacks of this machine learning method cited by the authors is the lack of fundamental understanding of the criteria used to estimate the various aspects of thermochemistry in their molecules of interest. Contrary to this machine learning approach, group additivity estimations allow for the user to clearly view the contributions of each of the different groups that led to the thermochemistry estimation of a molecule. This work indicates that users of RMG and other chemical models should be wary of the shortcomings of both estimation methods when estimating the thermochemistry of unknown compounds, and consider other necessary alternatives based on these shortcomings.

4.3.5. Kinetics of Intermolecular Addition

The rate coefficients for 21 of the 24 reactions outlined in Table 13 were calculated at the CBS-QB3 level of theory (Table 17). Transition state geometries can be found in the supporting information of Lai and Green [77].

Table 17 Modified Arrhenius rate parameters and rate at 723K for aromatic intermolecular addition reactions in CBS-QB3 level of theory.

Species	A (cm ³ /mole-s)	N	Ea (kcal/mol)	Rate at 723K (cm ³ /mol-s)
Toluene + H•				
Ortho	1.0x10 ⁹	1.4	4.5	1.3x10 ¹³
Meta	1.1x10 ⁹	1.4	5.4	1.3x10 ¹³
Para	1.1x10 ⁹	1.4	5.4	1.3x10 ¹³
Substituted	2.2x10 ⁸	1.6	6.4	6.7x10 ¹²
Hexylbenzene + H•				
Substituted	8.8x10 ⁷	1.7	6.1	6.7x10 ¹²
Toluene + •CH₃				
Ortho	6.8x10 ³	2.3	9.0	2.7x10 ¹⁰
Meta	6.7x10 ³	2.3	9.8	3.0x10 ¹⁰
Para	4.0x10 ³	2.3	9.9	1.6x10 ¹⁰
Substituted	1.4x10 ²	2.6	10.4	5.3x10 ⁹
Toluene + •C₂H₅				
Ortho	1.0x10 ³	2.6	7.7	3.5x10 ¹⁰
Meta	1.8x10 ³	2.6	8.3	4.4x10 ¹⁰
Para	5.7x10 ²	2.7	9.2	2.1x10 ¹⁰
Substituted	2.2x10 ¹	3.0	9.0	7.7x10 ⁹
Toluene + Benzyl Radical				
Ortho	7.5x10 ¹	2.9	11.3	1.2x10 ¹⁰
Meta	3.3x10 ²	2.8	12.5	3.6x10 ¹⁰
Para	2.0x10 ²	2.8	12.4	1.8x10 ¹⁰
Substituted	3.0 x10 ⁰	3.2	11.9	5.1x10 ⁹
Toluene + 1-Phenyl-1-ethyl Radical				
Ortho	1.0x10 ¹	3.1	11.4	5.2x10 ⁹
Meta	6.4x10 ⁰	3.2	11.3	9.7x10 ⁹
Para	3.8x10 ⁰	3.2	11.4	4.8x10 ⁹
Substituted	2.9x10 ⁻²	3.7	12.1	9.2x10 ⁸

RMG's training reaction algorithm allows extrapolation of known reaction rate coefficients to analogous reaction types; the objective of this work is to therefore appropriately populate RMG's training reaction database to allow for the accurate extrapolation of reaction rates to the many

possibilities of aromatic intermolecular addition in our systems of interest; more details on how RMG utilizes training reactions can be found in Gao et al. [16]. This section outlines the trends that were observed across our calculations to assess if the training reactions are appropriately populated to improve future estimates.

Figure 26 compares the Evans-Polanyi relationship (activation energy vs enthalpy of reaction) of the aromatic intermolecular addition reactions in Table 17 to aliphatic intermolecular additions, the latter of which had kinetics and thermochemistry approximated using RMG for additions to propylene, by the radicals H, CH₃, C₂H₅, Benzyl, and 1-phenyl-1-ethyl. It could be seen in this figure that the Evans-Polanyi relationship between the two classes of radical addition are extremely different. The slope of the Evans-Polanyi plot for aromatic intermolecular addition reactions is much steeper than usual, making us suspect it is not reliable, e.g. it is possible that aromatic + H reactions are so different from the other reactions they should be isolated on a different curve. The differences of aromatic intermolecular addition reactions from its aliphatic counterpart exemplifies the need for the calculation of training reactions to improve the accuracy of estimates in this reaction class' kinetics.

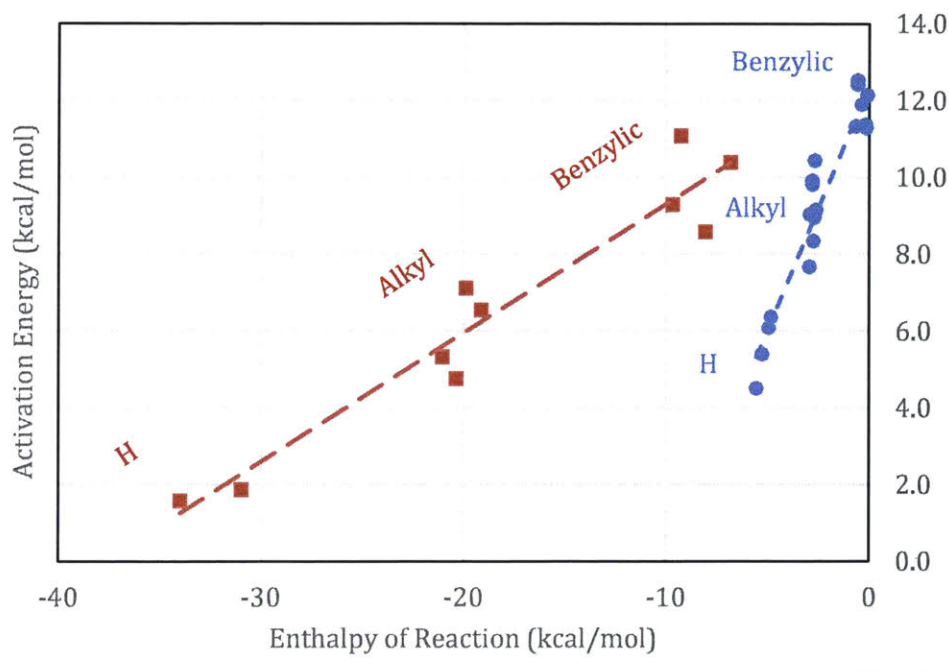


Figure 26 Evans-Polanyi relationship for aromatic intermolecular addition reactions calculated by CBS-QB3 (blue circles) and aliphatic intermolecular addition reactions approximated by RMG using propylene + radical (red squares). It can be observed that the two classes of reactions exhibit very different Evans Polanyi relationships.

4.3.5.1. Comparison with Previous RMG estimates

Figure 27 shows the RMG estimated rate coefficients and CBS-QB3 calculated rate coefficients for toluene + five different types of radicals (averaged among four addition positions ortho/meta/para/substituted). At our temperature of interest (723K), RMG overestimates the rate coefficient by 2-4 orders of magnitude, depending on the type of radical added.

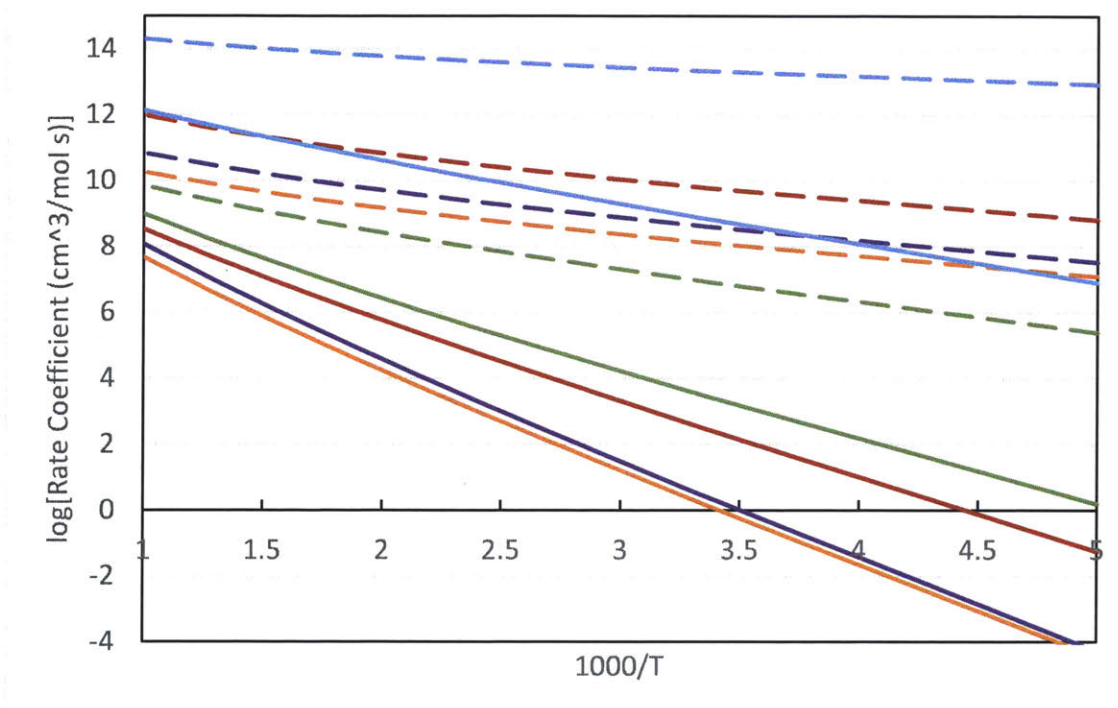


Figure 27 RMG estimated rate coefficients (dashed) and CBS-QB3 calculated rate coefficients (solid) for 1. Toluene + H (Blue), 2. Toluene + CH₃ (Red), 3. Toluene + C₂H₅ (Green), 4. Toluene + Benzyl (Purple), and 5. Toluene + 1-phenyl-1-ethyl (Orange). Rate coefficients for each class of reaction are averaged between four different addition sites. It can be observed that RMG's rate estimates are much faster than CBS-QB3 calculations because of RMG's questionable source.

The original source of these RMG's estimates come from CBS-QB3 calculations using 1,3,5-hexatriene or 3-methyl-1,3,5-hexatriene as model compounds. Due to the lack of an aromatic

structure of the model compound, the effects of losing aromaticity are not properly captured. The previous RMG estimates have an activation energy between 0.4 – 8.5 kcal/mol based on the site of addition and radical species used, whereas the CBS-QB3 calculations have an activation energy between 6.4 – 16.1 kcal/mol, highlighting the importance of capturing loss of aromaticity in aromatic intermolecular addition.

4.3.5.2. Effects of alkyl chain on aromatic species

Figure 28 shows the rate coefficients of toluene + H and hexylbenzene + H in the substituted position calculated using CBS-QB3. The calculated rates for the two reactions differ by no more than factor of 1.5 across all temperatures shown.

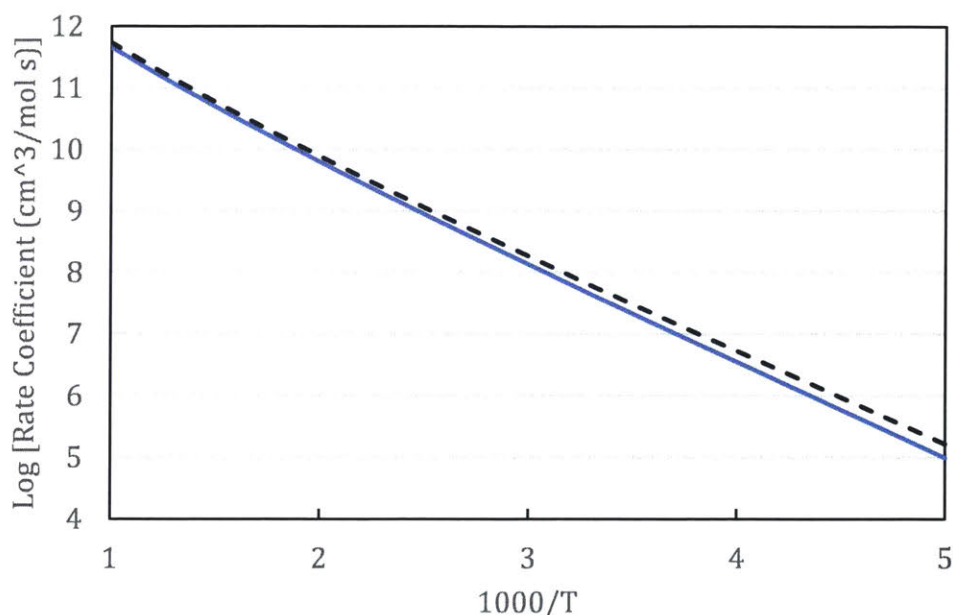


Figure 28 CBS-QB3 calculated rate coefficients for toluene + H (Blue Solid) and hexylbenzene + H (Black dashed) in the substituted position. Rate coefficients for two reactions differ by no more than factor of 1.5 across all temperatures shown.

This suggests that the length of the side chain does not affect the rate coefficient significantly. In the interest of conserving computational resources, training reactions for the aromatic intermolecular addition of other radicals to longer chain alkylaromatics (such as hexylbenzene) were not constructed.

4.3.5.3. Dependence of rate to the radical structure

The effects of radical added is displayed in Figure 29; rates are averaged among the four different sites of addition. This figure outlines the general trend that larger more stable radical groups tend to result in slower rate coefficients.

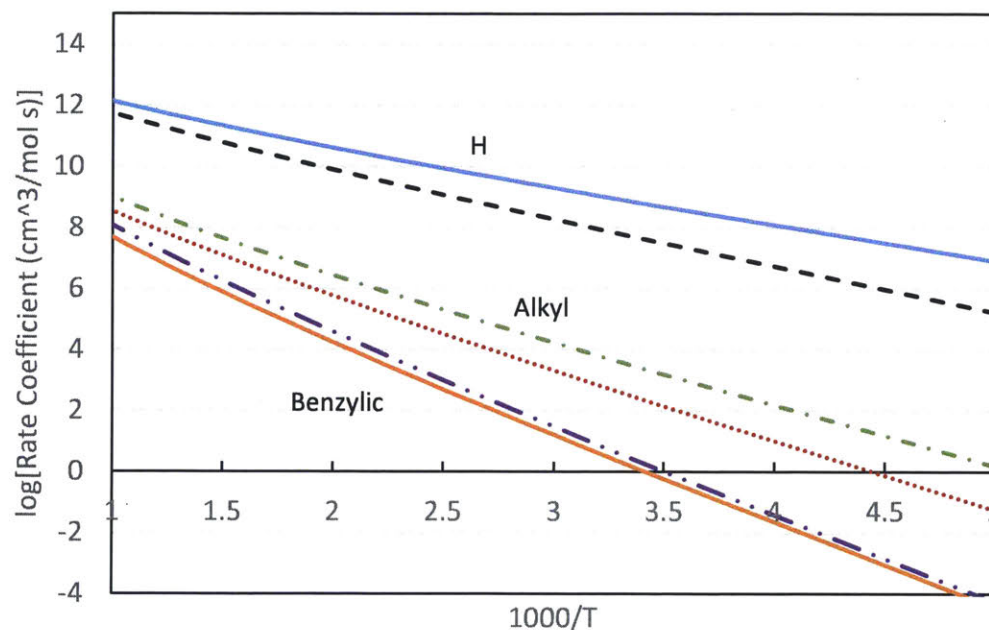


Figure 29 Rate coefficients for 1. Toluene + H (**Blue Solid**), 2. Hexylbenzene + H (**Black Dashed**), 3. Toluene + CH₃ (**Red Dotted**), 4. Toluene + C₂H₅ (**Green Dash Dotted**), 5. Toluene + Benzyl (**Purple Dash Double Dotted**), and 6. Toluene + 1-phenyl-1-ethyl radical (**Orange Solid**). Rate coefficients for each class of reaction are averaged between four different addition sites. The calculated rate coefficient is slower for the addition of larger radical species.

The activation energy increases with the size of radical added from ~7 kcal/mol (+H) to ~15 kcal/mol (+Benzyl/+1-phenyl-1-ethyl). This is likely due to the relative stabilities of these radicals; due to high stability of benzyl radicals (through resonance stabilization), the energy difference between the reactants and the transition state of aromatic intermolecular addition reactions are much higher, and thus, create a larger activation barrier for radicals to be added to the aromatic ring.

All the reactions listed in Figure 29 were added as training reactions in the RMG database, since the addition of different radicals can yield a 6 order of magnitude difference in rate coefficient (between H radical and 1-phenyl-1-ethyl radical).

4.3.5.4. Effects of addition position

Figure 30 shows the effect of the different positions of addition in toluene + H. Addition to the ortho, meta and para positions have comparable rate coefficients, and addition to the substituted position has the slowest rate, which is an order of magnitude slower than addition to the other positions.

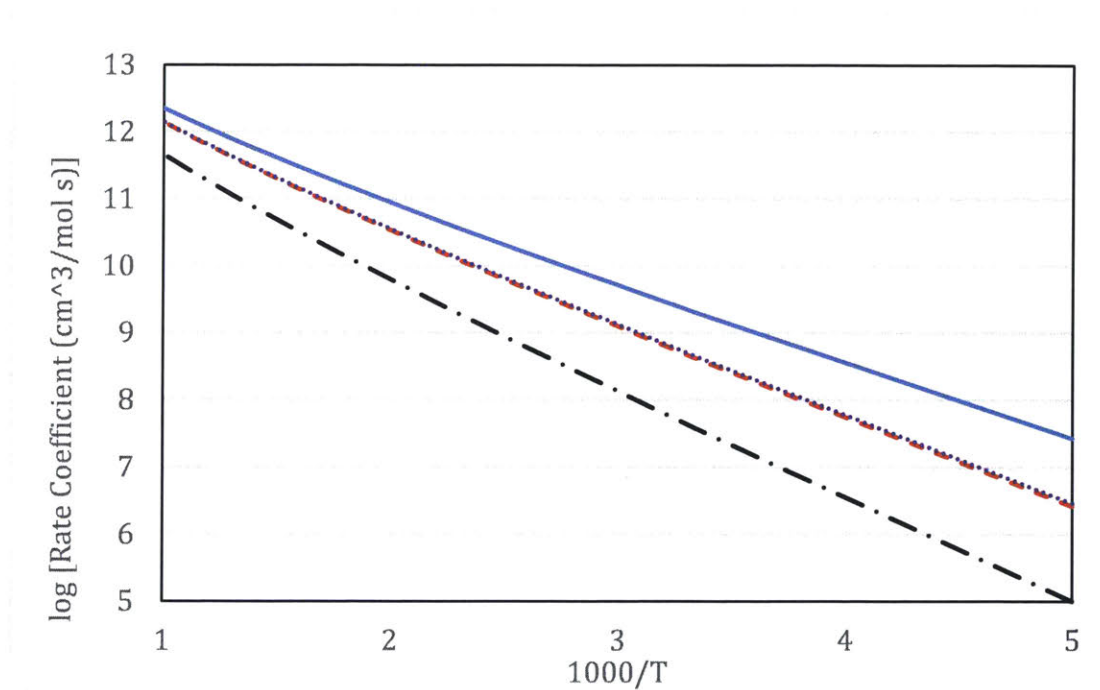


Figure 30. Rate coefficients for 1. Toluene + H (Ortho) (Blue Solid), 2. Toluene + H (Meta) (Red Dashed), 3. Toluene + H (Para) (Purple dotted), and 4. Toluene + H (Substituted) (Black Dash Dotted). Differences in the rate coefficients up to an order of magnitude can be observed.

This work finds that these trends also apply to the addition of larger radical groups. We surmise that the steric effects from adding to the substituted position contribute towards the energy of the transition state, making addition to the substituted position more difficult by 1.1-2.0 kcal/mol. In

the interest of appropriately populating RMG's training reaction database, reaction groups were further designed for different addition positions due to the potential for difference in kinetics.

4.3.6. Summary to rate coefficients of Aromatic Intermolecular Addition

This work finds that the previous RMG estimates for aromatic intermolecular addition rate coefficients to be highly overestimated compared to CBS-QB3 calculations done in this work, reason being the inappropriate use of 1,3,5-hexatriene and 3-methyl-1,3,5-hexatriene as a model compound to estimate these reactions, which does not account for effects resulting from breaking the aromatic structure. Other patterns observed in the kinetic rates of aromatic intermolecular addition are: (1) length of the alkyl side chain does not significantly affect rate, (2) increase in stability of radical reactant leads to a slower rate, and (3) addition to the substituted position is slower than addition to the three other positions. RMG's training reaction database was appropriately populated based on these trends to ensure maximum accuracy in rate estimates in the future for aromatic intermolecular addition reactions.

4.4. Conclusions

This work investigates the thermochemistry and kinetics of intermolecular addition, grounded by CBS-QB3 calculations. Aromatic intermolecular addition (and its reverse) is a class of reactions that could carry significant relevance in the reactivity of aromatics at moderate temperatures (~450°C) [19]. Upon investigating the thermochemistry of the products of this class of reactions, it can be found that Benson et al.'s group additivity and Lay et al.'s hydrogen bond increment corrections implemented in the RMG software package are insufficient for estimating the thermochemistry of this class of species. As a result, a new radical correction is derived through CBS-QB3 calculations, and the resulting group value will be instrumental to estimating the thermochemistry of aromatic pi radicals. Previous rate estimates for these reactions made using RMG are far from the true values, due to the software making analogies with wrong model species. Detailed rate calculations are used in this work to better understand the characteristics of this class of reactions. The newly calculated thermochemistry and rate coefficients added to RMG's database are expected to significantly improve the accuracy of future rate estimations.

5. Chapter 5

Formation of 2-Ring Aromatics in Hexylbenzene Pyrolysis

This work is closely related to the article by Lai, Pang, and Green, "Formation of 2-Ring Aromatics in Hexylbenzene Pyrolysis" [101]. The GCxGC-qMS calibration was performed by Hao-Wei Pang, and quantification of GC peaks in this work depended on her efforts.

Chapter Abstract

The formation of 2-ring aromatics in hexylbenzene pyrolysis is used in this work as a model system to better understand the coking behavior of crude oil upgrading processes. In this work, batch reactor experiments were done at 55 bar and 450 °C to study the pyrolysis of hexylbenzene utilizing GCxGC-qMS as an analysis tool. This work finds many different classes of aromatic species with > 1 aromatic ring, including bridged 2-ring aromatics, non-fully aromatized fused 2-ring aromatics, fully aromatized fused 2-ring aromatics, as well as > 2 ring species. A new detailed kinetic model is constructed using Reaction Mechanism Generator (RMG) using thermodynamic and kinetic parameters calculated at the CBS-QB3 quantum chemistry method for relevant 2-ring aromatic compounds. The results of the generated model were compared to batch reactor experiments; this work finds agreement between model results and experiments within a factor of 2 for many compounds, and the formation pathways of previously not well understood species were proposed based on evidence of intermediates found in this work's experiments and model.

5.1. Introduction

According to the 2018 World Oil Outlook, oil is forecasted to remain the largest contributor to the energy mix up to 2040, with a share of 28%. Oil demand is projected to grow at ~0.6 million barrels per day each year from 2020 to 2025 [1]. This increasing demand in oil will eventually

deplete lighter oil sources, and increase the demand for heavy oils, containing higher amounts of heavy hydrocarbons and heteroatoms [3]. To utilize heavy oils, upgrading processes are necessary to convert high molecular weight components in crude oil to low molecular weight species and reduce heteroatom content [4] to facilitate better combustion [5], to meet environmental and regulatory standards [3], to be compatible with modern combustion engines [102], and to produce high value chemicals for the chemical process industry [103].

Carbon rejection is a common process strategy to convert large hydrocarbons to lighter species, a process which has the tendency to produce coke as an undesirable side product [104]. To fundamentally understand the chemistry of coke formation, this work uses hexylbenzene and its formation of two ring aromatics in pyrolysis as a model system to imitate the behavior of the conversion of alkylaromatics to coke in carbon rejection based crude oil upgrading processes.

Alkylaromatics such as hexylbenzene are major components in jet fuel, and are expected to pyrolyze rapidly in combustors. Polycyclic aromatics formed in this step are thought to contribute to particulate emissions. Previous studies on the pyrolysis of alkylaromatics include Mandal et al. [20], Leigh and Szwarc [21], Khorasheh and Gray [22]. These works report the final product composition resulting from pyrolysis, but do not contain much information on the fundamental chemical mechanisms. Works dedicated to elementary step chemistry of alkylaromatic pyrolysis include Chen and Froment [23], Savage and Klein [24], Freund and Olmstead [25], and Guerra et al. [15]; the chemical mechanism construction of these works are rule based, and possibly neglect important pathways that lead to 2-ring aromatics. However, Guerra et al. [15] presented clearly documented pathways for the formation of fused aromatics such as tetralin and indane.

This work builds on the foundation of previous works from this research group [18] [19] [44] [77], using similar experimental and modelling methodologies, building on previous thermochemistry and kinetic data. This work also features updated analytical chemistry utilizing a GCxGC-qMS to experimentally validate our chemical mechanism.

5.2. Experimental Methods

Methodology for the batch reactor, Chemkin simulations, Gaussian 03 calculations, and RMG-Arkane can be found in sections 2.2.1, 2.2.7, 2.2.8, and 2.2.9 respectively.

5.2.1. GCxGC-qMS/FID Method for Liquid Analysis

The organic phase liquid product from the experiments was analyzed using a GCxGC-qMS/FID (Base unit Agilent 7890, modified by Zoex Corporation ZX2 thermal modulator). The primary column of this instrument is an RXi-5HT column with dimensions of 30 m x 0.25 mm ID x 0.25 μ m film thickness; a secondary column was used for separation through polarity, and is a BPX-50 column with dimensions of 2 m x 0.15 mm ID x 0.25 μ m film thickness. The modulation section between the primary and secondary columns is made using Agilent Ultimate Plus Deactivated Fused Silica Tubing (Part number 160-2255-5) 1.5 m x 0.25 mm. The thermal modulation period for the liquid analysis was set to a time of 16 seconds. Species were quantified using a FID detector and identified using a quadrupole mass spec (Agilent 5975C). Volume under GCxGC peaks are quantified using the software GC-Image, developed by Zoex Corporation. The quantification and identification of products were based on response factors found through analysis of standards containing alkanes, alkenes, alkylbenzenes, and alkylnaphthalenes; for species where standards were not available, their response factors were interpolated based on existing standards and their number of carbons. 3-Chlorothiophene was used as an external standard to improve the accuracy of quantification.

5.2.2. Constructing Chemical Kinetics Simulations with RMG

The detailed algorithm of Reaction Mechanism Generator (RMG) has been discussed extensively in the literature [28] [29]. In short, the mechanism generation follows a flux-based algorithm to select important species and reactions that are important at the chosen reaction conditions, and omits reactions with much slower rates. Thermochemistry of species and rate coefficients of reactions are estimated using the RMG-database, which contains parameters from various sources of information, including experimental and calculated values from both the literature and the

Green Group. Some of the parameters are accurately known, in those cases the known values are used rather than the RMG estimates.

Previous works by this group [19], [77], [44] and [62] highlighted the sparseness of thermochemical and kinetic database for aromatic intramolecular and intermolecular reactions. As a result, the thermochemistry of 132 species and kinetics of 41 reactions directly relevant to this model compound study was calculated at the CBS-QB3 level of theory. Moreover, 27 thermochemical groups and 41 training reactions were developed to allow for extrapolation to estimate analogous unknowns, highly improving the chemical accuracy of the formation of 2-ring aromatics compared to the model generated in Lai et al. [19]. Analysis of the model led us to compute the thermochemistry and rate coefficients of an additional 11 species and 3 reactions.

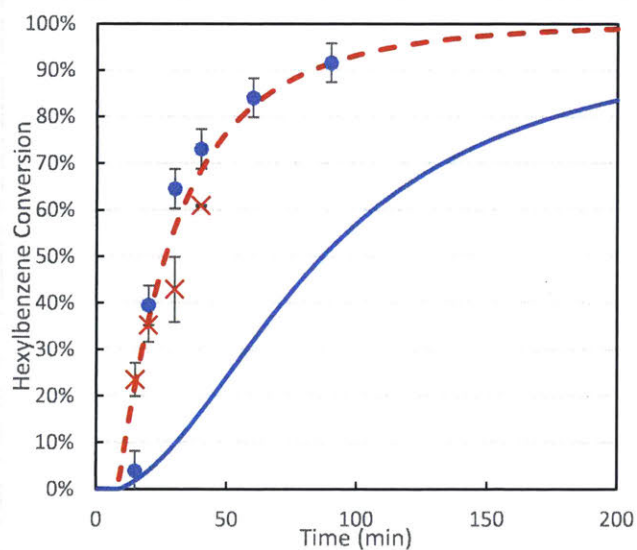
In addition, aromatic reactions are treated differently in the newest version of RMG compared to our previous work. This change eliminates all duplicate reactions that would take place if benzene bonds are treated as conjugated single/double bonds. The way RMG handles resonance forms was also updated recently [105]. These changes were made possible with addition of benzene bond-based training reactions outlined previously.

In this work, hexylbenzene was specified as an initial species with a mole fraction of 1, and 97 other species are specified in the input with a mole fraction of 0 to expedite the reaction discovery; this was found to be necessary due to the vast number of ways hexylbenzene and its intermediates may react. A copy of this work's RMG input file can be found in the supporting information of Lai et al. [101].

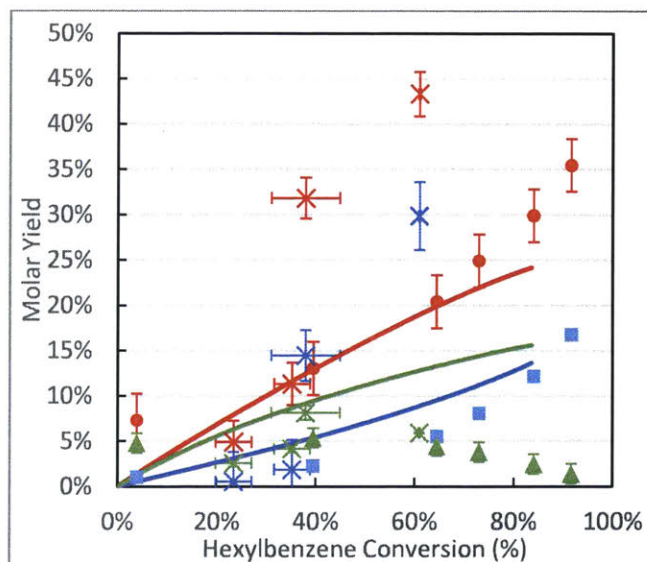
RMG is an active open-source software project, so its database is constantly being improved, and the software is also frequently updated; to exactly reproduce an RMG model one should use exactly the same version of the database and the software. GitHub version commit strings of RMG-Py and RMG-database used for the generation of the different versions of the mechanisms shown in this work can be found in the supporting information of Lai et al. [101].

5.3. Results and Discussion

Some of the experimental conditions of this work replicate our previous work [19]. Full experimental data are given in the supporting information of Lai et al. [101]. The measurements are similar but differ in important details because the GCxGC resolution is significantly better than the simple GC used previously [19]. Figure 31 highlights the resemblance of our current work to our previous work. Some differences were introduced due to the use of the GCxGC-qMMS as the method of quantification. Figure 31 shows that our previous work [19] tends to quantify major species at a higher concentration (lower conversion of hexylbenzene, higher molar yield of other species); this effect is more pronounced at later time points. This is due in part to the separation of species by GCxGC that were overlapped using one dimensional gas chromatography. In addition, this work uses a background correction algorithm by Reinchenbach et al. [106], which slightly alters peak sizes.



a)



b)

Figure 31 a) Experimental conversion of hexylbenzene for previous work [19] (red crosses), this work (blue circles) and model predicted conversion of hexylbenzene for previous work [19] (red dashed lines), this work (blue solid lines); b) molar yield of toluene (red), ethylbenzene (blue), and styrene (green) for previous work [19] (crosses) and this work (solid shapes). Reactor temperature of 450°C with 10 minutes heat up time. Reactor pressure 55 bar. Error bars represent standard deviation in replicated experiments.

This work's model contains 220 species and 3277 reactions (compared to 453 species and 3812 reactions in previous work [19]). This change reflects the removal of many invalid compounds in the previous model that were formed by poorly predicted pathways. The new model still contains many products of intermolecular addition between hexylbenzene and other radicals [77], but not as many as the old model. The full model is given in the supporting information of Lai et al. [101].

The conversion of hexylbenzene and molar yield predicted by our model is shown in Figure 31a; model prediction by this work shows a slower conversion than our previous work [19]. The predicted conversion time scale is about a factor of 3 slower in the new model. This is due to the discovery of many species by RMG that are intermolecular addition products; previous work shows that the rate rules of this class of reaction to be overestimated by RMG by 2-4 orders of magnitude [77]; with the update of the rate rules, the molar yield of products produced by radical addition to hexylbenzene greatly reduces, and in turn, decreases the conversion of hexylbenzene. In many free radical processes, the selectivity and conversion are somewhat decoupled: the selectivity (product yields vs conversion) is controlled by ratios of propagation rate coefficients, while the conversion (absolute overall reaction rate) is controlled primarily by the radical concentration, set by initiation and termination rate coefficients. Here we focus primarily on product selectivities, as a result we plot molar yields against conversion, shown e.g. in Figure 31b.

Figure 31b shows the model predicted molar yields for toluene, ethylbenzene, and styrene, the highest yield aromatic products of hexylbenzene pyrolysis. The model yields of toluene and ethylbenzene are found to match with experiments within 30%, whereas the model over-predicts the experimental yield of styrene by an order of magnitude at high conversions. The misprediction of styrene at high conversions can be attributed to styrene's propensity to react to form larger alkylaromatics in this work's experiments, such as to form the $C_{20}H_{26}$ species, but these styrene consumption pathways aren't well characterized by the model.

5.3.1. GCxGC Analysis of 2-ring aromatics

This work uses GCxGC-qMS/FID to identify and quantify the formation of 2-ring aromatics. Figure 32 shows the resulting chromatogram of hexylbenzene pyrolysis at 450°C, 55 bar, 40 minutes. Key species and groups of compounds have been labelled. In Figure 47, 134 peaks were identified. Of the 134 peaks, 67 were identified as known species in the MS library. The remaining peaks could only be identified by the C_xH_y formula based on the fragmented mass spectra and relative locations on the GCxGC. A complete list of the measured peaks and their assignments is given in the supporting information of Lai et al. [101].

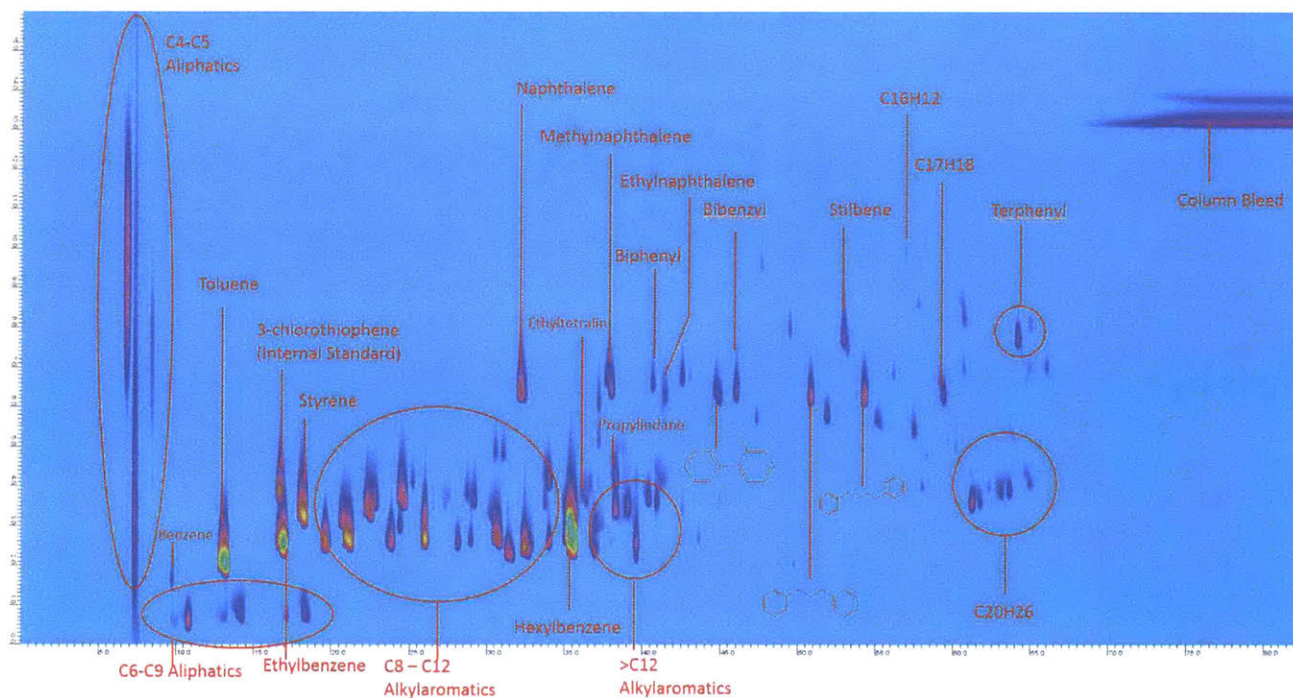


Figure 32 GCxGC chromatogram of products produced by hexylbenzene pyrolysis at 40 minutes, 450°C, and 55 bar. Key compounds and groups labelled.

Chromatograms for hexylbenzene pyrolysis at the same conditions for various different time points are shown in Figure 33 through Figure 38.

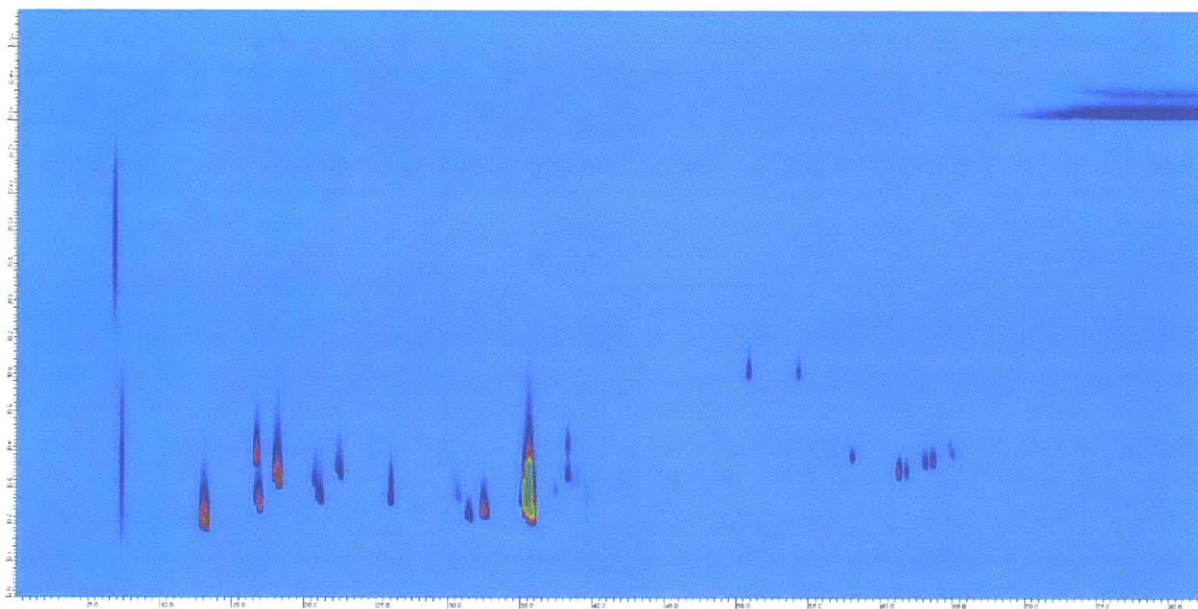


Figure 33 GCxGC chromatograms of hexylbenzene pyrolysis, 15 minutes, 450°C, and 55 bar.

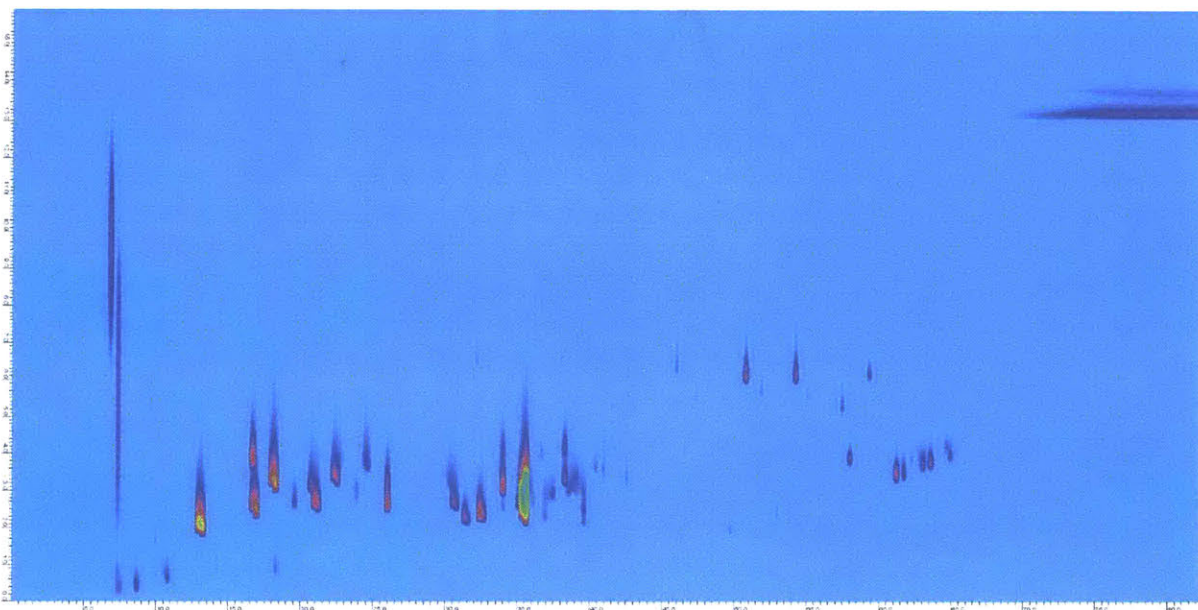


Figure 34 GCxGC chromatograms of hexylbenzene pyrolysis, 20 minutes, 450°C, and 55 bar.

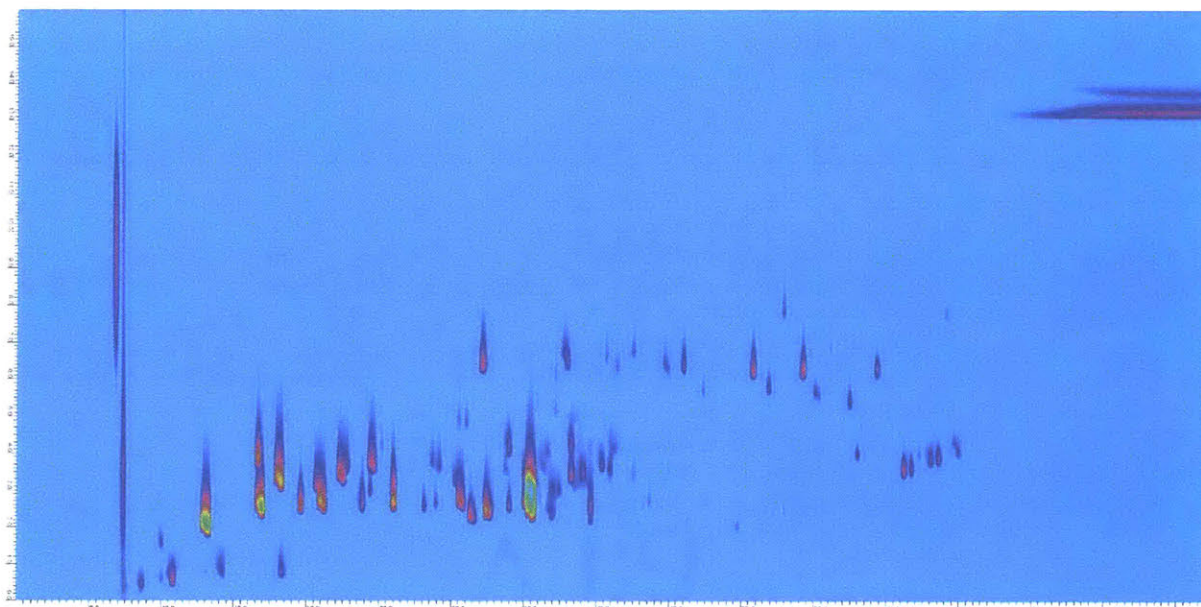


Figure 35 GCxGC chromatograms of hexylbenzene pyrolysis, 30 minutes, 450°C, and 55 bar.

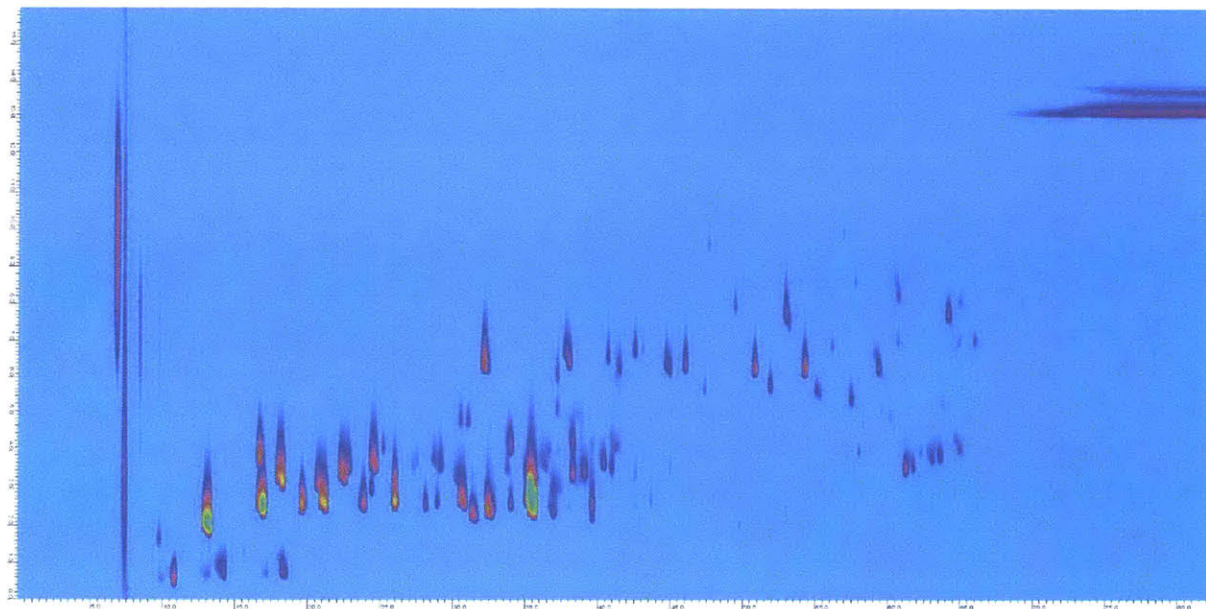


Figure 36 GCxGC chromatograms of hexylbenzene pyrolysis, 40 minutes, 450°C, and 55 bar.

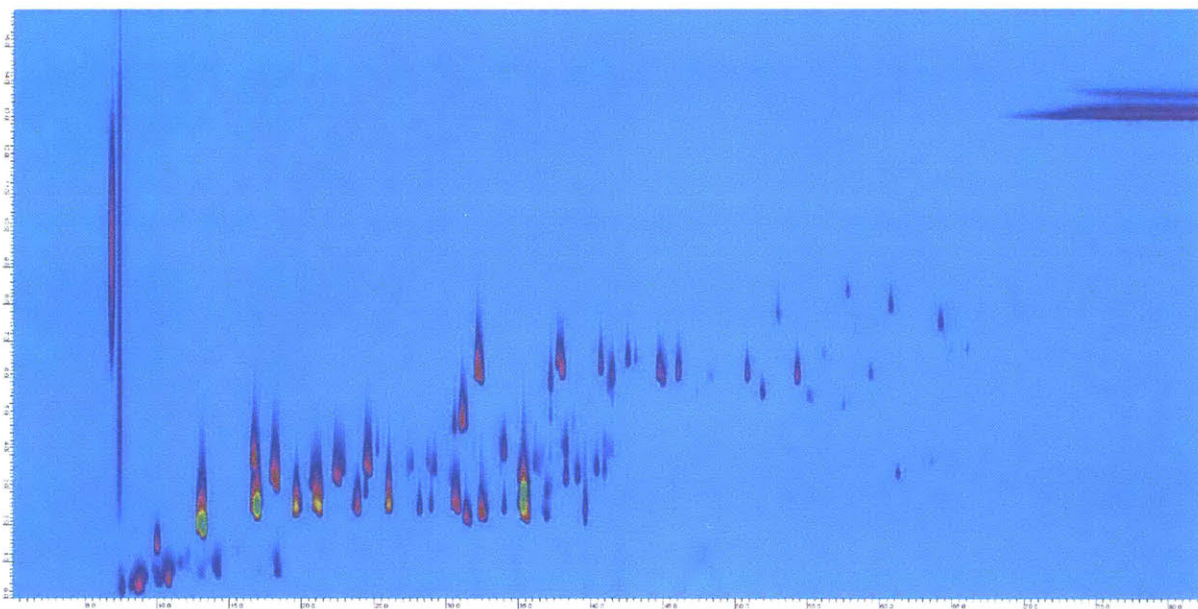


Figure 37 GCxGC chromatograms of hexylbenzene pyrolysis, 60 minutes, 450°C, and 55 bar.

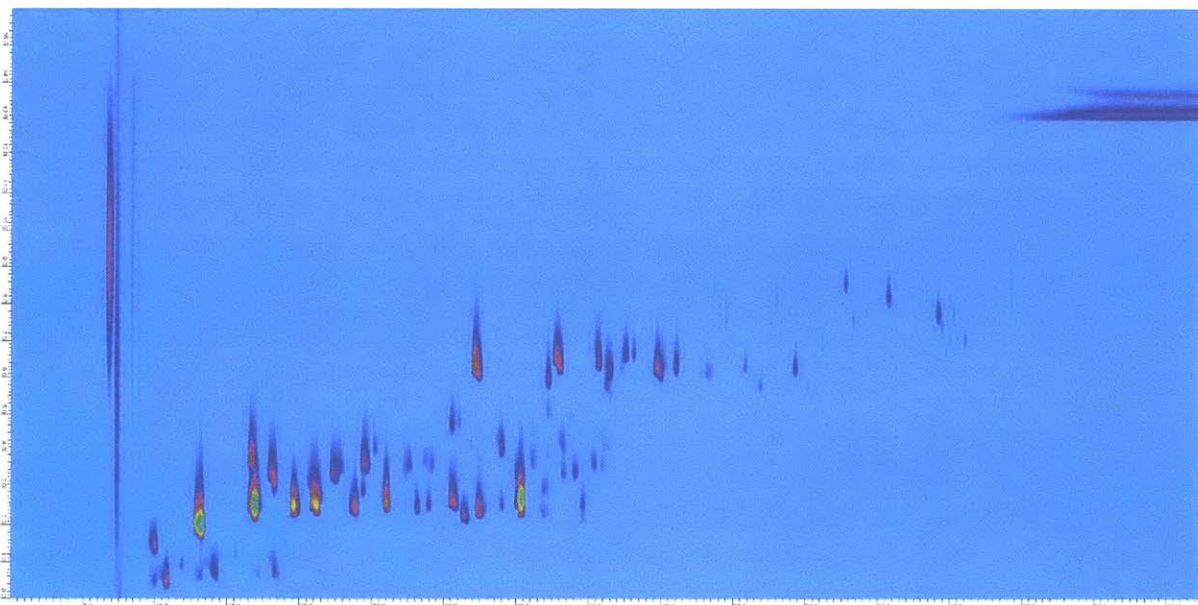


Figure 38 GCxGC chromatogram of hexylbenzene pyrolysis, 90 minutes, 450°C, and 55 bar.

This work finds many interesting classes of compounds that were not extensively studied previously [19]. The GCxGC-qMS enables the analysis of 2-ring products formed by this pyrolysis; observations are discussed below.

5.3.2. Bridged 2-Ring Aromatics

This work finds many bridged 2-ring aromatics, where the two rings are not fused. This class of species has an experimental total molar recovery of $\sim 1\%$, shown in Figure 39a, which is one quarter of the highest yield product (toluene). The most prominent products of this class are bibenzyl, 1,3-biphenylpropane, 1,4-biphenylbutane, and $C_{20}H_{26}$; experimental molar yields shown in Figure 39b.

Figure 39a shows the total molar yield of bridged 2-ring aromatics predicted by this work's model, which agrees with experimental work within a factor of 2. The individual yields of the bridged 2-ring aromatics are shown in Figure 39b. According to the model, bibenzyl is predicted to form by radical recombination of two benzyl radicals, whereas 1,3-biphenylpropane and 1,4-biphenylbutane are predicted to form by intermolecular addition to styrene (with benzyl and ethylbenzyl respectively), followed by hydrogen abstraction from hexylbenzene or other major species. It is interesting that bibenzyl forms through a different pathway than the other two aforementioned compounds, but the resulting concentrations in both the model and experiment are similar.

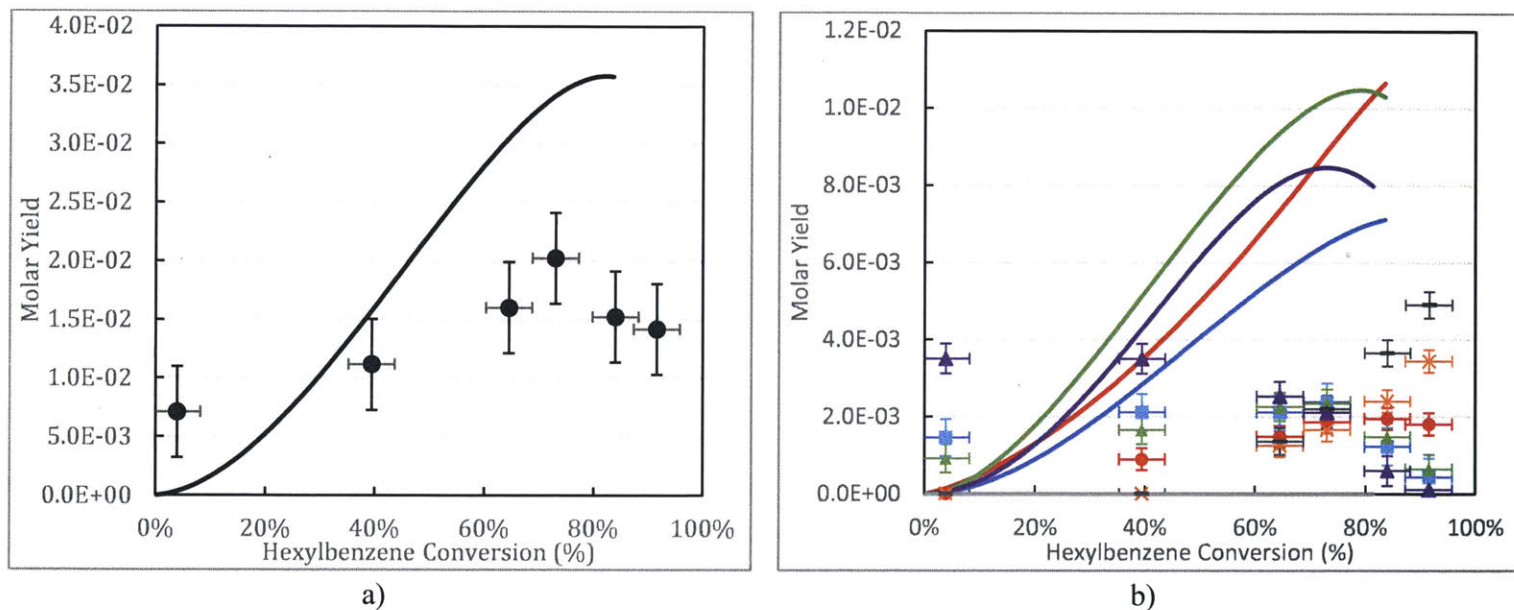


Figure 39 a) Experimental (circles) and model predicted (line) total molar yield of bridged 2-ring aromatics, b) experimental molar yield of bibenzyl (red circles), 1,3-biphenylpropane (blue squares), 1,4-biphenylbutane (green diamonds), biphenyl (orange crosses), sum of selectivities of $C_{20}H_{26}$ (purple triangles), and total alkyl biphenyl (grey dashes). Model predicted molar yield of

bibenzyl (red lines), 1,3-biphenylpropane (blue line), 1,4-biphenylbutane (green line), biphenyl (orange line), sum of molar yield of $C_{20}H_{26}$ (purple line), and sum of molar yield of alkylbiphenyl compounds (grey line). Batch reactor conditions of 450°C, and 55 bar.

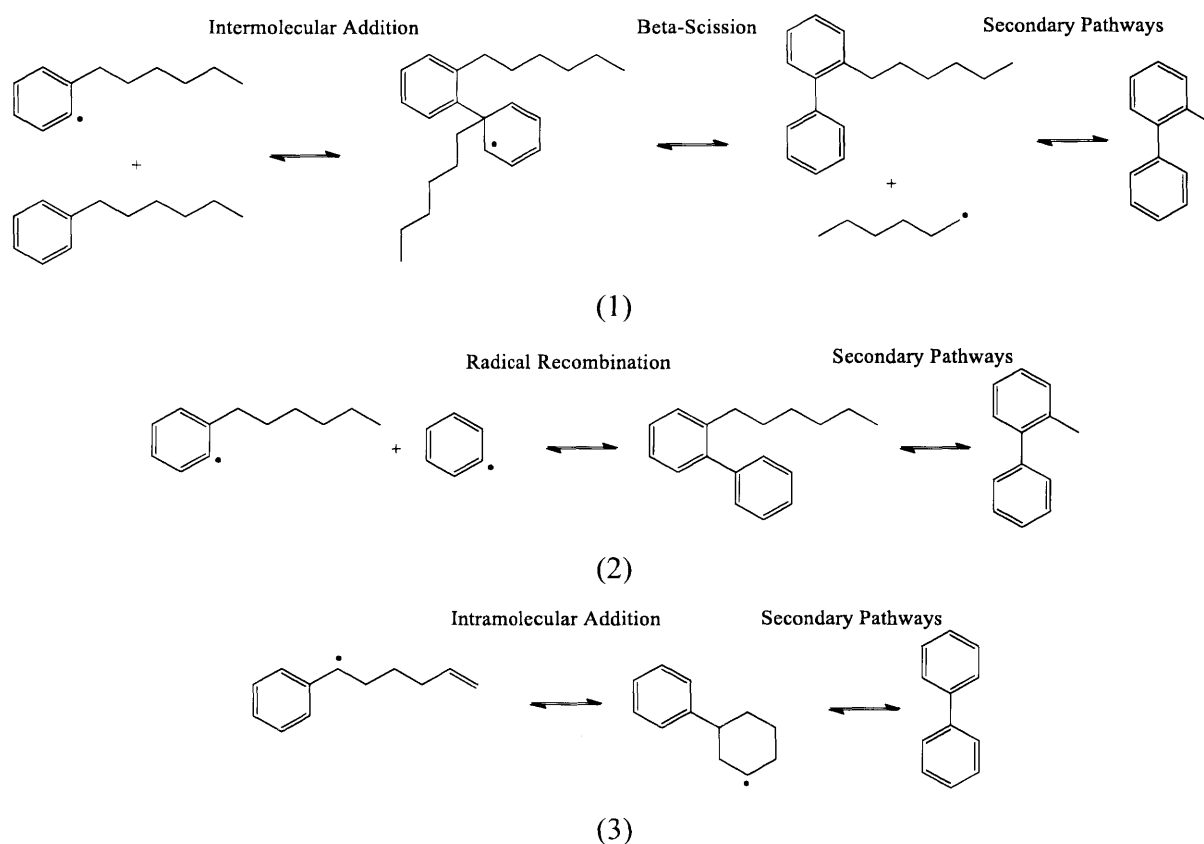
A notable group of products of this class have the formula $C_{20}H_{26}$. Products of this molecular weight are produced up to a significant experimental molar yield of 3.5×10^{-3} , and decreases to $< 6 \times 10^{-4}$ after 40 minutes of reaction time, shown in Figure 39b. This group of products show up very distinctly in the chromatogram (shown in Figure 32). Due to the extraordinarily high selectivity towards C_{20} specifically (almost no $C_{19}H_{24}$ or $C_{21}H_{28}$ products are formed), we infer that $C_{20}H_{26}$ species are formed by the addition of a hexylbenzene radical to styrene, as opposed to being products of radical recombination between hexylbenzene radical and ethylbenzene radicals. A radical recombination pathway would favor the formation of $C_{19}H_{24}$ over $C_{20}H_{26}$ due to the higher concentration of C_7H_8 radicals compared to C_8H_9 radicals (as produced by the model and suggested by the higher experimental concentration of toluene).

For the two $C_{20}H_{26}$ compounds seeded in our model (shown in Figure 40), the main flux towards these compounds is by addition of hexylbenzene radicals to styrene, followed by hydrogen abstraction. Figure 39b shows the model prediction of $C_{20}H_{26}$ species is in reasonable accord with experiment at low conversions, but greatly exceeds the molar yield found in experiments at high conversions. This is possibly because the model lacks pathways to consume the $C_{20}H_{26}$ species either by beta-scission of the long alkyl tail or by addition to form larger aromatics. These further reaction pathways will be of future interest.



Figure 40 The two $C_{20}H_{26}$ species seeded in the kinetic model.

One unexpected pair of bridged 2-ring aromatic compounds that formed were biphenyl and methylbiphenyl, at experimental molar yields from $\sim 1.0 \times 10^{-3}$, shown in Figure 39b, which is comparable in yield with bibenzyl. Possible biphenyl formation pathways include: (1) addition of phenyl radicals to aromatic bonds, followed by beta scission of an aliphatic radical, (2) radical recombination of two phenyl radicals, (3) cyclization of a phenylhexenyl radical, (4) Diels-Alder addition between styrene and 1,3-butadiene, or (5) intramolecular hydrogen abstraction [107] followed by phenyl radical addition to the second aromatic ring in bridged aromatics such as $C_{20}H_{26}$. Pathways are shown in Figure 41. Based on the concentrations of intermediates in our model and the high barrier to Diels Alder reactions, pathways (2) and (4) are unlikely. This work further studies pathway (1) due to the availability of information on its intermediates and the likelihood of this pathway; future work should be done to investigate other pathways.



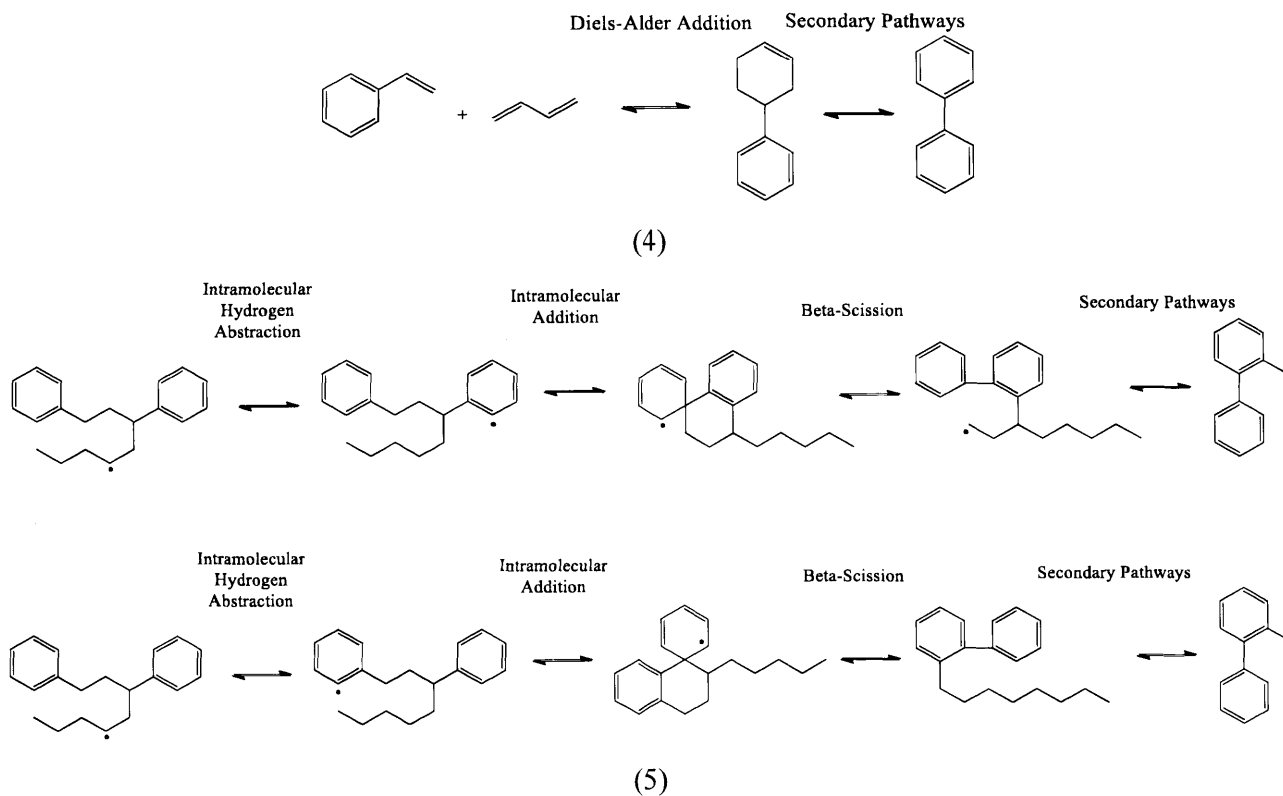


Figure 41 Proposed formation pathway for biphenyl compounds by (1) addition of phenyl radicals to aromatic bonds, followed by beta scission of an aliphatic radical, (2) radical recombination of two phenyl radicals, (3) cyclization of a phenylhexenyl radical, (4) Diels-Alder addition between styrene and 1,3-butadiene, or (5) intramolecular hydrogen abstraction followed by phenyl radical addition to the second aromatic ring in bridged aromatics

Biphenyl and hexylbiphenyl were seeded to form through the proposed pathway shown in Figure 41; despite RMG finding pathways (1) and (2) mentioned above, the predicted molar yields of these compounds are $<10^{-8}$, 5 orders of magnitude lower than experimental results. As a result, the thermochemistry and kinetics associated to this pathway for the phenyl + ethylbenzene system (shown in Figure 42) which were based on RMG estimates, were more accurately computed at CBS-QB3 level of theory. A summary of all thermochemistry and kinetic rates calculated with computed transition state geometries are summarized in the supporting information of [101].

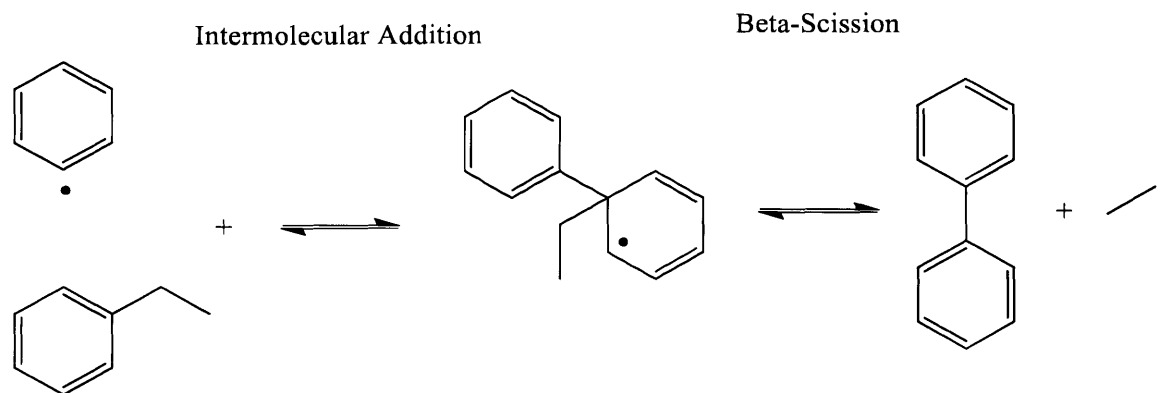


Figure 42 Phenyl + ethylbenzene pathway studied to model the behavior of biphenyl formation in hexylbenzene pyrolysis

Table 18 shows the thermochemistry of the five species shown in Figure 42 from RMG estimates, CBS-QB3 calculations, and the literature. Gibbs free energies calculated by CBS-QB3 match RMG estimates within 1 kcal/mol with the exception of the phenyl radical; however, the RMG estimate for phenyl radical matches the Active Thermochemical Tables [49] with entropy by the Computational Chemistry Comparison and Benchmark Data-Base [108]. The Gibbs free energy of biphenyl from both RMG estimate and CBS-QB3 calculation are 1 kcal/mol lower than literature sources.

Table 18 Thermochemistry of biphenyl, ethylbenzene, ethylbiphenyl, ethyl radical, and phenyl radical.

Species Name	Gibbs Free Energy (kcal/mol)		
	RMG Estimate (Group Additivity [53])	CBS-QB3 Calculation	Literature Source
Biphenyl	14.9	14.5	15.6 [37], 15.8 [109]
Ethylbenzene	-18.7	-18.9 [19]	-18.1 [37]
Ethylbiphenyl Radical	28.6	28.3	Not available
Ethyl Radical	10.8	11.4	10.4 [49] [108]
Phenyl Radical	60.1	62.8	59.8 [49] [108]

Figure 43 shows the rate coefficients of phenyl radical + ethylbenzene and beta scission of ethylbiphenyl radical; the rate rules of the phenyl addition step estimated by RMG is 2 orders of magnitude slower than the CBS-QB3 calculation, and the ethyl scission step is 1 order of magnitude faster than the CBS-QB3 calculation.

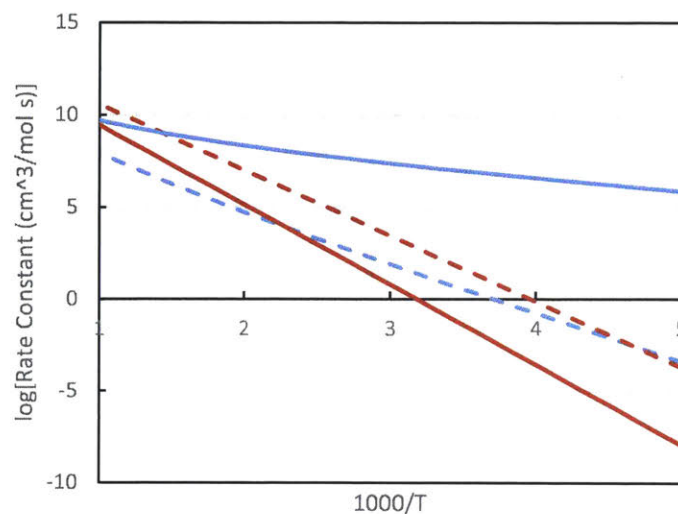


Figure 43 Rate coefficients of phenyl radical + ethylbenzene (in $\text{cm}^3/\text{mol}\cdot\text{s}$) (blue) and ethylbiphenyl radical beta scission (in s^{-1}) (red) estimated by RMG (dashed) and calculated by CBS-QB3 (solid)

Sensitivity analysis of biphenyl and hexylbiphenyl shows that the most sensitive reactions to these two species is the intermolecular phenyl addition steps leading to the radical intermediates (Figure 42).

Figure 44 shows a comparison of the experimental yield, model yield, and model yield with rate rule changes from Figure 43 for biphenyl and methylbiphenyl/hexylbiphenyl. It can be seen that while the updated rate rules increase the model predicted yield of the two species by more than two orders of magnitude, the updated model yield remains 3-4 orders of magnitude lower than our experimental results, suggesting the model is missing additional pathways leading to biphenyl compounds.

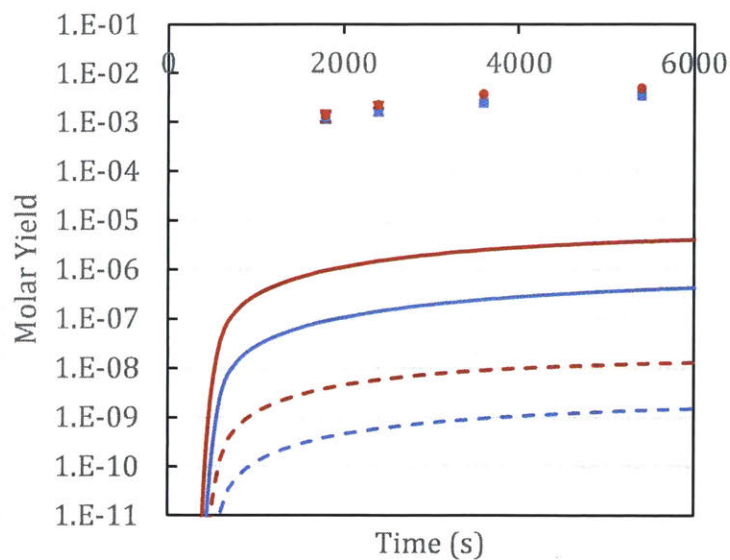


Figure 44 Molar yields of biphenyl (blue), methylbiphenyl/hexylbiphenyl (red). Experiments are represented in circles/squares, model yield in dashed lines, and model yield with updated kinetics from Figure 43 in solid lines.

5.3.3. Fused 2-Ring Species

From the GCxGC-FID data, the molar yield of fused aromatic 2-ring species in the experiments ranges from 0.0035 – 0.04, see Figure 45. The model predictions for total fused 2-ring species agree with experiments within 40%. However, the predicted individual product yields of each species are quite different from the experimental data, and the model omits several species which were observed experimentally (see Figure 46 and Figure 48).

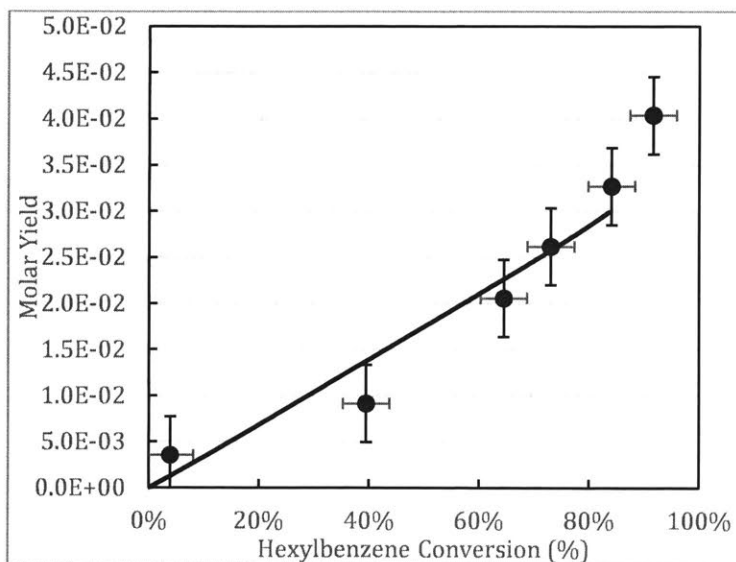


Figure 45 Total molar yield of all fused 2-ring aromatics (including non-fully and fully aromatic species) for experiments (circles) and model (line). Batch reactor conditions of 450°C, and 55 bar.

5.3.3.1. Non-fully Aromatic Fused 2-Ring Precursors

Non-fully aromatic fused 2-ring precursors propylindane and ethyltetralin were both formed experimentally; other experimentally observed fused 2-ring aromatic precursors are indane, methylindane, and tetralin. Indane and methylindane are produced at a lower experimental yield than propylindane at early conversions; this is due to the reactant requiring less steps to reach propylindane. Tetralin is produced at a comparable yield to ethyltetralin, possibly indicating the loss of the ethyl chain from ethyltetralin is a fast process. Figure 46 shows the experimental molar yield of indane, methylindane, propylindane, tetralin, and ethyl tetralin.

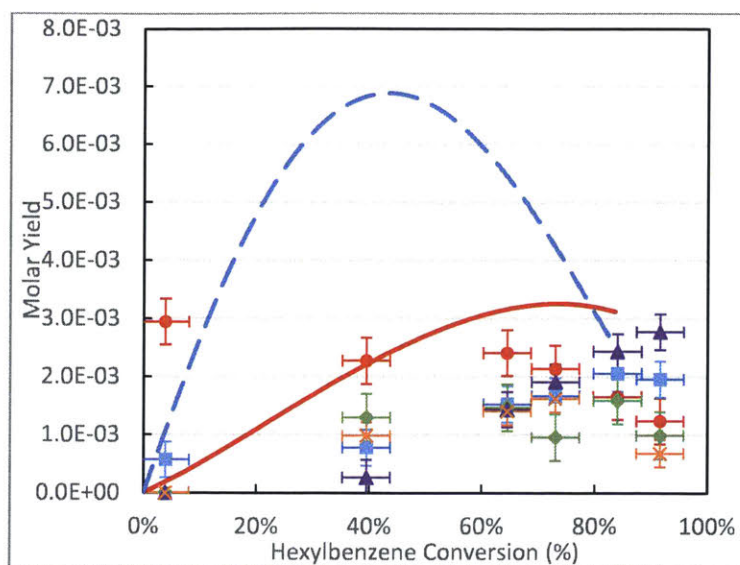


Figure 46. Experimental molar yield of propylindane (red circles), ethyltetralin (blue squares), indane (green diamonds), methylindane (purple triangles), and tetralin (orange crosses). Model predicted molar yields of indane (red solid line) and ethyltetralin (blue dashed line). Batch reactor conditions of 450°C, and 55 bar.

The model predictions of molar yield of non-fully aromatic fused 2-ring can be found Figure 46. Propylindane and ethyltetralin are the only fused 2-ring precursors that the model predicts to form. The model prediction for propylindane agrees very closely with experimental data at higher conversions, whereas the model prediction of ethyltetralin is an order of magnitude over-predicted by the model; since formation pathways of ethyltetralin were well studied in the past [44], the model and experimental mismatch of ethyltetralin indicates consumption pathways of ethyltetralin are not well represented in the model.

5.3.3.2. Fully Aromatized Fused 2-Ring Species

This work finds fully aromatized 2-ring species starting at 20 minutes (no fully aromatized 2-ring species are detected at 15 minutes); this class of species yields the highest concentration out of all 2-ring species, up to 2% experimental molar yield. Alklynaphthalenes, including naphthalene, methylnaphthalene, and ethylnaphthalene are formed.

This work finds the experimental molar yield of naphthalene to be highest out of the alkylnaphthalenes, followed by methylnaphthalene and ethylnaphthalene, shown in Figure 46; a likely formation pathway of naphthalene is shown in Figure 47. The formation path for methylnaphthalene is likely similar to the pathway for formation of toluene from ethylbenzene presented by Carr et al. [18]

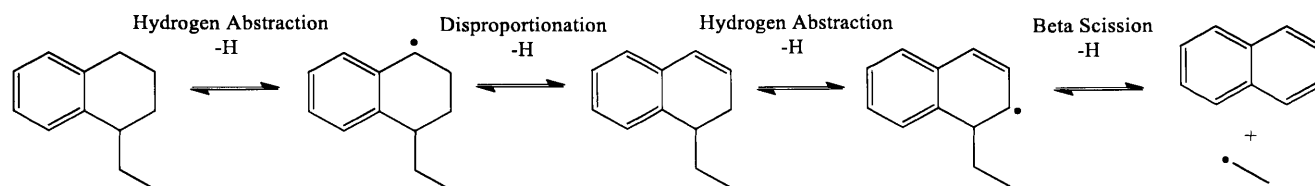


Figure 47 Most plausible formation pathway for naphthalene from ethyltetralin.

Ethyldihydronaphthalene and propylindene were not detected in this experiment. This can be due to (1) the mass spectral library not having data for both ethyldihydronaphthalene and propylindene [110], (2) the products of hexylbenzene pyrolysis contain many compounds in similar molecular weight range of these two compounds, which might overlap in the GCxGC, and (3) the conversion of dihydronaphthalenes to naphthalenes is fast, leaving the former with a low concentration.

Figure 48 shows the molar yield of the three alkylnaphthalenes and benzocycloheptatriene with respect to time.

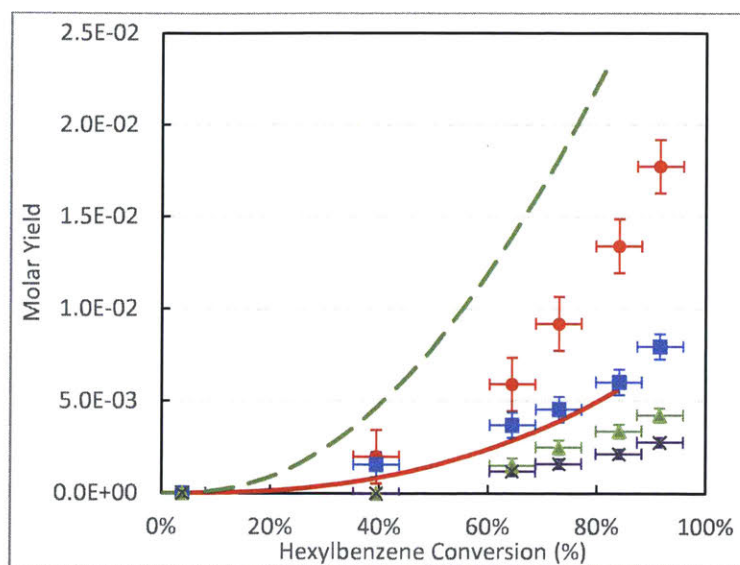


Figure 48 Experimental molar yield of naphthalene (red circles), methylnaphthalene (blue squares), ethylnaphthalene (green triangles), and benzocycloheptatriene (purple crosses). Model molar yield of naphthalene (red solid line) and ethylnaphthalene (green dashed line). Batch reactor conditions of 450°C, and 55 bar.

The model predictions of naphthalene and ethylnaphthalene agree with experiments fairly well (Figure 48). The molar yield of naphthalene is under-predicted, whereas the molar yield of ethylnaphthalene is significantly over-predicted; this suggests that conversion paths from ethylnaphthalene to naphthalene are not well represented in the RMG model, or the final beta-scission step shown in Figure 47 is not well understood. Methylnaphthalene was predicted to form at a molar yield of 10^{-10} ; it is very likely that the model is missing some of the pathways of conversion from ethylnaphthalene to naphthalene and methylnaphthalene.

The general performance of the model in predicting 2-ring aromatics is fairly good, considering that these are pure predictions, not calibrated to any experimental data. The model predicted molar yield of the two most expected species from intramolecular reaction pathways, propylindane and ethylnaphthalene, agree with experiments within an order of magnitude. The predicted total yield of fused 2-ring species closely matches the experiments. It is likely that recent thermochemistry corrections [44] allowed for a better prediction for the formation of fused 2-ring species.

Benzocycloheptatriene was also found to form at an appreciable concentration experimentally; this compound is likely formed through the 7 membered ring intramolecular addition using an alkylaromatic radical; Figure 49 shows one such pathway.

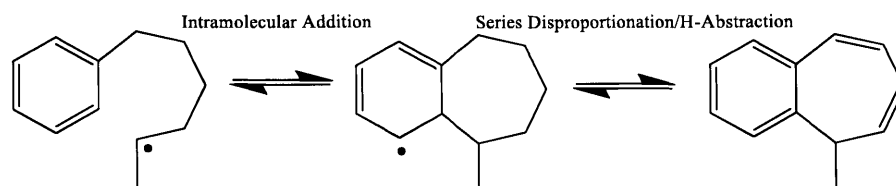
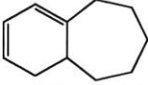
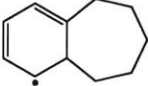
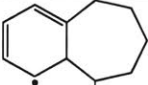
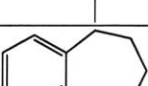
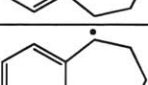
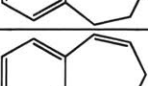
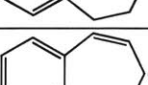
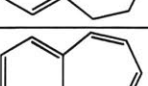


Figure 49 Proposed formation pathway of benzocycloheptatriene.

Benzocycloheptatriene was predicted to form at 10^{-6} molar yield, 3 orders of magnitude lower than its experimental yield. Due to the mismatch, CBS-QB3 calculations were performed to find the thermochemistry for 2-ring aromatic species with a 7-membered secondary ring (Table 19) and the rate coefficient (Figure 50) of the intramolecular addition step shown in Figure 49. Developed group values for thermochemistry can be found in Table 20. Full thermochemistry data including enthalpy, entropy, and heat capacity, uncertainties for group additivity values, and calculated transition state geometries can be found in the supporting information of Lai et al. [101].

Table 19 Thermochemistry of fused 2-ring species with seven membered secondary rings; including benzocycloheptene, benzocycloheptadiene, benzocycloheptatriene, and various radical species.

Species Structure	Gibbs Free Energy (kcal/mol)	
	RMG Estimate (Group Additivity [53])	CBS-QB3 Calculation
	-12.3	-19.6
	10.3	3.6
	1.1	-3.7
	-23.0	-26.9
	15.8	13.5
	2.4	1.1
	37.0	29.4
	36.2	24.6

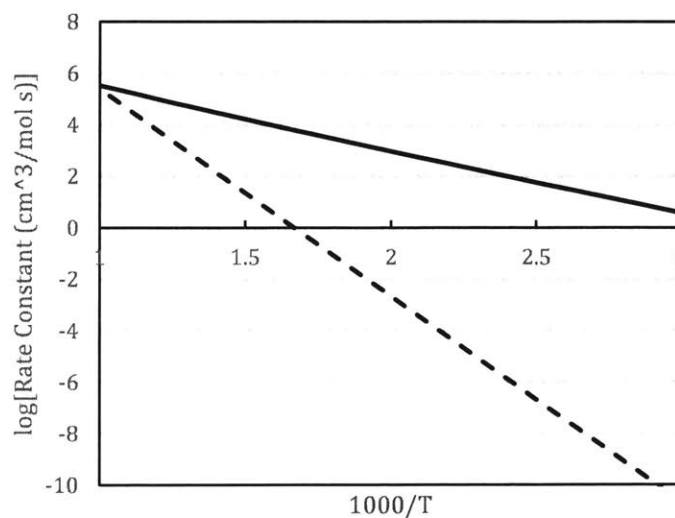


Figure 50 Rate coefficient of hexylbenzene intermolecular addition (1/s) to form methylbenzocycloheptene radical precursor (in shown in Figure 49) estimated by RMG (dashed) and calculated by CBS-QB3 (solid)

Table 20 Group Additivity Values Developed in chapter 5

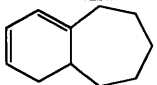
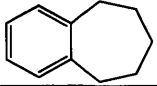
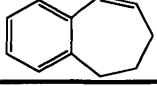
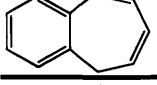
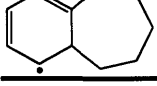
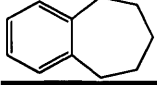
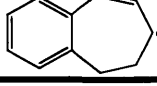
Group	H298 (kcal/mol)	S298 (cal/mol K)	C _p (cal/mol K)						
			300K	400K	500K	600K	800K	1000K	1500K
	6.9	41.1	-10.2	-10.3	-9.8	-8.3	-5.4	-3.1	-0.6
	0.8	14.2	-5.7	-5.3	-4.8	-3.9	-2.0	-0.4	1.7
	3.0	17.5	-5.2	-5.0	-4.6	-3.8	-2.1	-0.7	0.8
	2.0	28.8	-4.1	-4.5	-4.7	-4.2	-3.1	-2.0	-1.6
	92.1	4.7	-1.4	-1.6	-1.9	-2.2	-2.7	-3.3	-4.5
	76.4	0.5	0.1	-0.4	-1.0	-1.6	-2.5	-3.3	-4.6
	80.7	1.0	-0.3	-0.5	-1.0	-1.5	-2.5	-3.3	-4.5

Table 19 shows a stark difference between group additivity estimates and the new CBS-QB3 calculations. This is due to RMG lacking training data for 2-ring aromatic species with seven membered secondary ring structures. RMG's estimates use Han et al.'s algorithm [57], utilizing features of single rings such as cyclohexadiene, benzene, cycloheptane, cycloheptene, etc. as opposed to characterizing the polycyclic ring structures as a feature. As a result, the differences between RMG's estimates and CBS-QB3 calculations were up to 12 kcal/mol in Gibbs free energy.

Similarly, due to lack of training data, the rate estimates of RMG for the intramolecular addition of hexylbenzene to form a seven membered secondary ring is 2 orders of magnitude slower than the CBS-QB3 calculated rate coefficient at 723K.

Updated thermochemistry of methylbenzocycloheptene and its radical precursor, as well as the rate parameters for the intramolecular addition of hexylbenzene radical to form this precursor

was updated in the CHEMKIN input to preview the effect of the CBS-QB3 calculations' effects on the yield of benzocycloheptatriene. Figure 51 shows the effects of the updated parameters.

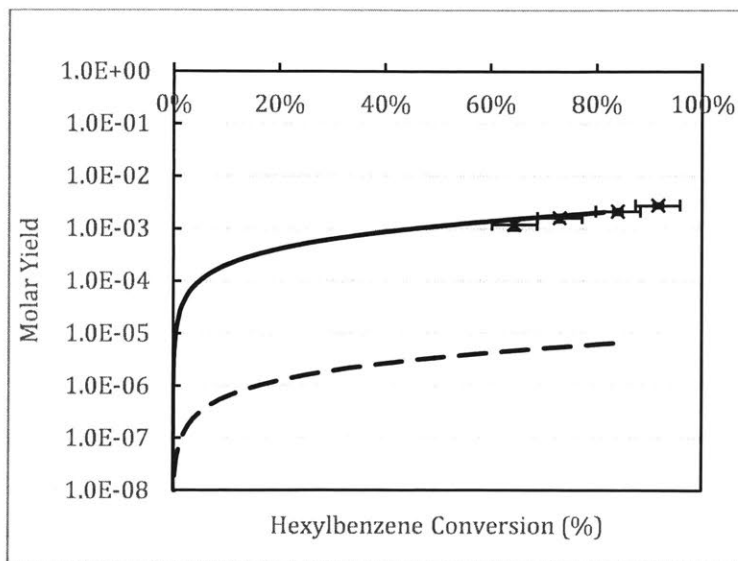


Figure 51 Experimental molar yield of benzocycloheptatriene (crosses). Model predicted molar yields of methylbenzocycloheptene using RMG estimates (dashed), and using CBS-QB3 calculations (solid).

The molar yield of methylbenzocycloheptene, a likely precursor of benzocycloheptatriene, increased by 2.5 orders of magnitude due to the changes in thermochemistry and kinetics related to its formation. The model used here does not include reactions which convert methylbenzocycloheptene to benzocycloheptatriene.

5.3.4. Species Beyond 2 Rings

Compounds that contain more than 2 rings were observed starting at a reaction time of 30 minutes. The total molar yield of compounds with more than 2 rings is $< 8 \times 10^{-3}$, an order of magnitude lower than bridged and fused two ring compounds.

Only a few > 2 ring compounds can be conclusively identified using the MS, but many can be identified as >2 ring species based on the retention time in the polar column of the GCxGC and the carbon to hydrogen ratio detected by the mass spec. Some that can be identified with high confidence include methylfluorene, phenylnaphthalene, terphenyl, and methylterphenyl. Among

these known species, terphenyl has the highest molar yield, at $\sim 1.3 \times 10^{-3}$. The molar yields of these compounds and the total molar yield of > 2 ring compounds are shown in Figure 52.

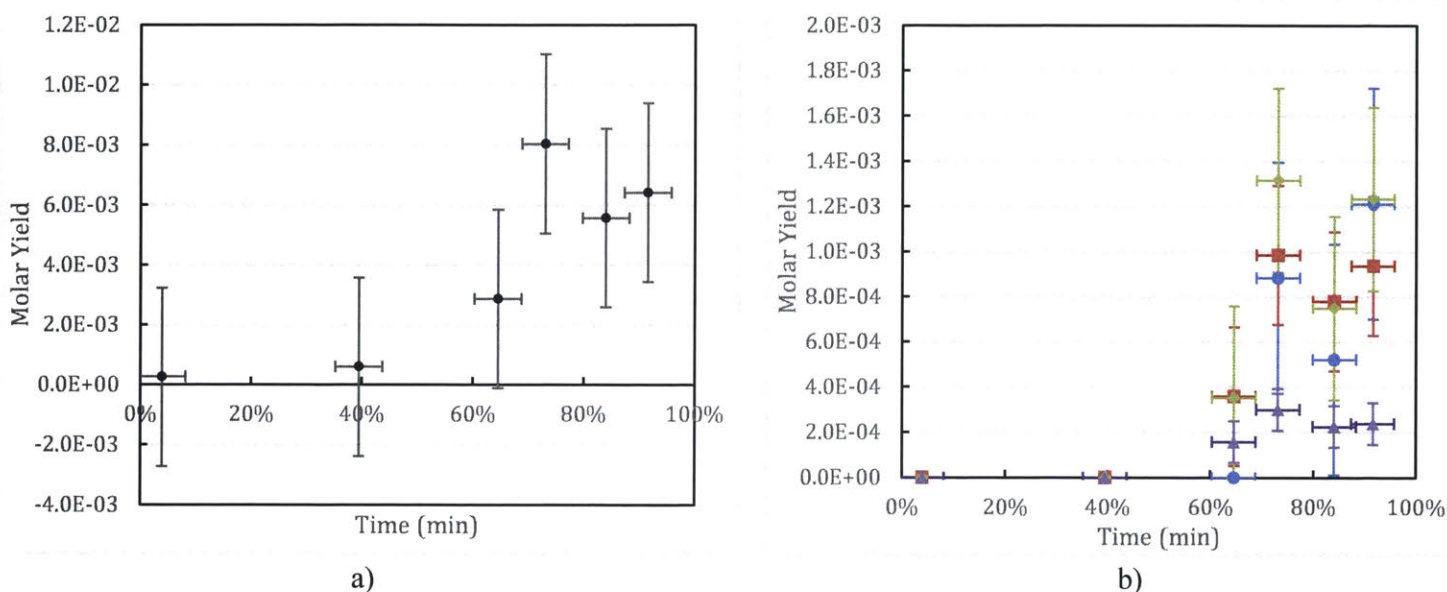
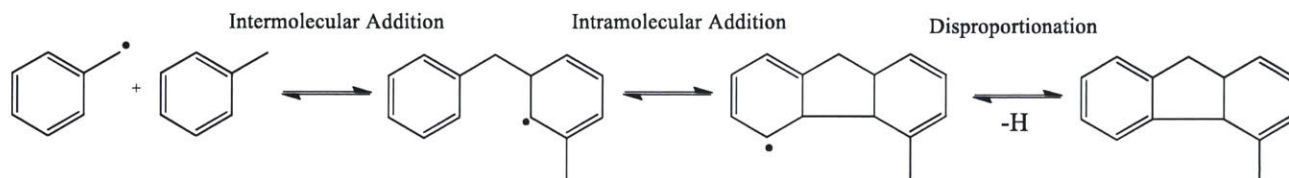


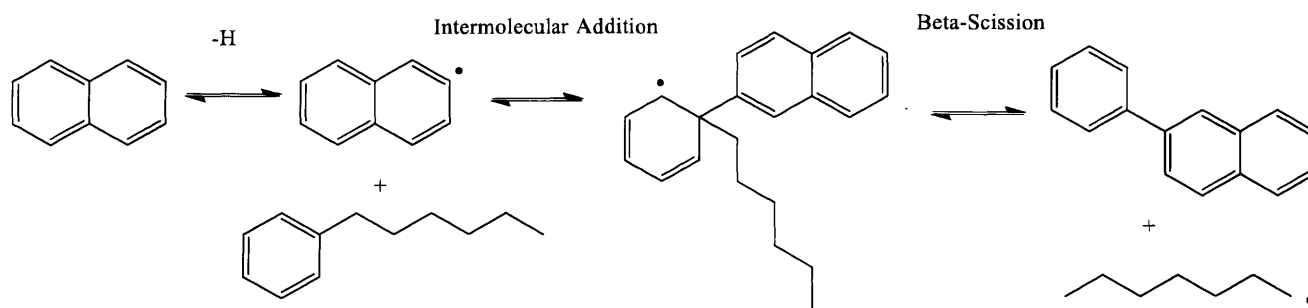
Figure 52 a) Total molar yield of > 2 ring species, and b) molar yield of methylfluorene (blue circles), phenylnaphthalene (red squares), terphenyl (green diamonds), methylterphenyl (purple triangles). Batch reactor conditions of 450°C, and 55 bar.

The formation pathways for these compounds are hypothesized in Figure 53. All pathways utilize reactants that are found in this experiment or are otherwise predicted to form by this work's model. All of these pathways involve aromatic intermolecular addition pathways, which was previously studied in [77]. Currently RMG does not predict these formation pathways due to computational difficulty in processing the vast number of edge species in our work's model.

Methylfluorene



Phenylnaphthalene



Terphenyl/Methylterphenyl

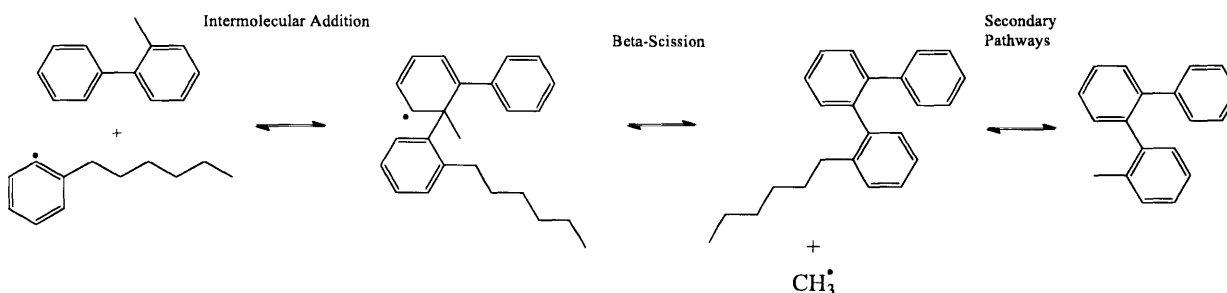


Figure 53 Proposed formation pathways for methylfluorene, phenylanthracene, and terphenyl/methylterphenyl in this work's batch reactor conditions.

5.3.5. Hexylbenzene Isomers

In this work, all species found with a molecular weight of 162 g/mol and are in the vicinity of the hexylbenzene peak are characterized as hexylbenzene isomers; the total molar yield of these species is ~1-2%, exact numbers plotted in Figure 54. We are unable to characterize the exact hexylbenzene isomer due to the lack of data of hexylbenzene isomers in the NIST Mass Spectral Library [110]. It is plausible to conclude that the formation of these compounds is due to the phenyl migration pathways studied by Khanniche et al [62].

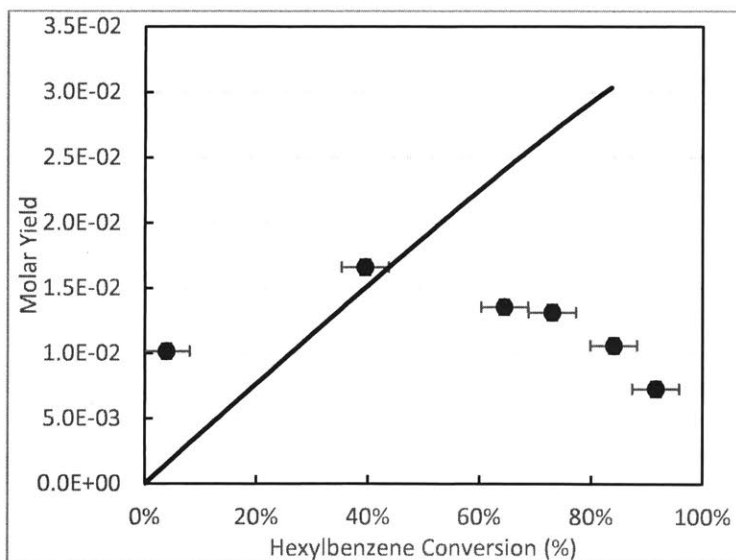


Figure 54 Total molar yield of hexylbenzene isomers (excluding n-hexylbenzene) measured by experiments (circles) and predicted by model (line). Batch reactor conditions of 450°C, and 55 bar. Exact identity of hexylbenzene isomers unknown due to lack of reference data.

Figure 54 shows the model predictions for hexylbenzene isomers formed through the phenyl migration pathway referenced in Lai [44] and Khanniche [62]. The model prediction for hexylbenzene isomers monotonically increases, whereas in experiments, hexylbenzene isomers peak at 40% conversion. This discrepancy is due to the lack of consumption pathways for hexylbenzene isomers in the model.

5.4. Conclusions

Hexylbenzene pyrolysis experiments were performed at 55 bar and 450 °C, analyzed by GCxGC-qMS with FID. Results were consistent with previous work [19] within factor of 2-3. Many aromatic species were resolved and identified by GCxGC-qMS, including bridged 2-ring aromatics, fused 2-ring aromatics, partially-aromatic fused ring species, species with >2 rings, and several isomers of hexylbenzene. The possible formation paths of newly identified products were discussed. The updated model for hexylbenzene pyrolysis includes improved thermochemistry and kinetics estimates from recent quantum chemical calculations [77] [44] [62]. The resulting model has 220 species and 3277 reactions. Many model predictions match experimental results

within an order of magnitude. Some of the model-data discrepancies were discussed in detail. In particular, the biphenyl formation pathway was studied in great detail, and results indicate that there are formation pathways leading to biphenyl and methyl biphenyl that this work does not expect.

6. Chapter 6

Recommendations

This chapter first summarizes the previous chapter conclusions, and makes recommendations for future researchers should they want to further pursue this work. Standard operating procedures (SOPs) used for this work are referenced in Appendix B so that the developed methods can be reused for future work. Troubleshooting tips can be found in Appendix C.

6.1. Summary of chapter conclusions

In the previous chapters, the following conclusions were made about the chemistry of alkylaromatics:

Chapter 2 highlights a major past misconception that the retroene reaction plays a major role in the conversion of hexylbenzene to toluene. This was found to be extremely inaccurate based on quantum calculations by this work, and the chemistry of alkylaromatic systems was re-characterized in the absence of the retroene reaction. The main reaction paths of alkylaromatic systems are initiation by homolytic radical scission, hydrogen abstraction to form alkylaromatic radicals on non-aromatic carbons, and beta scission to convert long chain alkylaromatic radicals into smaller species. In order to generate accurate predictions for product compositions, thermochemistry of species must be accurate within <2 kcal/mol, as this size of error can cause a factor of 2-3 difference. This conclusion sets the foundation to pursue accurate predictions for the formation of 2-ring aromatics.

Chapter 3 describes aromatic intramolecular addition reactions to form fused 2-ring aromatics, an important method to form species such as naphthalene and indane. In this work, formation of fused 2-ring aromatics were hypothesized to form by the unimolecular addition of hexylbenzene radicals to the ortho or ipso position in the relevant process conditions of 450°C and 70 bar. In this work, the feasibility of this method to form 2-ring aromatics is investigated by calculating the thermochemistry of relevant 2-ring species as important data for hexylbenzene pyrolysis model

generation. In addition, to generalize the thermochemistry calculations made in this chapter, group additivity values that are used to describe the polycyclic and radical features of the calculated compounds were updated or created. As a result of this work, thermochemistry of 83 species were calculated in the CBS-QB3 level of theory, and 26 new group additivity values were updated/introduced, reducing the Gibbs Free energy training error of relevant species from 7.3 ± 4.1 kcal/mol using old group additivity values to 0.4 ± 0.9 kcal/mol using new group additivity values.

Chapter 4 describes aromatic intermolecular addition reactions to form bridged 2-ring aromatics. This class of bimolecular reaction takes place by the addition of a radical species to the aromatic carbon of an alkylaromatic. A similar study on the thermochemistry of this class of reaction was performed akin to Chapter 3; 49 species thermochemistry were calculated in the CBS-QB3 level of theory, and one new radical group was created to describe the aromatic pi radical produced by this type of reaction, reducing the Gibbs Free energy training error of intermolecular addition products from 5.3 kcal/mol \pm 4.5 kcal/mol to 0.5 kcal/mol \pm 0.6 kcal/mol. In addition, the kinetics of this class of reaction was extensively studied to provide 21 training reactions. Through studying the differences of the new training reactions and old rate estimations, inappropriate features used to describe this class of reaction used by RMG in the past were found, and corrective measures were made by further defining reaction groups; the training reactions calculated were sufficient to cover a wide variety of analogous reactions, capable of discerning the differences in kinetics for the addition of different radicals (H, CH₃, C₂H₅, benzyl radical, and 1-phenyl-1-ethyl radical), different aromatic chain lengths (toluene and hexylbenzene), and additions to the four different positions (ortho, meta, para, and substituted).

Chapter 5 incorporated all features defined between chapters 2 and 4 into RMG, and generated a detailed kinetic model for hexylbenzene pyrolysis to describe the formation of 2-ring aromatics. The model was seeded with ~100 species in the core, including many species found in experiments. This study was supported by a parallel experimental study of hexylbenzene pyrolysis using a high-pressure batch reactor, coupled with GCxGC-qMS analysis. This chapter was able to identify a broad range of species resulting from the pyrolysis of hexylbenzene using

GCxGC-qMS; the molar yield of many of these species were compared to the kinetic model generated with updated thermochemistry, group values, and training reactions from Chapters 2-4. Many of the broad features of the detailed kinetic model match experiments within a factor of 2, such as the total molar yield of bridged species, fused aromatics, and hexylbenzene isomers. However, individual molar yields such as naphthalene and ethylbenzene do not exactly match experiments due to the lack of secondary pathways that convert ethylbenzene to naphthalene, and some species such as biphenyl was predicted to form at extremely low yields in the model, indicating key pathways for its formation is missing. Species larger than 2-rings were also found in this work.

6.2. Future of CBS-QB3 calculations

This work exploits the limits of the CBS-QB3 level of theory quite thoroughly. In Chapter 4, some of the species thermochemistry and rate coefficients, such as toluene + 1-phenyl-1-ethyl, are the largest hydrocarbon system that can be calculated in the CBS-QB3 level of theory given the limited memory Pharos (the shared server between Green and Ghoniem groups), and these calculations can take up to thirty days to complete. Based on the conclusions of chapter 2, using a lower level of theory to avoid the computational costs of the CBS-QB3 level of theory is discouraged due to the importance of accurate thermochemistry.

Many methods under development can avert the steep computational costs of quantum computational methods; such as Li's method of convolutional neural network with dropout training [59], isodesmic reactions (automation currently under development by Mark Payne). ARC, currently under development by Alon Grinberg Dana will also decrease the demand for human interference in making quantum calculations. Currently, ARC is capable of performing geometry energy, frequency, and 1-D rotor calculations, but its functionality is limited in multi-dimensional rotors and transition state calculations.

In conclusion, future work should be pursued in the future to secure new, faster, and less labor-intensive ways to generate accurate training data to improve thermochemistry estimates of RMG.

6.3. Additional Chemical Systems to Study

The chemical systems studied in chapters 3, 4, and 5 can have room to be expanded upon.

For chapter 3, in intramolecular addition, similar work for intramolecular addition can be performed for larger ring systems (e.g. intramolecular addition of butylnaphthalene to phenanthrene). Pathway (5) in Chapter 5 (to form biphenyl related species and methylfluorene) is a good example of intramolecular addition reactions of higher complexity that have not been studied in Chapter 3, indicating that there is vast room for improvement for relevant intramolecular reactions of interest. Generating the training data to improve Li et al's thermochemistry estimation method [59] and developing new group additivity values (such as the benzocycloheptane related compounds in chapter 5) will further improve RMG's performance, and improve models generated by RMG users that work with alkylaromatics.

In chapters 4 and 5, many interesting pairings of aromatic intermolecular addition have not been investigated. Most notably, the intermolecular addition between hexylbenzene and styrene (albeit not an addition to aromatic bond) should be investigated in detail, given the importance of $C_{20}H_{26}$ species displayed in chapter 5. Other radicals to consider include allyl, vinyl, propargyl, and cyclopentadienyl radicals, whereas other stable aromatic species to consider include benzene, xylene, styrene, and polycyclic aromatics. It will be extremely rewarding to further understand the kinetics of different radical and aromatic pairings to ensure RMG's rate estimates for aromatic intermolecular addition are covered in sufficient depth.

For the benzocycloheptatriene system, some key group additivity values can be further developed. In the development chapter 5, some key structures from the species C[C]1CCCCc2ccccc21, C[C]1CCC=Cc2ccccc21, CC1=CCC[CH]c2ccccc21, CC1=CCC=Cc2ccccc21 were not accounted for. These structures may be important in the future for heavy oil pyrolysis mechanisms.

6.4. Future of Hexylbenzene Model for 2-Ring Aromatics

Chapter 5 leaves a gold mine of data for improvement. Some aspects of the model that have not been fully developed include re-generating the model with updated thermochemistry and rate coefficients for the biphenyl formation pathways and the benzocycloheptene formation pathway. None of the three ring aromatics have been seeded in the model's core in current work, and it will be interesting to observe whether if RMG's current database that is heavily developed around 2-ring aromatics can be extrapolated to the formation of 3-ring species.

6.5. Fully automated chemical mechanism generation of alkylaromatic pyrolysis

A much more difficult, but higher impact improvement to the work in chapter 5 is to improve RMG to be able to fully automatically generate a chemical mechanism for hexylbenzene. The current hexylbenzene mechanism presented in chapter 5 has 150k edge species and 700k edge reactions (with pruning, these numbers drop to 15k species, 18k reactions, a significant improvement). An unseeded hexylbenzene mechanism (mechanism with hexylbenzene and nothing else at the start) has 150k species and 700k reactions, but the individual molar yields and the species involved in the mechanism will be vastly different; the resulting conversion of hexylbenzene for this model at 200 minutes is 15%, as opposed to the > 80% presented in chapter 5, indicating that the unseeded model forms too many erroneous species for the main features of hexylbenzene pyrolysis to be identified.

Due to the vast number of edge species and reactions that RMG must work with, the model will not easily identify key reaction features on its own. This results in predictions such as ethylnaphthalene and naphthalene, where the model yield of ethylnaphthalene/naphthalene highly overpredicts/underpredicts experimental data respectively, because reaction paths converting ethylnaphthalene to naphthalene were not able to be found.

RMG could be greatly improved by parallelization and other forms of acceleration, work currently pursued by Agnes Jocher. Her work investigates the effect of reaction filtering, which prevents low concentration core species from reacting and consuming computational resources, on the fly

quantum calculations that could avoid faulty group additivity values, preventing a vast number of erroneous species from forming, and pruning, where edge species will be removed periodically based on a maximum number of allowed species and a flux criterion to limit the edge space. Agnes is also developing parallelization of tasks in RMG to enable the utilization of multiple processors. Finally, according to Matt Johnson, some of RMG's functions and algorithms that are currently in use are not efficiently written, can redesigning can be done to improve the speed of model generation.

However, proper speed up alone will not solve the problems of fully automating RMG. Some reaction pathways feature a thermodynamically stable global reactant and product, but contain many steps and intermediates in between. A prime example is hexylbenzene's conversion to ethylnaphthalene, which contains 10 intermediate species and a minimum of 6 reaction steps for conversion, and every single species on the way to ethylnaphthalene is at a low concentration compared to the global reactant (hexylbenzene) and product (ethylnaphthalene). Intermediate species will be difficult to discover using the flux criteria due to this behavior. According to the expertise of Matthew Johnson, one feasible way to solve this problem is to adapt RMG to save compressed templates of past models. These compressed templates would contain information on the most important pathways of their respective models, and in future model generations, whole sequence of reactions based on these templates will be added instead of a single step, and evaluated as an extended unit by the flux criteria.

6.6. Improvements in Gas Chromatography Instrumentation

Many experimental components presented in Chapter 5 can also be improved. While the GCxGC-qMS is a powerful addition to the analytical chemistry of this work, it isn't without its own drawbacks. The Leco GCxGC-FID in the group (responsible for generating Figure 3 and Figure 4) has a higher sampling rate and resolution than the Zoex GCxGC-qMS (responsible for generating Figure 32). The limiting component to the sampling rate is the quadrupole MS, but it is also possible that the thermal modulation device used in the Zoex GCxGC-qMS doesn't allow for fast

sampling. Investigating the cause of the difference in sampling rate is highly encouraged to improve resolution of future GCxGC chromatograms.

The Shimadzu GC, used in Chapter 2 and previous work by Carr et al. [18] is also highly underdeveloped. The GC unit is currently unable to detect gases that are larger than 5 carbons, and the TCD attached to this unit is heavily underutilized, because the column set causes carbon dioxide, carbon monoxide, and other light gases to co-elute with methane and nitrogen. The detection of carbon dioxide and monoxide could be extremely instrumental to finding the effect of water on supercritical water treatment of hexylbenzene similarly to Kida et al. [8]. To accomplish the objectives listed above, an appropriate column set to better separate light gases but retains peak structure for heavy gases is required, but if accomplishing both at the same time is not possible, a decision should be made to at least fulfill one of the two objectives at a time.

6.7. Improvements in Batch Reactor Method

Finally, the batch reactor setup of the lab is highly inefficient. While it only takes roughly three hours for an experienced experimentalist to run one experiment the setup suffers from many drawbacks. These problems are listed with possible solutions.

- Each experiment will only provide one data point.
 - o The gold tube reactor setup Appendix B avoids part of this issue by allowing multiple reactions to be run at the same time. This method can be used to investigate different reactant compositions at the same time, and can also allow for replicated data for uncertainty control, but these reactions will share the same temperature and reaction time (doesn't solve the multiplex problem very well). Gold tube reactors is also not a good setup for water, due to water's high specific volume, limiting the quantity of reagent that may be added to the gold tube.
 - o A flow reactor setup will allow for better multiplex data collection. However, this suffers from the drawback of consuming more reactant, and it is much more time

consuming to complete one flow reactor experiment. The advantages and disadvantages of using flow reactors should be carefully considered.

- Note that the batch reactor has a limited life span due to the many cycles of heating and cooling it experiences. Maximizing the utility of the reactor in each experiment will be advantageous for many practical purposes.
- There is no direct temperature measurement
 - It is possible to insert a 1/32 inch thermocouple into the batch reactor setup for direct temperature measurement, but this will require an additional inlet or a Tee at an appropriate location (one of the sidearms).
- The heat up time raises many questions for as to whether if any secondary chemistry at lower temperatures during the course of heat up
 - Can be avoided using a flow reactor
- Small volume of product does not allow for more elaborate downstream analysis methods, such as fractional distillation
 - Can also be avoided using a flow reactor or a larger reactor.

6.8. Incorporation of Water to investigation

Throughout this work, supercritical water (SCW) has been left out of the investigation due to hexylbenzene pyrolysis being a sufficiently complicated system for investigation. However, using the methodologies outlined in this work, one should be able to characterize and quantify the effects of water towards the formation of 2-ring aromatics in SCW treatment of hexylbenzene.

In work performed by Carr et al. [18], it was reported that the RMG does not output any difference in the model generated in the presence and absence of water, presumably because all reactions involving water were limited in the model's edge. Since then, many improvements have been made to RMG, including expanded training data, new atom types throughout RMG's many updates, and better handling of resonance structures. It is possible that some reactions involving water will make it past the flux criteria.

However, this leads back to the full automation of the hexylbenzene pyrolysis system. Depending on the relative rates of water reaction, reaction generation may be heavily favored towards generating hexylbenzene isomers and intermolecular addition products. Per usual, to circumvent this, one may seed the core of the mechanism with likely products of reactions involving water. One key compound that was found in SCW treatment of hexylbenzene that was absent in hexylbenzene pyrolysis was acetophenone, discovered by Bob Nelson's GCxGC-TOF-MS at the Woods Hole Oceanographic Institution. The formation of this species is possibly due to the addition between styrene and water.

6.9. Transition from 2-Ring Species to Coke

The most complex topic that was barely touched upon in this work is the formation of coke. In this work, the formation 2-ring aromatics was studied, with the underlying idea that the chemistry of formation of 2-ring species can be extrapolated to formation of larger polyaromatic hydrocarbons, which is the possible identity of coke.

Much work can be accomplished to this end. As a simple objective, one may choose to correlate the concentration of 2-ring aromatics (or a specific class of 2-ring aromatics) with a measurement that more closely describes coke concentration, such as a UV-vis measurement of the sample. The correlation of certain species (or ratio of species) to coke will allow for a more industrially relevant interpretation of RMG's output.

The study of coke formation can be approached in many more directions, due to the vast number of unknowns surrounding coke's identity. Presumably, more analytical chemistry work can be pursued to further identify coke. In the past, NMR, column chromatography, SARA fractionation, Raman spectroscopy, FT-IR, x-ray fluorescence, and vacuum distillation have all been used in by Gudiyella et al. [78] in attempts to better understand the composition of crude oil and its components. While invaluable knowledge was uncovered, much future work will be needed to further characterize crude oil, coke, and other crude oil constituents.

7. References

- [1] Organization of the Petroleum Exporting Countries, "World Oil Outlook 2040," Vienna, Austria, 2018.
- [2] S. Zhao, B. D. Sparks, L. S. Kotlyar and K. H. Chung, "Correlation of processability and reactivity data for residua from bitumen, heavy oils and conventional crudes: Characterization of fractions from super-critical pentane separation as a guide to process selection," *Catalysis Today*, pp. 122-136, 2007.
- [3] R. O. Caniaz and C. Erkey, "Process Intensification for Heavy Oil Upgrading Using Supercritical Water," *Chemical Engineering Research and Design*, pp. 1845-1863, 2014.
- [4] K.-H. Choi and M. F. Aljishi. United States Patent US 8,535,518 B2, 2013.
- [5] I. C. Allen, Heavy Oil as Fuel for Internal-Combustion Engines, Ann Arbor, MI: Govt. Print. Off., 1913.
- [6] E. Furmsky, "Emissions of carbon dioxide from tar sands plants in Canada," *EnergyFuels*, vol. 17, pp. 1541-1548, 2003.
- [7] V. A. Gembicki, T. M. Cowan and G. R. Brierley, "Update processing operations to handle heavy feedstocks," *Hydrocarbon Processing*, pp. 41-53, 2007.
- [8] Y. Kida, C. A. Class, A. J. Concepcion, M. T. Timko and W. H. Green, "Combining experiment and theory to elucidate the role of supercritical water in sulfide decomposition," *Phys. Chem. Chem. Phys.*, vol. 16, pp. 9220-9228, 2014.
- [9] P. R. Patwardhan, M. T. Timko, C. A. Class, R. E. Bonomi, Y. Kida, H. H. Hernandez, J. W. Tester and W. H. Green, "Supercritical Water Desulfurization of Organic Sulfides Is Consistent with Free-Radical Kinetics," *EnergyFuels*, vol. 27, no. 10, pp. 6108-6117, 2013.
- [10] N. Li, B. Yan and X. Xiao, "A review of lab scale research on upgrading heavy oil in supercritical water," *Energies*, vol. 8, pp. 8962-8989, 2015.
- [11] Criterion Catalysts and Technologies, "Hydrocracking Process Description and CRITERION/ZEOLYST Hydrocracking Catalyst Applications," Zeolyst International, Houston, TX, 2005.
- [12] J. M. Oelderick, S. T. Sie and D. Bode, "Progress in the Catalysis of the upgrading of petroleum residue - a review of 25 years of R&D on shell residue hydroconversion technology," *Appl. Catal.*, pp. 1-24, 1989.
- [13] J. Ancheyta, Modeling and Simulation of Catalytic Reactors for Petroleum Refining, Hoboken, New Jersey: John Wiley & Sons, 2011.
- [14] T. Morita, H. Sato, M. Uematsu and K. Watanabe, "PVT Properties and Vapor-PPressures of Ordinary Water Substance in the Critical Region.," *Physica A: (Amsterdam)*, vol. 15, pp. 436-453, 1989.
- [15] N. C. Leguizamon Guerra, J. C. Lizardo Huerta, C. Lorgeoux, R. Michels, R. Fournet, B. Sirjean, A. Randi, R. Bounaceur and V. Burkle-Vitzthum, "Thermal cracking of n-butylbenzene at

- high pressure: Experimental study and kinetic modelling," *Journal of Analytical and Applied Pyrolysis*, vol. 133, pp. 234-245, 2018.
- [16] C. W. Gao, J. W. Allen, W. H. Green and R. H. West, "Reaction Mechanism Generator: Automatic construction of chemical kinetic mechanisms," *Computer Physics Communications*, vol. 203, pp. 212-225, 2016.
- [17] W. H. Green and R. H. West, "Reaction Mechanism Generator," 2013. [Online]. Available: <http://rmg.mit.edu/>.
- [18] A. G. Carr, C. A. Class, L. Lai, Y. Kida, T. Monroe and W. H. Green, "Supercritical Water Treatment of Crude Oil and Hexylbenzene: An Experimental and Mechanistic Study on Alkylbenzene Decomposition," *Energy & Fuels*, pp. 5290-5302, 2015.
- [19] L. Lai, S. Gudiyella, M. Liu and W. H. Green, "Chemistry of Alkylaromatics Reconsidered," *Energy & Fuels*, vol. 32, no. 4, pp. 5489-5500, 2018.
- [20] P. C. Mandal, S. Chowdhury and M. Sasaki, "Comparison Study of Heptylbenzene and hexylbenzene Decomposition under Supercritical Water," *International Journal of Chemical Engineering and Applications*, vol. 7, no. 3, pp. 156 - 160, 2016.
- [21] C. H. Leigh and M. Szwarc, "The Pyrolysis of n-Propyl-Benzene and the Heat of Formation of Ethyl Radical," *The Journal of Chemical Physics*, vol. 20, no. 3, pp. 403-406, 1952.
- [22] F. Khorasheh and M. R. Gray, "High-Pressure Thermal Cracking of n-Hexadecane in Aromatic Solvents," *Ind. Eng. Chem. Res.*, vol. 32, pp. 1864-1876, 1993.
- [23] C. Qi. and G. F. Froment, "Thermal cracking of substituted aromatic hydrocarbons. II. Kinetic study of the thermal cracking of n-propylbenzene and ethylbenzene," *Journal of Analytical and Applied Pyrolysis*, vol. 21, pp. 51-77, 1991.
- [24] P. E. Savage and M. T. Klein, "Discrimination between molecular and free-radical models of 1-phenyldodecane pyrolysis," *Ind. Eng. Chem. Res.*, vol. 26, no. 2, pp. 374-376, 1987.
- [25] H. Freund and W. N. Olmstead, "Detailed Chemical Kinetic Modeling of Butylbenzene Pyrolysis," *International Journal of Chemical Kinetics*, vol. 21, pp. 561-574, 1989.
- [26] Chemkin-Pro 15112, Reaction Design, San Diego, 2011.
- [27] M. J. Frisch, G. W. Trucks, H. B. Schlegel, G. E. Scuseria, M. A. Robb, J. R. Cheeseman, J. A. Montgomery Jr., T. Treven, K. N. Kudin, J. C. Burant, J. M. Millam, S. S. Iyengar, J. Tomasi, V. Barone, B. Mennucci, M. Cossi, G. Scalmani, RegaN., G. A. Petersson, H. Nakatsuji, M. Hada, M. Ehara, K. Toyota, R. Fukuda, J. Hasegawa, M. Ishida, T. Nakajima, Y. Honda, O. Kitao, H. Nakai, M. Klene, X. Li, J. E. Knox, H. P. Hratchian, J. B. Cross, V. Bakken, C. Adamo, J. Jaramillo, R. Gomperts, R. E. Stratmann, O. Yazyev, A. J. Austin, R. Cammi, C. Pomelli, J. W. Ochterski, P. Y. Ayala, K. Morokuma, G. A. Voth, P. Salvador, J. J. Dannenberg, V. G. Zakrzewski, S. Dapprich, A. D. Daniels, M. C. Strain, O. Farkas, D. K. Malick, A. D. Rabuck, K. Raghavachari, J. B. Foresman, J. V. Ortiz, Q. Cui, A. G. Baboul, S. Clifford, J. Ciolowski, B. B. Stefanov, G. Liu, A. Liashenko, P. Piskorz, I. Komaromi, R. L. Martin, D. J. Fox, T. Keith, M. A. Al-Laham, C. Y. Peng, A. Nanayakkara, M. Challacombe, P. M. Gill, B. Johnson, W. Chen, M. W. Wong, C. Gonzalez and J. A. Pople, Gaussian 03, Revision C.02, Wallingford, CT: Gaussian, Inc., 2003.
- [28] J. W. Allen, F. C. Goldsmith and W. H. Green, "Automatic estimation of pressure-dependent rate coefficients," *Phys. Chem. Chem. Phys.*, pp. 1131-1155, 2012.

- [29] M. R. Harper, K. M. Van Geem, S. P. Pyl, G. B. Marin and W. H. Green, "Comprehensive reaction mechanism for n-butanol pyrolysis and combustion," *Combustion and Flame*, pp. 16-41, 2011.
- [30] S. Sharma, S. Raman and W. H. Green, "Intramolecular Hydrogen Migration in Alkylperoxy and Hydroperoxyalkylperoxy Radicals: Accurate Treatment of Hindered Rotors," *J. Phys. Chem. A*, vol. 114, pp. 5689-5701, 2010.
- [31] J. W. Allen and W. H. Green, "CanTherm User Guide," 2017. [Online]. Available: <http://reactionmechanismgenerator.github.io/RMG-Py/users/cantherm/>.
- [32] G. A. Petersson, D. K. Malick and W. G. Wilson, "Calibration and comparison of the Gaussian-2, complete basis set, and density functional methods for computational thermochemistry," *The Journal of Chemical Physics*, vol. 109, pp. 10570-10579, 1998.
- [33] V. Burklé-Vitzthum and R. Michels, "Experimental Study and Modeling of the Role of Hydronaphthalenics on the Thermal Stability of Hydrocarbons under Laboratory and Geological Conditions," *Ind. Eng. Chem. Res.*, pp. 8972-8987, 2005.
- [34] M. T. Klein and P. S. Virk, "Model Pathways in Lignin Thermolysis. 1. Phenethyl Phenyl Ether," *Ind. Eng. Chem. Fundam.*, vol. 22, pp. 35-45, 1983.
- [35] W. Tsang, "Chemical Kinetic Data Base for Combustion Chemistry Part V. Propene," *J Phys Chem Ref Data*, pp. 221-274, 1991.
- [36] M. V. Roux, M. Temprado, J. S. Chickos and Y. Nagano, "Critically Evaluated Thermochemical Properties of Polycyclic Aromatic Hydrocarbons," *J. Phys. Chem. Ref. Data*, vol. 4, no. 1855-1996, p. 37, 2008.
- [37] K. Narayanaswamy, G. Blanquart and H. Pitsch, "A Consistent Chemical Mechanism for Oxidation of Substituted Aromatic Species," *Combustion and Flame*, vol. 10, no. 157, pp. 1879-1898, 2010.
- [38] B. Ruscic, J. E. Boggs, A. Burcat, A. G. Csaszar, J. Demaison, R. Janoschek, J. M. Martin, M. L. Morton, M. J. Rossi, J. F. Stanton, P. G. Szalay, P. R. Westmoreland, F. Zabel and T. Berces, "IUPAC Critical Evaluation of Thermochemical Properties of Selected Radicals Part I," *Phys. Chem. Ref. Data.*, vol. 34, no. 2, p. 573, 2005.
- [39] E. J. Prosen and F. D. Rossini, "Heats of formation and combustion of 1,3-butadiene and styrene," *J. Res. NBS*, vol. 34, pp. 59-63, 1945.
- [40] A. Miller, "Chemical thermodynamic properties of ethylbenzene," *J. Chem. Phys.*, vol. 68, pp. 1317-1319, 1978.
- [41] K. S. Pitzer, "The heat capacity, heats of fusion and vaporization, vapor pressure, entropy, vibrational frequencies, and barrier to internal rotation of styrene," *J. Am. Chem. Soc.*, vol. 68, pp. 2209-2212, 1946.
- [42] K. P. Somers and J. M. Simmie, "Benchmarking Compound Methods (CBS-QB3, CBS-APNO, G3, G4, W1BD) against the Active Thermochemical Tables: Formation Enthalpies of Radicals," *The Journal of Physical Chemistry*, vol. 119, pp. 8922-8933, 2015.
- [43] P. A. Dennis, "Coupled cluster, B2PLYP and M06-2X investigation of the thermochemistry of five-membered nitrogen containing heterocycles, furan, and thiophene," *Theoretical Chemistry Accounts*, vol. 129, no. 2, pp. 219-227, 2011.

- [44] L. Lai, S. Khanniche and W. H. Green, "Thermochemistry and Group Additivity Values for Fused Two Ring Aromatic Species and Radicals," *J. Phys. Chem. A*, vol. 123, no. 15, pp. 3418-3428, 2019.
- [45] Q. Chen and G. F. Froment, "Thermal Cracking of Substituted Aromatic Hydrocarbons I. Kinetic Study of the Thermal Cracking of i-propylbenzene," *Journal of Analytical and Applied Pyrolysis*, vol. 21, pp. 27-50, 1992.
- [46] Q. Chen and G. F. Froment, "Thermal Cracking of Substituted Aromatic Hydrocarbons II. Kinetic Study of the Thermal Cracking of n-Propylbenzene and Ethylbenzene," *Journal of Analytical and Applied Pyrolysis*, vol. 21, pp. 51-77, 1991.
- [47] M. Chase, NIST-JANAF thermochemical tables 4th ed., New York: American Institute of Physics for the National Institute of Standards and Technology, 1998.
- [48] E. Goos, A. Burcat and B. Ruscic, Extended Third Millennium Ideal Gas and Condensed Phase Thermochemical Database for Combustion with Updates from Active Thermochemical Tables, Argonne: Argonne National Laboratory, 2014.
- [49] B. Ruscic, R. E. Pinzon, G. von Laszewski, D. Kodeboyina and a. Burcat, "Active Thermochemical Tables: thermochemistry for the 21st century," *Journal of Physics: Conference Series*, vol. 16, p. 561/570, 2005.
- [50] J. B. Pedley, R. D. Naylor and S. P. Kirby, Thermochemical Data of Organic Compounds, New York: Chapman and Hall, 1977.
- [51] G. R. Magoon, W. H. Green and C. F. Goldsmith, "Database of Small Molecule Thermochemistry for Combustion," *J. Phys. Chem. A*, vol. 116, pp. 9033-9057, 2012.
- [52] S. W. Benson and J. H. Buss, "Additivity Rules for the Estimation of Molecular Properties. Thermodynamic Properties," *J. Chem. Phys.*, vol. 29, pp. 546-572, 1958.
- [53] S. W. Benson, F. R. Cruickshank, D. M. Golden, G. R. Haugen, H. E. O'Neal, A. S. Rodgers, R. Shaw and R. Walsh, "Additivity Rules for the Estimation of Thermochemical Properties," *J. Chem. Phys.*, vol. 29, no. 546, pp. 279-324, 1958.
- [54] E. R. Ritter and J. W. Bozzelli, "THERM - THERMODYNAMIC PROPERTY ESTIMATION FOR GAS-PHASE RADICALS AND MOLECULES," *International Journal of Chemical Kinetics*, vol. 23, no. 9, pp. 767-778, 1991.
- [55] T. H. Lay, J. W. Bozzelli, A. M. Dean and E. R. Ritter, "Hydrogen Atom Bond Increments for Calculation of Thermodynamic Properties of Hydrocarbon Radical Species," *J. Phys. Chem.*, vol. 99, no. 39, pp. 14514-14527, 1995.
- [56] J. Yu, R. Sumathi and W. H. Green, "Accurate and Efficient Method for Predicting Thermochemistry of Polycyclic Aromatic Hydrocarbons – Bond-Centered Group Additivity," *J. Am. Chem. Soc.*, vol. 126, no. 39, pp. 12685-12700, 2004.
- [57] K. Han, A. Jamal, C. A. Grambow, Z. J. Buras and W. H. Green, "An Extended Group Additivity Method for Polycyclic Thermochemistry Estimation," *International Journal of Chemical Kinetics*, vol. 50, no. 4, pp. 294-303, 2018.
- [58] Y. Li and H. J. Curran, "Extensive Theoretical Study of the Thermochemical Properties of Unsaturated Hydrocarbons and Allylic and Super-Allylic Radicals: The Development and Optimization of Group Additivity Values," *J. Phys. Chem. A*, vol. 122, no. 20, pp. 4736-4749, 2018.

- [59] Y.-P. Li, K. Han, C. A. Grambow and W. H. Green, "Self-Evolving Machine: A Continuously Improving Model for Molecular Thermochemistry," *J. Phys. Chem. A*, p. Just accepted, 2019.
- [60] A. A. Clifford, *Multivariate Error Analysis: A Handbook of Error Propagation and Calculation in Many-parameter Systems*, New York: Wiley, 1973.
- [61] J. A. J. Montgomery, M. J. Frisch, J. W. Ochterski and G. A. Petersson, "A complete basis set model chemistry. VI. Use of density functional geometries and frequencies," *J. Chem. Phys.*, vol. 110, no. 6, pp. 2822-2827, 1999.
- [62] S. Khanniche, L. Lai and W. H. Green, "Kinetics of Intramolecular Phenyl Migration and Fused Ring Formation in Hexylbenzene Radicals," *J. Phys. Chem. A*, vol. 122, no. 51, pp. 9778-9791, 2018.
- [63] N. Cohen and S. W. Benson, "Estimation of Heats of Formation of Organic Compounds by Additivity Methods," *Chem. Rev.*, vol. 93, no. 7, pp. 2419-2438, 1993.
- [64] S. P. Verevkin, V. N. Emel'yanenko, A. A. Pimerzin and E. E. Vishnevskaya, "Thermodynamic Analysis of Strain in Heteroatom Derivatives of Indene," *J. Phys. Chem. A*, vol. 115, no. 44, pp. 12271-12279, 2011.
- [65] A. E. Long, S. S. Merchant, A. G. Vandeputte, H.-H. Carstensen, A. J. Vervust, G. B. Marin, K. M. Van Geem and W. H. Green, "Pressure dependent kinetic analysis of pathways to naphthalene from cyclopentadienyl recombination," *Combustion and Flame*, vol. 187, pp. 247-256, 2018.
- [66] A. Li, H. S. Muddana and M. K. Gilson, "Quantum Mechanical Calculation of Noncovalent Interactions: A Large-Scale Evaluation of PMx, DFT, and SAPT Approaches," *J. Chem. Theory Comput.*, vol. 10, no. 4, pp. 1563-1575, 2014.
- [67] X. Rozanska, J. J. Stewart, P. Ungerer, B. Leblanc, C. Freeman, P. Saxe and E. Wimmer, "High-Throughput Calculations of Molecular Properties in the MedeA Environment: Accuracy of PM7 in Predicting Vibrational Frequencies, Ideal Gas Entropies, Heat Capacities, and Gibbs Free Energies of Organic Molecules," *J. Chem. Eng. Data*, vol. 59, pp. 3136-3143, 2014.
- [68] W. R. Roth, F. Bauer, A. Beitat, T. Ebbrecht and M. Wüstefeld, "Die Bildungsenthalpie des Allyl- und Methallyl-Radikals," *Chem. Ber.*, vol. 124, no. 1191, pp. 1453-1460, 1991.
- [69] D. A. Robaugh and S. E. Stein, "Stabilities of highly conjugated radicals from bond homolysis rates," *J. Am. Chem. Soc.*, vol. 108, no. 12, pp. 3224-3229, 1986.
- [70] H. Hippler and J. Troe, "Thermodynamic properties of benzyl radicals: enthalpy of formation from toluene, benzyl iodide, and dibenzyl dissociation equilibria," *J. Phys. Chem.*, vol. 94, no. 9, pp. 3803-3806, 1990.
- [71] Y.-R. Luo, *Handbook of Bond Dissociation Energies in Organic Compounds*, Boca Raton: CRC Press, 2002.
- [72] E. T. Denisov and T. G. Denosova, *Handbook of Antioxidants*, New York: CRC Press, 2000.
- [73] E. A. Kromkin, V. Tumanov and E. T. Denisov, "Evaluation of C-H bond dissociation energies in alkylaromatic hydrocarbons and the enthalpies of corresponding radicals from kinetic data," *Neftekhimiya*, vol. 42, no. 1, pp. 3-14, 2002.
- [74] V. Tumanov and E. T. Denisov, "Evaluation of C-H bond dissociation energies in hydrocarbons and the enthalpies of the relevant radicals from kinetic data," *Neftekhimiya*, vol. 41, no. 2, pp. 109-118, 2001.

- [75] L. J. Laarhoven, and P. J. Mulder, " α -C-H Bond Strengths in Tetralin and THF: Application of Competition Experiments in Photoacoustic Calorimetry," *J. Phys. Chem. B.*, vol. 101, no. 1, pp. 73-77, 1997.
- [76] C. R uchardt, M. Gerst and J. Ebenhoch, "Uncatalyzed Transfer Hydrogenation and Transfer Hydrogenolysis: Two Novel Types of Hydrogen-Transfer Reactions," *Angew. Chem. Int. Ed. Engl.*, vol. 36, no. 13-14, pp. 1406-1430, 1996.
- [77] L. Lai and W. H. Green, "Thermochemistry and Kinetics of Intermolecular Addition of Radicals to Toluene and Alkylaromatics," *J. Phys. Chem. A.*, vol. Submitted (In review), 2019.
- [78] S. Gudiyella, L. Lai, I. H. Borne, G. A. Tompsett, M. T. Timko, K.-H. Choi, M. H. Alabsi and W. H. Green, "An Experimental and Modeling Study of Vacuum Residue Upgrading in Supercritical Water," *AIChE Journal*, vol. 64, pp. 1732-1743, 2018.
- [79] K.-C. Xie, "Coal Pyrolysis Reactions," in *Structure and Reactivity of Coal*, New York, Springer, 2015, pp. 119-179.
- [80] S. J. Klippenstein, L. B. Harding and Y. Georgievskii, "On the formation and decomposition of C7H8," *Proceedings of the Combustion Institute*, vol. 31, pp. 221-229, 2007.
- [81] V. V. Kislov, A. M. Mebel, J. Aguilera-Iparraguirre and W. H. Green, "Reaction of Phenyl Radical with Propylene as a Possible Source of Indene and Other Polycyclic Aromatic Hydrocarbons: An Ab Initio/RRKM-ME Study," *J. Phys. Chem. A*, vol. 116, pp. 4176-4191, 2012.
- [82] J. O. Terry and J. H. Futrell, "Disproportionation and combination reactions of simple alkyl radicals: methyl, ethyl, n-propyl, and isopropyl," *Canadian Journal of Chemistry*, vol. 45, no. 2327-2333, 1967.
- [83] R. S. Zhu, Z. F. Xu and M. C. Lin, "Combination and Disproportionation Reactions of Alkyl Radicals: An Ab Initio Kinetics Study For CH₃ + C₂H₅," *Prepr. Pap.-Am. Chem. Soc., Div. Fuel Chem.*, vol. 49, no. 1, pp. 447-448, 2004.
- [84] S. H. Mousavipour and Z. Homayoon, "A Theoretical Study on the Kinetics of Disproportionation versus Association Reaction of CH₃ + C₂H₅," *J. Phys. Chem. A*, vol. 107, no. 41, pp. 8566-8574, 2003.
- [85] F. Lannuzel, R. Bounaceur, R. Michels, G. Scacchi and P.-M. Marquaire, "An extended mechanism including high pressure conditions (700 bar) for toluene pyrolysis," *Journal of Analytical and Applied Pyrolysis*, vol. 87, no. 2, pp. 236-247, 2010.
- [86] A. S. Semenikhin, A. S. Savchenkova, I. V. Chechet, S. G. Matveev, Z. Liu, M. Frenklach and A. M. Mebel, "Rate Constants for H Abstraction from benzo(a)pyrene and chrysene: a theoretical study," *Phys. Chem. Chem. Phys.*, vol. 19, pp. 25401-25413, 2017.
- [87] T. V.-T. Mai, A. Ratkiewicz, M. V. Duong and L. K. Huynh, "Direct ab initio study of the C₆H₆ + CH₃/C₂H₅ = C₆H₅ + CH₄/C₂H₆ reactions," *Chemical Physics Letters*, vol. 16, pp. 102-109, 2016.
- [88] H. Ismail, J. Park, B. M. Wong, W. H. Green and M. C. Lin, "A theoretical and experimental kinetic study of phenyl radical addition to butadiene," *Proceedings of the Combustion Institute*, vol. 30, no. 1, pp. 1049-1056, 2005.

- [89] M. K. Sabbe, M.-F. Reyniers, V. Van Speybroeck, M. Waroquier and G. B. Marin, "Carbon-Centered Radical Addition and β -Scission Reactions: Modeling of Activation Energies and Pre-exponential Factors," *Chem Phys Chem*, vol. 9, no. 1, pp. 124-140, 2008.
- [90] A. M. Mebel, M. C. Lin and K. Morokuma, "Theoretical Study of Potential Energy Surface and Thermal Rate Constants for the C₆H₅ + H₂ and C₆H₆ + H Reactions," *J. Phys. Chem. A*, vol. 101, no. 17, pp. 3189-3196, 1997.
- [91] K. Lorenz and R. Zellner, "Kinetics of the Reactions of OH-Radicals with Benzene, Benzene-d₆ and Naphthalene," *Ber. Bunsenges. Phys. Chem.*, vol. 87, pp. 629-636, 1983.
- [92] K. Yang, "Free Radical Reactions Initiated by Ionizing Radiation. II. Rate Constants for Hydrogen Atom Addition Reactions with Mono-olefins, Butadiene and Benzene," *J. Am. Chem. Soc.*, vol. 84, no. 20, pp. 3795-3799, 1962.
- [93] I. Da Costa, R. Fournet, F. Billaud and F. Battin-Leclerc, "Experimental and Modeling Study of the Oxidation of Benzene," *Int. J. Chem. Kinet.*, vol. 35, no. 10, pp. 503-524, 2003.
- [94] B. Shukla, A. Susa, A. Miyoshi and M. Koshi, "Role of Phenyl Radicals in the Growth of Polycyclic Aromatic Hydrocarbons," *J. Phys. Chem. A*, vol. 112, pp. 2363-2369, 2008.
- [95] M. Morimoto, S. Sato and T. Takanohashi, "Effect of water properties on the degradative extraction of asphaltene using supercritical water," *J. Supercrit. Fluids*, vol. 68, pp. 113-116, 2012.
- [96] A. Zaker, P. Guerra, Y. Wang, G. Tompsett, X. Huang, J. Bond and M. Timko, "Evidence of heterogeneous catalytic activity of ZSM-5 in supercritical water for dodecane cracking," *Catalysis Today*, vol. In Press, 2018.
- [97] M. W. Haenel, "Recent Progress in coal structure research," *Fuel*, vol. 71, no. 11, pp. 1211-1223, 1992.
- [98] L. Artok, Y. Su, Y. Hirose, M. Hosokawa, S. Murata and M. Nomura, "Structure and Reactivity of Petroleum-Derived Asphaltene," *Energy & Fuels*, vol. 13, no. 2, pp. 287-296, 1999.
- [99] T. W. Mojelsky, T. M. Ignasiak, Z. Frakman, D. D. McIntyre, E. M. Lown, D. S. Montgomery and O. P. Strausz, "Structural Features of Alberta Oil Sand Bitumen and Heavy Oil Asphaltenes," *Energy & Fuels*, vol. 6, no. 1, pp. 83-96, 1992.
- [100] A. Burcat and B. Ruscic, Third Millennium Ideal Gas and Condensed Phase Thermochemical Database for Combustion with Updates from Active Thermochemical Tables, Argonne: Argonne National Laboratory, 2005.
- [101] L. Lai, H.-W. Pang and W. H. Green, "Formation of 2-Ring Aromatics in Hexylbenzene Pyrolysis," *Energy & Fuels*, vol. To be submitted, 2019.
- [102] A. K. Hossain and P. A. Davies, "Pyrolysis liquids and gases as alternative fuels in internal combustion engines – A review," *Renewable and Sustainable Energy Reviews*, vol. 21, pp. 165-189, 2013.
- [103] A. V. Bridgewater and M.-L. Cottam, "Opportunities for biomass pyrolysis liquids production and upgrading," *Energy & Fuels*, vol. 6, no. 2, pp. 113-120, 1992.
- [104] M. S. Rana, V. Samano, J. Ancheyta and J. A. Diaz, "A review of recent advances on process technologies for upgrading of heavy oils and residua," *Fuel*, vol. 86, pp. 1216-1231, 2007.

- [105] M. Liu and W. H. Green, "Capturing aromaticity in automatic mechanism generation software," *Proceedings of the Combustion Institute*, vol. 37, no. 1, pp. 575-581, 2018.
- [106] S. E. Reichenbach, M. Ni, D. Zhang and E. B. Ledford, "Image background removal in comprehensive two-dimensional gas chromatography," *Journal of Chromatography A*, vol. 985, no. 1-2, pp. 47-56, 2003.
- [107] Z. J. Buras, T.-C. Chu, A. Jamal, N. W. Yee, J. E. Middaugh and W. H. Green, "Phenyl radical + propene: a prototypical reaction surface for aromatic-catalyzed 1,2-hydrogen-migration and subsequent resonance-stabilized radical formation," *Phys. Chem. Chem. Phys.*, vol. 20, pp. 13191-13214, 2018.
- [108] R. D. Johnson, "NIST Standard Reference Database Number 101," NIST Computational Chemistry Comparison and Benchmark Database, 19 April 2018. [Online]. Available: <http://cccbdb.nist.gov/>. [Accessed 12 April 2019].
- [109] V. Chernov, M. J. Thomson, S. B. Dworkin, N. A. Slavinskaya and U. Riedel, "Soot formation with C1 and C2 fuels using an improved chemical mechanism for PAH growth," *Combustion and Flame*, vol. 161, no. 2, pp. 592-601, 2014.
- [110] S. Stein, Y. Mirokhin, D. Tchekhovskoi, G. Mallard, A. Miskaia, P. Neta, D. Sparkman, E. White, X. Yang, V. Zaikin and D. Zhu, "The NIST Mass Spectra Search Program for the NIST/EPA/NIH Mass Spectral Library," NIST, Foster City, CA, 2011.

Appendix A

List of changes made to RMG:

The following are a summary of changes that I have contributed to RMG. To see a full view of my commits, type in the following command:

```
git log -author="laitcl"
```

To view the details of each commit, type

```
git show <commit string>
```

RMG-Database

Thermochemistry of the following classes of species have been added to the Lai_Hexylbenzene Library:

- Hexylbenzene
- Hexylbenzene aliphatic radicals
- Styrene
- 1-butyl and 1-pentyl radical
- Alkylbenzenes from toluene to pentylbenzene
- Benzyl radicals of alkylbenzenes from benzyl radical to pentylbenzyl radical
- All fused species shown in chapter 3
 - o All fused species shown in chapter 3 with shorter or no alkyl chains. For example, naphthalene and methylnaphthalene were calculated alongside ethylnaphthalene
- Additional fused species from the s2_5_6_diene and s2_6_6_diene family
- Intermolecular addition products outlined in chapter 4
- 1,3-cyclohexadiene-5-methylene and 1,4-cyclohexadiene-3-methylene
- Species in biphenyl reaction pathway shown in Chapter 5

- Species in benzocycloheptene pathway shown in Chapter 5

Rate coefficients of the following species has been added to Lai_Hexylbenzene Library

- Reaction 3 from chapter 2
- All intramolecular addition steps shown in chapter 3
- Many steps involving beta scission of hydrogen shown in chapter 3 (for example, beta-scission of dihydronaphthalene radical to form naphthalene)
- All intermolecular addition reactions shown in chapter 4
- Two reactions of the ethylbiphenyl system shown in chapter 5 (phenyl addition and ethyl scission)
- Intramolecular addition of Rad5 to form methylbenzocycloheptene rad

The following group additivity values were added or updated

- Secondary benzyl radical (Benzyl_S)
- Primary benzyl radical (Benzyl_P)
- Polycyclic groups for 2_5_6_dienes and 2_6_6_dienes
- Polycyclic and radical groups shown in chapter 3
- Aromatic pi radicals (there are many types all labelled Aromatic_pi_S_(something))
- The Allyl_T group was previously overspecified, leading to the phenomenon highlighted in chapter 4. This has been fixed.
- 13cyclohexadiene5methylene and 14cyclohexadiene5methylene
- Polycyclic and radical groups shown in chapter 5

The following Training reactions were added

- Intra_H_Migration reactions from Wang, Villano, and Dean, "The Impact of Resonance Stabilization on the Intramolecular Hydrogen-Atom Shift Reactions of Hydrocarbon Radicals", ChemPhysChem, 2015.
- All reactions in R_Addition_MultipleBond that used single/double bond notation are now switched to use benzene bond notation in the species dictionary wherever necessary.
- All reactions highlighted two paragraphs above; these were added to the following families:

- Intramolecular addition to ortho position → Intra_R_Addition_Endocyclic
- Intramolecular addition to substituted position → Intra_R_Add_Exocyclic
- Beta-scission reactions → R_Addition_MultipleBond
- Intermolecular addition reactions → R_Addition_MultipleBond

The following reaction groups have been added to RMG-database

- Many benzene bond containing groups found in R_Addition_MultipleBond
 - Notably, nodes were made for most reactions that were outlined in Chapter 4 so that they are classified something different from what was previously in the family.
- Reaction groups for reactions in chapter 3 were added with more depth
- Reaction groups for reactions in chapter 5 were added with more depth

RMG-Py

Changed Fourier fitting in Arkane, function name FitFourierPotentialToData.

- Fitting begins with twelve fourier parameters (6 sine 6 cosine), and adds two fitting parameters at a time when a negative barrier height is found to avoid errors.

Some minor bug fixes to statmech.py and documentation changes

Appendix B

**Standard Operation Procedures for All
Developed Methods**

Procedure for Performing Stainless Batch Reactor Experiment

Overview

This experiment involves the potential for toxic gas (hydrocarbons) generation and high pressure/temperature. Caution is advised during the procedure. The most important point to keep in mind is to have ventilation and never to touch heated elements.

Written by Lawrence Lai

Date Written: 4/15/2019

1. Purpose

The purpose of this document is to provide standard operating procedures for lab members who wish to use the stainless-steel batch reactor for experimentation.

2. Location of Equipment

Batch reactors are stored in fume hoods adjacent to the main faucet in the Green lab, E18-566. Work bench tools can be found to the right of the walk-in hood, and the heated sand bath can be found in the enclosure at the center of the lab near the office area.

3. Required Materials

3.1. Reactor components

The reactors sold by SITEC can be bought from Island Automation, contact dean@islandautomation.ca to purchase part number 740.8036. Other parts include 620.0110 Gland nuts and 620.0120 Ferrules.

Additional sand can be found underneath lab bench near batch reactor enclosure, should sand be replenished in the sand bath.

4. Reactor Operation

4.1. Loading

The reactor can be loaded by injection of liquid.

Load reactor using micropipettes based on the mass needed by experimentalist.

The batch reactor is too heavy for measurement using analytical balance. Experimentalist should measure weight difference of chemical container as opposed to batch reactor for precise mass measurements.

Caution: Many chemicals of interest are hazardous on contact, through inhalation or ingestion. Consult MSDS before conducting experiment. Load reactor inside fume hood to avoid inhalation risks.

To tighten reactor, the pressure tight ring should be screwed on after inserting the fastening nut. The pressure tight ring is reverse threaded, and tightens when turned counter-clockwise. Apply high temperature grease to the threading of the reactor to avoid pressure tight ring being stuck after thermal cycling. Place reactor cap on top of reactor body, before raising fastening and tightening reactor nut; make sure the reactor cap and base do not rotate in this process to avoid leaks in reactor. Once fastening nut has been tightened, clamp fastening nut with the vice located on the work bench, and tighten reactor cap using wrench by an additional 90°.

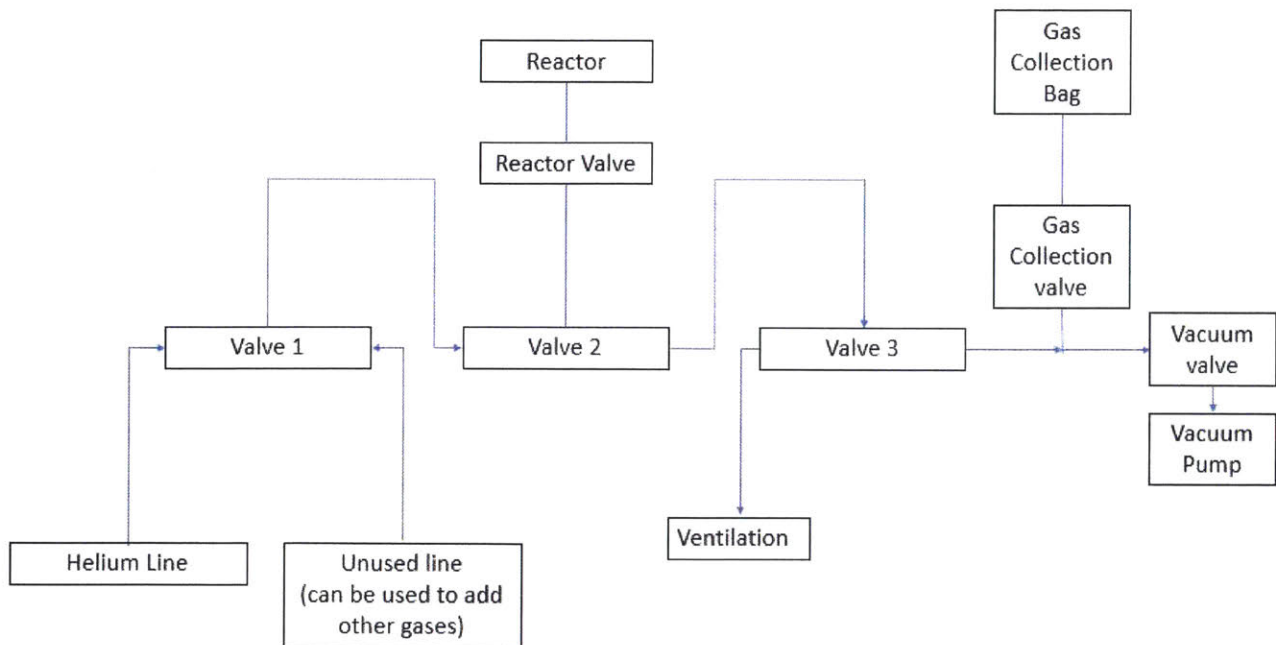
4.2. Operation of heated sand bath

To operate heated sand bath, turn on power switch of the heated sand bath, located inside reactor enclosure. Once the power switch is turned on, increase fluidization air flow until temperature control turns on. Heating will not take place without fluidization air to prevent uneven heat transfer. Set the appropriate temperature to sand bath by changing setpoint on temperature control. There is no confirm button; heating takes place once setpoint is changed.

The hanging wire of the reactor can be hung onto the orange hook located inside batch reactor. The pressure transducer and reactor outlet valve should be attached to the two sidearms. The purge line leading to the quenching water should be attached to the rupture disk. Finger tight nuts, and turn additional 10° with wrench to ensure pressure tightness.

4.3. Purging reactor

It is important to purge any air or oxygen from the reactor with helium. The three valves installed on the reactor enclosure will allow experimentalist to manipulate gas flow in and out of the pressure. The following diagram shows the configuration of valves



The valves connect one side (left or right) to the center. The base configuration of the reactor is valve 1 = left, valve 2 = right, valve 3 = left.

To load reactor with helium, first, turn on pressure transducer laptop to begin data acquisition of pressure data. Turn valve 2 to the left configuration to connect the helium line with the reactor and observe pressure increase in reactor as it gets filled with helium. Turn valve 2 to the right configuration to send helium to ventilation. Repeat 10 times to ensure reactor headspace is filled with helium instead of air. Afterwards, close reactor valve, and turn valve 2 to the right configuration to stop helium feed to the reactor. The pressure transducer reading should not drop in the next 10 minutes. If it does, there is a leak in reactor; the reactor should be re-tightened.

4.4. Heating Reactor

Reactor can be inserted into sand bath for heating. Pull overhead device to the left to position reactor over sand bath. To properly move device, hold handlebars as close as possible to the reactor enclosure, and pull parallel to the surface of the reactor enclosure. It is advised to use a step stool for shorter members. Once reactor is positioned on top of sand bath opening, descend

reactor using the lever; experimentalist should guide the wire above the orange hook to ensure reactor and side arms enter the sand bath. Observe hanging wire to ensure that there is tension between wire and orange hook; if the orange hook is lowered past this point, reactor may become trapped in sand bath as the wire becomes loosened from the hook.

Caution: Beware to heated elements. Never touch the sand bath. Never allow plastic components to touch the sand bath.

Caution: During reaction, reactor pressure may be high. Typical reactor pressure can reach 300 bar, and rupture disk has rating of 450 bar. Ensure all doors to reactor enclosure are closed during operation.

4.5. Product Collection

To terminate reaction, quench reactor using water bath. Ascend reactor from sand bath; remove sand from reactor quickly using pressurized air, and descend reactor into water bath to the right of the sand bath. Turn off the sand bath if not in use to avoid risks associated to heated elements.

After reactor has been cooled down to room temperature, gas can be collected using the 3-valve system and a gas collection bag. Gas bag should be opened and connected to gas collection valve. Valve 2 and valve 3 should be facing the right configuration. Vacuum valve should be closed. To purge gas bag with helium, repeatedly turn valve 2 between left and right configurations to fill gas bag with helium. Turn on vacuum and open vacuum valve to purge gas bag. Close vacuum valve and observe pressure gauge to ensure gas bag and gas collection piping are pressure tight.

Once gas collection is ready, make sure Valves 2 and 3 are facing the right configuration. Gas collection valve and vacuum valve should both be closed. Open the reactor outlet valve, observe pressure of reactor gas outlet if needed, and open gas collection valve to fill gas bag with sample. Close gas bag first, before removing from gas collection piping.

Unload reactor by loosening side arms and purge piping. Move reactor underneath a fume hood promptly to unfasten the rest of the reactor in reverse order to tightening reactor.

Caution: Hazardous gases may have formed during course of reaction. Do not expose reactor to unventilated areas for extended period of time. If any gas alarms in batch reactor enclosure come off (gas alarms currently set up for CO and H₂S), do not unload reactor until exposure limit is safe.

Unload reactor liquid to falcon tube. Proceed to analysis.

5. Safety Hazards

The safety hazards of operating this setup include:

1. High temperature of sand bath.
2. Possibility of high operating pressure of batch reactor.
3. Chemical exposure risks from loading reactor.
4. Gas exposure from reactor products.
5. Ergonomic risks from loading reactor and heating reactor.
6. Electrical risks when trouble shooting electrical elements for this setup.

Procedure for Performing Gold Tube Batch Reactor Experiment

Overview

This experiment involves the potential for toxic gas (hydrocarbons) generation and high pressure/temperature. Caution is advised during the procedure. The most important point to keep in mind is to have ventilation and never to touch heated elements.

Written by Lawrence Lai

Date Written: 4/15/2019

1. Purpose

The purpose of this document is to provide standard operating procedures for lab members who wish to use the gold tube batch reactor for experimentation.

2. Location of Equipment

Batch reactors are stored in fume hoods adjacent to the main faucet in the Green lab, E18-566. Work bench tools can be found to the right of the walk-in hood, and the heated sand bath can be found in the enclosure at the center of the lab near the office area.

3. Required Materials

The reactors sold by SITEC can be bought from Island Automation, contact dean@islandautomation.ca to purchase part number 740.8036. Other parts include 620.0110 Gland nuts and 620.0120 Ferrules.

Gold tubes are expensive, and therefore locked in one of the drawers of the lab. Consult Allen Mark Payne for keys and access to materials.

Argon is required to seal gold tubes

Additional sand can be found underneath lab bench near batch reactor enclosure, should sand be replenished in the sand bath.

4. Reactor Operation

4.1. Sealing gold tubes

Heat gold tubes with Bunsen burner until they glow. Let them cool. This annealing step makes removes organic contaminants from gold tube.

The Ono lab has a welder and argon for sealing gold tubes. Before sealing, make sure welding surface is free of any water or chemicals.

Clamp bottom of gold tube shut, cut clamped section with pliers to ensure a sharp surface. Proceed to welding from left to right using Energy of 8ms at 21%.

Caution: Use safety glasses and never look directly at arc flash; directly looking at flash may lead to blindness.

Caution: Never touch the welding needle, as it is a heated element. Any water that comes in contact with the needle could also cause welding to fail.

Re-perform annealing step to remove impurities.

Acid rinse gold tubes in 6M HCl for 6 hours to remove any iron impurities that may be in gold tubes.

4.2. Loading

The gold tubes can be loaded by injection of liquid.

Load reactor using micropipettes based on the mass needed by experimentalist.

Caution: Many chemicals of interest are hazardous on contact, through inhalation or ingestion. Consult MSDS before conducting experiment. Load reactor inside fume hood to avoid inhalation risks.

Fill gold tube headspace with argon; argon has a high density and will naturally sink; position argon needle at the inlet of the gold tube for 1 minutes to allow displacement of argon. Weld top of gold tube similarly to the bottom.

4.3. Tightening Reactor

To tighten reactor, the pressure tight ring should be screwed on after inserting the fastening nut. The pressure tight ring is reverse threaded, and tightens when turned counter-clockwise. Apply high temperature grease to the threading of the reactor to avoid pressure tight ring being stuck after thermal cycling. Place reactor cap on top of reactor body, before raising fastening and tightening reactor nut; make sure the reactor cap and base do not rotate in this process to avoid leaks in reactor. Once fastening nut has been tightened, clamp fastening nut with the vice located on the work bench, and tighten reactor cap using wrench by an additional 90°.

4.4. Operation of heated sand bath

To operated heated sand bath, turn on power switch of the heated sand bath, located inside reactor enclosure. Once the power switch is turned on, increase fluidization air flow until temperature control turns on. Heating will not take place without fluidization air to prevent

uneven heat transfer. Set the appropriate temperature to sand bath by changing setpoint on temperature control. There is no confirm button; heating takes place once setpoint is changed.

The hanging wire of the reactor can be hung onto the orange hook located inside batch reactor. The pressure transducer and reactor outlet valve should be attached to the two sidearms. The purge line leading to the quenching water should be attached to the rupture disk. Finger tight nuts, and turn additional 10° with wrench to ensure pressure tightness.

4.5. Filling Reactor

Reactor should be filled with water using syringe pumps located nearby. Pressure transducer and water line should be attached to side arms, and purge line should be connected to the rupture disk. Turn on syringe pump to appropriate pressure to fill reactor with water at desired pressure using the constant pressure setting on the syringe pump controls. Note that as water vaporizes, there will be flow in and out of the reactor from the syringe pump; this is normal.

Caution: During setup, reactor pressure may be high. Typical reactor pressure can reach 300 bar, and rupture disk has rating of 450 bar. Ensure all doors to reactor enclosure are closed during operation.

4.6. Heating Reactor

Reactor can be inserted into sand bath for heating. Pull overhead device to the left to position reactor over sand bath. To properly move device, hold handlebars as close as possible to the reactor enclosure, and pull parallel to the surface of the reactor enclosure. It is advised to use a step stool for shorter members. Once reactor is positioned on top of sand bath opening, descend reactor using the lever; experimentalist should guide the wire above the orange hook to ensure reactor and side arms enter the sand bath. Observe hanging wire to ensure that there is tension

between wire and orange hook; if the orange hook is lowered past this point, reactor may become trapped in sand bath as the wire becomes loosened from the hook.

Caution: Beware to heated elements. Never touch the sand bath. Never allow plastic components to touch the sand bath.

Caution: During reaction, reactor pressure may be high. Typical reactor pressure can reach 300 bar, and rupture disk has rating of 450 bar. Ensure all doors to reactor enclosure are closed during operation.

4.7. Product Collection

To terminate reaction, quench reactor using water bath. Ascend reactor from sand bath; remove sand from reactor quickly using pressurized air, and descend reactor into water bath to the right of the sand bath. Turn off the sand bath if not in use to avoid risks associated to heated elements.

After reactor has been cooled down to room temperature, water can be released using the pump controls, and gold tubes can be collected.

Insert gold tube into septum vials. Puncture gold tube with syringe and needle to collect gas for analysis as needed. Draw deeper to analyze liquid phase; dilute with DCM if needed.

5. Safety Hazards

The safety hazards of operating this setup include:

1. Electrical risks associated to welding
2. Arc flash from welder may cause blindness
3. Hydrochloric acid is corrosive
4. Annealing step has risk of exposed heated gold tube.
5. High temperature of sand bath.
6. Possibility of high operating pressure of batch reactor
7. Chemical exposure risks from loading reactor

8. Gas exposure from reactor products
9. Ergonomic risks from loading reactor and heating reactor

Procedure for Measuring Liquid Composition with 2-dimensional with Quadrupole Mass Spec

Written by Lawrence Lai

Date Written: 4/15/2019

1. Purpose

The purpose of this document is to provide standard operating procedures for lab members who wish to analyze samples using the GCxGC-qMS (2-dimensional gas chromatography with quadrupole mass spec).

2. Location of Equipment

GC unit provided by Agilent 7890A and modified by Zoex corporation is located on top of lab bench nearest to E17, located across window office.

3. Required Materials

Cleaning solvents (Acetone, Toluene, DCM, or CS₂) should be loaded prior to operation on cleaning rack.

GC vials can be found near the main faucet. Maintenance components can be found in nearby drawers.

4. GC Operation

4.1. Modifying GC Method

The base GC method as of 4/15/2019 is named "10312018_LAI_GCXGC_MS_SPLIT150.M". This method has the following settings:

- 1 microliter injection
- 1:150 split ratio
- Temperature ramp up to 300 degrees over 90 minutes
- Flowrate of 1mL/min
- Uses solvent A for washing

Any changes to the method can be made using this method, and saving as a new name.

4.2. Loading sample

Sample should be loaded in GC vials. Roughly 0.5mL is required for the sampling needle to touch the sample. If there is insufficient sample, glass inserts can be used to boost the liquid level of samples. One may also choose to use a diluent based on the sample's concentration.

Throughout the course of this thesis' work, 3-chlorothiophene is often added as an external standard to improve accuracy. Sample and standard weights must be precisely measured using an analytical balance.

4.3. Modulation Elements

The following are a list of elements used for modulation installed by Zoex corporation. They often function independently of the Agilent components, and specific instructions are given if necessary.

- Cooling component is located underneath GC unit. This device uses a refrigerant and a cooling cycle to cool to -90°C. Turn this device on before the first measurement; it takes roughly 15 minutes to cool to setpoint temperature.

- Nitrogen purge gas generator: Located behind pillar near Leco GCxGC device. Purge gas generator contacts with aforementioned cooling device and is used for the cold jet. No operation is needed to use this device; however, this device is shared with the Leco GCxGC, and piping must be swapped in order to use the Leco GCxGC instrument (two instruments can't run at the same time).
- Modulation control panel: Located on the right side of equipment. Modulation control allows user to set modulation time and hot jet time; this part electrically communicates with Agilent GC to open and close valves 2 and 3 periodically (controls the hot and cold jets). User must press the start button before beginning measurement.
- Modulation loop: Modulation loop is installed inside oven. The modulation loop passes the outlet of the hot and cold jet twice, at 1 meter apart. User does not have to tamper with modulation loop for measurement, but will likely encounter this component in maintenance.
- Hot and cold jet: Hot and cold jets are controlled by valves 1 and 2, controllable on the GC device. The two valves are set to be opened by the method file outlined above, and the modulation control panel will automatically toggle the two valves.
- Secondary Oven: Secondary oven is installed to provide secondary column with higher temperature than the primary column. Temperature of the secondary oven should be set 15° higher than the primary oven for optimal results. (Prevents flow from secondary column back to the primary).
- Valve 4: Valve 4 is installed to cool secondary oven between runs. Turn on valve 4 from the GC control panel between two runs to accelerate cooling.
- Auxiliary heating elements: Aux temperature 1 is used for heating the hot jet, Aux 2 for the secondary oven, and Aux 3 for the MSD transfer line. Aux 3 heating is stolen from the front inlet heating; as a result, the front inlet cannot be used (it's a redundant inlet for the most part).

4.4. Running a sample

Turn on the cooling device beneath the GC. Device takes 15 minutes to fully cool down. Press start on the modulation control to enable modulation.

Open gas cylinders for hydrogen and air to ignite flame ionization detector (FID). Helium should be always opened to ensure column is filled with inert gas.

Write the GC sequence by clicking the button with the vials and a piece of paper on it. Label each of your sample names, select a vial to analyze, and load the proper method.

Load the Standby.M before starting the sequence. This will revert the GC back to Standby.M after the measurement, allowing for resources to be conserved without user interference.

Press the start button (button with a running person and vials). The GC will start it's injection sequence.

Analyze sample with GC Image.

5. Safety Hazards

The safety hazards of operating this setup include:

1. The GC has many heated and cooled elements. Do not touch.
2. Hydrogen is used to ignite the flame ionization detector. Ensure that there are no leaks in the hydrogen; this gas is highly flammable.
3. Chemical risks with preparing sample and solvent washes. In particular, carbon disulfide is a very toxic substance, and should only be used as a solvent if no substitutes are available.

Procedure for Measuring Gas Composition with Shimadzu GC

Written by Lawrence Lai
Date Written: 4/15/2019

1. Purpose

The purpose of this document is to provide standard operating procedures for lab members who wish to analyze gas samples using the Shimadzu GC 2014.

2. Location of Equipment

GC unit is provided by Shimadzu 2014 series, to the left of the GCxGC-qMS and to the right of the flow reactor enclosure.

3. Required Materials

Syringes and needles will be used to transfer gas sample into the GC

4. GC Operation

4.1. Modifying GC Method

The base GC method as of 4/15/2019 is named "03212016_Lai_Method_GasInjection.gcmj".

Any changes to the method can be made using this method, and saving as a new name.

4.2. Running a sample

Turn on GC by pressing "GC On" on the left of the computer screen. This should turn on all gas flow and heating elements. Once the FID temperature is ready, press the ignition button to turn on FID, and press the detector on button to turn on detector.

Press single sample to prepare instrument to run a single sample. The sample log in button allows the user to specify the name of the sample and the file location.

Clean syringe by repeatedly pumping air (syringe is open using the white valve), followed by three sample washes. The nearby hood can be used to purge sample washes.

Draw 10mL of sample with syringe; press the black valve to seal the syringe. Press start on the computer to put GC in standby mode, then inject gas sample to the bottom right inlet of the GC, and then press start on the GC machine. Sample will be collected.

5. Safety Hazards

The safety hazards of operating this setup include:

1. The GC has many heated elements. Do not touch.
2. Hydrogen is used to ignite the flame ionization detector. Ensure that there are no leaks in the hydrogen; this gas is highly flammable.
3. Chemical risks with preparing sample and solvent washes. This GC is built for gas samples; ensure all gas waste is purged in fume hoods.

Standard Operating Procedures for Horiba Sulfur-In-Oil Analyzer SLFA-1000 Series

Written by Lawrence Lai and Isaiah Borne

Date Written: 5/22/2017

1. Purpose

The purpose of this document is to provide standard operating procedures for lab members who wish to use the Horiba SLFA-1000 in analyzing chemical samples for sulfur content.

2. Location of Equipment

The location of this piece of equipment is in the end of Green lab, E18-566, underneath the window and beside the secondary water faucet of the lab.

The supplies required to use this piece of equipment can be found in drawers right beneath the equipment. This includes this SOP, sample cells, sample windows, and the manufacturer's manual for this machine.

3. Required Materials to use equipment

The required materials to run this equipment include:

3.1. Sample cells

Sample cells are specialized containers used to hold sample for sulfur content analysis. These sample cells are designed to secure the sample window, as well as designed to fit properly in the SLFA-1000 unit.

3.2. Sample windows

Sample windows are transparent and colorless windows made by the manufacturer for the purposes of sample analysis using the SLFA-1000 series.

3.3. Solute and Solvent

The solute is the species of interest at which the user of this equipment will measure sulfur content for. Typically, due to the volume required to execute measurements, the solute is diluted by a solvent, either toluene, or mineral oil, or other species based on previous calibrations.

4. Calibration

Calibration is highly recommended prior to performing experiments, since the solvent of choice and range of sulfur content may vary from user to user.

4.1. Choice of solute and Solvent

For the purposes of calibration, the user has the freedom towards the choice of solute. The Green Group typically uses diethyl sulfide as our choice of solute. A series of four to six samples at different known solute concentrations are prepared.

Note: it is important that the weight percent of sulfur in the sample is known; this is as opposed to the weight percent of the sulfurous species (e.g. not the weight percent of diethyl sulfide in solution, but the weight percent of sulfur in solution).

The choice of solvent should best reflect the actual conditions while making measurements. If the sample of interest is going to be diluted in Toluene, calibrations should be done with a toluene solvent. Typical choices for solvent selection are toluene and mineral oil.

4.2. Sample Preparation

The method of sample preparation for calibration is identical to that of the method of sample preparation while making sulfur content measurements.

It is most important to note that the total volume of sample prepared should be as close to 5mL as possible.

A sample cell can be disassembled into two parts; a container component, and a ring shaped securing component. Sample must be diluted in another container, and 5mL of sample can be transferred into the container component of the sample cell.

The transparent cell window should then be placed on top of the sample cell, and the ring shaped securing component should be secured onto the cell window, down to the base of the

container component. While doing so, take special care to maintain a straight planar surface to the cell window to facilitate best measurements.

4.3. Operation of SLFA-1000 for Calibration

The following are steps to operate the SLFA-1000 for calibration

1. Make sure the SLFA-1000 is powered on; the power on switch is located at the back of the machine.
2. After the machine's startup, use the buttons and the screen to enter calibration mode..
3. Select an empty calibration setting, or a calibration setting to be overwritten.
Warning: Make sure calibration setting to be overwritten isn't currently in use by other lab members or projects.
4. Input weight percentages of sulfur for the samples to be used for calibration.
5. Input the number of repetitions per sample as desired.
6. Open the SLFA-1000 unit by flipping the latch to the right, and pushing the cover upwards. The latch cannot be opened during the machine's operation due to an electronic safety lock.
7. Insert samples into the unit, with cell windows facing downwards. Each sample should correspond to the weight percent inputted in step 4.
8. Close the lid. Press downwards onto the cover until latch flips towards the lock position on its own.
9. Press the calibrate button. The machine will automatically take measurements and print results out through the built in printer.

4.4. Tips on calibration

Often times the built in calibration isn't accurate. Perform a confirmation on the calibration samples to ensure consistence.

In the case where the built in calibration does not read accurate results, an external calibration can be done, correlating machine outputs to actual concentrations using math done externally.

5. Sulfur Measurements

The operation of the machine allows the user to find the sulfur content of a certain sample. The steps on choice of solvent and sample preparation are outlined in sections 4.1 and 4.2. The only difference between machine operation and calibration is the use of the SLFA-1000 unit, which is outlined below:

5.1. Operation of SLFA-1000 for making sulfur content measurements

The following are steps to operate the SLFA-1000 for sulfur content measurements.

1. Make sure the SLFA-1000 is powered on; the power on switch is located at the back of the machine.
2. After the machine's startup, use the buttons and screen to enter the measurement mode.
3. Choose the calibration setting and number of repetitions desired for each run. Also choose the amount of time for requisition.
4. Place samples into the SLFA-1000 unit similar to steps 6-8 outlined in section 4.3.
5. Press the measure button to begin acquisition. Results should be automatically collected and printed out through the printer.

6. Safety Hazards

The safety hazards of operating this machine include:

1. X-ray hazard; the machine employs the use of X-rays to measure sulfur content. While the X-ray light is on, be very sure not to open the lid of the machine.
 - a. The machine should not open itself during operating. Do not force the lid to open when the electronic lock is in effect.
2. Chemical hazards; while working with sample cells, make sure each cell is sealed tight to prevent any leakages. Many sulfur containing compounds are irritants to skin, and can have more serious health effects. Ensure that the sample stays contained within the sample cell through good loading.
3. Ergonomic hazards; since the equipment uses a latch door equipped with an electronic lock, it is possible for one to trap fingers, parts of clothing or personal protective equipment between the cover and the machine. Make very sure that this does not happen while closing the cover of the SLFA-1000 unit.

7. Registration

X-ray equipment is under Laws of registration for x-ray equipment. Please do not use the SLFA-1000 unit unless it is marked for being active and in use. Failure to do so will be a violation of Massachusetts State Law. Contact MIT-EHS to find out more, and to register the machine if the machine happens to be inactive.

Procedure for Using GC Image to Analyze GCxGC chromatograms

Written by Lawrence Lai

Date Written: 4/15/2019

1. Purpose

The purpose of this document is to provide standard operating procedures for lab members who wish to analyze GCxGC images using GC Image.

2. Location of Software Access

GC Image is provided by Zoex corporation. There is one physical USB activation key (it's teal colored), located on Hao-Wei Pang's desk.

3. Software Operation

3.1. Importing an Image

The data files ".ch" and ".MS" are compatible to be imported to GC Image. In general, GC Image requires a file with tabulated times (in seconds) and a signal.

On the import screen, select the correct sampling rate (divide 1 by the interval between two time points), select the correct run time (find the last time point), and most importantly, select the correct modulation period.

Note: This is particularly important for the GCxGC-qMS, since the modulation information is not stored in any GC file but controlled externally.

3.2. Image Processing

The color bar for the 2-dimensional chromatogram should be set so that the features of the GCxGC chromatogram can be clearly seen, but the instrument artifacts are not present. Some examples of instrument artifacts are diagonal streaks trailing the solvent, streaks leading to the column bleed, etc.

Use the correct baseline function to remove baseline noise. Shift phase to align the MS and FID images, and set aliphatics to the bottom of the chromatogram.

The interactive blob detection tool will allow users to interactively select for settings that are optimized to visualize GC peaks. In general, if background noise is being picked up as peak signal, the peak height and area thresholds of the blob detection should be set higher to avoid these background signals being picked up. If any main features are being omitted, the peak height and area thresholds should be set lower.

For MS chromatograms, the MS tool can be used for peak identification. Enable the MS setting, and use the left click to analyze MS signals. Typical tools for analyzing GC MS, such as isolated m/z ion views, are available on this software.

3.3. Extrapolating Data

The template mode of GC Image allows the extrapolation of identified peaks from one chromatogram to another. To use this feature, identify all peaks in one chromatogram. Highlight all peaks, press the template button, and add all the peaks to the template. Click File > Save Template to generate a template file.

On a new chromatogram, after blob detection, a template can be loaded, matched, and incorporated to fill in peak identities. This feature will greatly speed up GC analysis.

Procedure for Developing Group Additivity Values

Written by Lawrence Lai

Original script developed by Ryan Gillis

Date Written: 4/15/2019

1. Purpose

The purpose of this document is to provide standard operating procedures for lab members who wish develop group additivity values, given the thermochemistry values in the format of enthalpy, entropy, and heat capacities in 300K, 400K, 500K, 600K, 800K, 1000K, and 1500K.

2. File Name

The main file to develop group additivity values is named "Make Group Values.ipynb". This file will be made available to the group. This code is written in Python, using dependencies Numpy and Pandas.

3. Inputs

This code implements the weighted least squares outlined in Chapter 3. Proper operation of this code requires input files to be setup correctly.

Matrix A is set up as "coefficients.csv"; each column represents a training species, and each row represents the occurrence of an unknown group.

Matrix C is set up as "correction.csv"; very similar setup to Matrix A, but instead, each row represents the occurrence of a known group.

Matrix D is set up as “known.csv”; each column is a group value in Matrix C (the ordering of the columns must be same as the rows in matrix C); each row represents the H, S, and Cp values (in ascending order of temperature).

Matrix E is set up as “thermoparam.csv”; each column represents a species, and each row represents H, S, and Cp values similar to Matrix D. Source of this matrix is always a set of CBS-QB3 calculations for my work.

The csv file “labels.csv” is used to label the unknown groups.

The csv file “KnownGroupUncertainties.csv” is in the exact same format as Matrix D, but instead carries the values for uncertainties of H, S, and Cp values instead. If uncertainties are unknown, I typically assume the uncertainty is zero; this is obviously incorrect, and future lab members should set up a system to account for unknown uncertainty values.

4. File Operation

The only line of code that is important is the following:

```
SigmaE.iloc[0] = 1.08 #Add CBS-QB3 Error in all enthalpies according to Montgomery 1999
```

This line assumes that all enthalpies in Matrix E has an set uncertainty value. This value/line should be changed based on the source of the training data.

Everything should be ready to go upon pressing the restart and run button.

5. Output

This script currently outputs standard errors for group additivity values to a csv file. This script also prints thermochemistry groups to the standard output, with a few caveats.

- The index is always 2050
- The group structure is never drawn correctly (it currently always outputs methane)
- Radical species do not have their enthalpy corrections printed correctly; the proper enthalpy corrections for radicals should be the output value + 52.1 kcal/mol due to Lay and Tsan's HBI Scheme
- The comments for every single group value are set to be the same message. This should be changed when incorporated to the RMG-database

It is highly encouraged to use ThermoEstimator.py to estimate the thermochemistry of species in "thermoparam.csv" to ensure that RMG's new estimations are close to the training data.

6. Future Improvements to This Script

Should anybody want to make future improvements to this script, I have a few suggestions:

- A separate script should be developed to generate input files automatically. I have a preliminary scrip that generates "correction.csv" and "known.csv" given "thermoparam.csv", but this script is incomplete and relies on some manual tweaking. The name of this script is called "MakeGroupsSpreadsheets.ipynb", which will also be made available.
- This script can ideally be made to interact with RMG to generate group structures from the SMILES string specified in "thermoparam.csv".
- In general, this script lacks many aspects of automation that can be fixed in the hands of a better programmer.

Appendix C

The Lawrence Trick Book

Here are some undocumented tricks that Lawrence uses to solve many of his problems.

On the topic of the batch reactor

Batch reactor leaking

One of the side arms or the main batch reactor body is leaking. Snoop leak detector can be used to detect for leaks. Apply snoop on side arm connections, and the leak hole on the batch reactor to detect for leaks. A leak will manifest itself as bubbles appear on the applied area. To fix this, tighten the affected areas better.

Note: Just because snoop doesn't detect a leak doesn't mean there is no leak. You should always check for leaks by reading the pressure of a closed reactor for a duration of 10 minutes.

If there is a leak that snoop does not identify, the leak is usually on the reactor body. Re-tighten reactor, making sure cap and reactor body does not move (only allow the fastening nut to rotate until reactor is finger tight).

Pressure Tight Ring is Stuck

You can usually loosen the ring by lightly gripping ring with a vice and turning the reactor body. A few things to take note: (1) if the ring is gripped too tightly, the next use of the reactor will almost always fail, because the vice leaves markings on the ring; consider gripping it behind a couple pieces of wood. (2) if you manage to get the ring out, it usually means there is some external debris trapped in the threading or other parts of the ring; try to clean these out with acetone, but also expect the reactor to fail pretty soon.

Remember, greasing threading with high pressure grease will avoid this situation and increase the lifetime of a reactor, but reactors don't last forever.

There was one instance in the past where we took these reactors where the ring won't move to the machine shop for inspection. With some fine machine work they did, they were able to make the ring spin smooth again. Consider doing this in the future.

The Temperature Controller on the Sand Bath

It might seem like it's impossible to decrease the temperature setpoint of the sand bath. This is false. You just need to press very hard, because the controller's pretty old. I've found that pressing it with a 1/8 inch pipe works wonders.

On the Topic of Gas Chromatography

Inlet won't hold pressure

One of the few inlet components are defective. This includes the glass liner, the o-ring around the glass liner, and the septum. There are plenty of these parts underneath the LECO GCxGC at the top drawer, and these parts are pretty easy to replace.

If there is no helium flow, the inlet will not get any pressure.

FID won't ignite

The most common cause for this is that the hydrogen line was just turned on, and the line is still filled with air. Set the hydrogen flowrate to 50 and wait for 5 minutes before trying again.

The Leco GCxGC FID was not set up to ignite properly, because the SCD sits on top of it. The user needs to give it some help by (1) opening the ignition wire, but maintain its electrical contact with the FID (make sure they touch), (2) press the ignite button, (3), hold an open flame outside the FID hole. It may take a few tries to successfully ignite the FID on this machine. This method also helps the GCxGC-qMS if it won't ignite.

Lack of Signal

There are many reasons why there would be a lack of signal. Check the following cases.

If one detector shows signal and another doesn't (e.g. has MS signal but no FID), the problem is with the detector. Check that detector, and the connections leading up to that detector.

If both detectors show no signal, but there is column bleed at the end of the run, it means that connections are made properly, but the sample didn't get through to the inlet. Check the inlet, and also check the liquid level on the sample to make sure that the needle contacted.

If there is no column bleed, it implies there is no flow throughout the column. Check if the column is broken inside the oven. If all else fails, replace entire column to observe effects; unreplaced one piece at a time to isolate problem; the connections between column in a GCxGC device can leak.

Unintended Signal

If something is in the products that you do not expect, there is contamination, either in the sample, or in the machine. First, check if this signal belongs to a common cleaning solvent, such as acetone or toluene. If so, more sample washes should get rid of the cleaning solvent. In general, acetone is the better cleaning solvent regarding this problem; toluene should only be used if samples can't be washed with acetone, such as crude oil or heavy hydrocarbons.

Other unintended signals can originate from previous runs. There have been past examples where a crude oil sample was trapped in the column until the next run, contaminating the following user's results. Should this ever happen, set the oven temperature to 300°C and let the GC purge for 24 hours.

Remake the sample if possible to ensure there are no contaminants from the sample side.

Altered Peak Shapes/Bad Modulation

If peaks on a GCxGC appear in unintended shapes, it is very likely that something is wrong with the modulation.

On the GCxGC-qMS, the most likely cause is that the modulation loop is not properly aligned to the jets. Make sure the loop crosses the outlet of the both jets twice.

On the GCxGC-Leco, we have had experience in the past where a cold jet was clogged with ice, and one of the cold jets were not able to function. The instrument software has a debugging setting that lets you turn on the jets while a run is not in place; this is a good place to check whether the jets are working. If a cold jet is clogged, turn on the jet overnight, and allow the ice inside to melt.

In all cases, if jet is not working, try to identify the problem causing it, and fix the jet.

On the Topic of the XRF

Printer not printing properly

Depending on the humidity of the day and other reasons, the roller on the printer won't work. My advice is to get the part replaced if you are really irritated by it. The instrument still functions, and you can easily write down the output of the machine somewhere else and analyze it there.

In fact, the machine has been used without a printer for a while, and that was a much more tedious process. We had to restart the machine after every single measurement because it would crash upon finding out that there is no printer. Highly do not recommending going through that again.

On the Topic of GC Image

Correct baseline algorithm is killing signal

Often times seeing many small peaks go from a chromatogram bothers a lot of users. It is important to note that you will most likely not use that information on your final analysis, so step 1 is to stop being perfectionistic.

But in the case that some important information is being pruned, the baseline correction algorithm thresholds can be altered on the software. I have limited experience with this, however.

MS signal doesn't match anything in database library

This could be a result of one of many possibilities.

It is possible that the actual species that the peak matches is not in the NIST database library, therefore it tries to draw the closest analogies and isn't able to find anything. Do not rely on the MS signal and library to tell you what everything is in general; there is a lot of contextual clues based on the position of the GCxGC chromatogram and the reactants that could lead you to a more plausible answer than the library search alone.

Two or more isomers with similar MS signal can be present in the library. For example, the MS features of 1-methylnaphthalene and 2-methylnaphthalene aren't that different; the MS search will most likely be unable to tell between the two. If the MS can't tell you which one is which, and you are out of clues, report them as methylnaphthalene isomers.

It is also possible for two peaks to have eluted around the same region (it's still possible even using the GCxGC). If the MS signals from the two compounds are different, but their retention times are similar, it could cause this problem. There is not a lot that you can do about this other than changing the GC method or the column sets. Just be aware of whether if you really need that peak information.

MS search window doesn't show up

Really stupid problem that has costed me over a day. If it's not showing up, it's usually because (1) you're trying to do an MS search on an FID, or (2) the MS search window showed up on your "secondary display device" when there is no secondary display device. To solve problem (2), hold windows key and hit left a few times.

Template match isn't accurate

You will often find that the template match tool isn't accurate, even on two chromatograms that supposedly show the same species (same species being run twice). Just accept that the template match algorithm isn't perfect, and sometimes you will have to manually check everything and make a few changes.

Over long periods of time, however, the templates will stray further (especially if sections of the column have been cut or replaced). To GC Image's credit, the template match algorithm is still pretty good at detecting major shifts like this, but again, it's not going to be perfect.

The GC Image Key is missing

You guys need to clean up your stuff better and stop losing things.

On the Topic of Gaussian

Error by 1999.exe

This is by far the most common problem. Gaussian ran out of steps in a geometry optimization.

Use this input line on the checkpoint file of your previous run:

```
#B3LYP/6-311++G(d,p) OPT=ReadFC freq Geom=AllCheck Guess=Read
```

This will make gaussian calculate the frequency, and read force constants from that frequency calculation. Solves the problem most of the time.

CBS-QB3 Calculation terminates on couple cluster step

Sometimes this could happen when pharos runs out of memory. Do an ssh into the node that you were running, and type in "du -sh ../../scratch" to find out the memory that is in use in the scratch directory. If it says 204GB, it means the job terminated because the scratch memory is full. Rerun the job on a more empty node, or if all else fails, it means your molecule is a little too large.

Hindered rotor calculation fails

Usually, this means that the four atoms selected for dihedral angle was not specified correctly.

Check the atom numbers to make sure the four atoms were intended ones.

In some circumstances, it may also meant that the bond was not supposed to be rotated.

Obviously, if the rotating bond is bound inside a cyclic structure, the calculation will most likely fail. Other examples include when the rotation of the bond causes atoms to crash, there are coupled rotation effects (such as p-xylene).

On the Topic of Cantherm

My software says it's called Arkane

No. It's called Cantherm.

Cantherm says there is a lower energy conformation

You will unfortunately have to restart your calculations. Look in the conformer scan to find which scan has the lowest energy, and use that conformer as your initial guess for the geometry optimization.

Fourier fit does not fit rotor scan

Few reasons that this can happen other than not starting at the correct conformation. First, check the y-axis of the rotor scan. If it's small (< 1 kcal/mol), the erratic rotor scan may mean that the rotor is a free rotor, and Gaussian isn't able to find a very well defined energy minimum at the specific dihedral angle.

Then check for high barriers (< 10 kcal/mol). It may also mean that the bond was not supposed to be rotated. For example, the first bond of hexylbenzene rad 1 is not supposed to be rotatable, because the radical can be resonantly stabilized with the aromatic ring, and that bond can be drawn as a double bond. Saves you a lot of time to identify these mistakes ahead of time.

On the Topic of Group Additivity Development

Another reviewer tells me machine learning is the future

Politely agree and move on, saying that Yi Pei's work needs more training data.

I want RMG estimates of my training species

Use the molecule search tool on https://rmg.mit.edu/molecule_search, hit search thermochemistry, and look for the estimates.

You can also use the thermoEstimator found in RMG/scripts to process a batch of species.

RMG's unit tests say new group cannot be accessed

When you write a new group, there are many nuances that you need to account for to make sure that this group works, and didn't break any other groups. For one, the group structure that you have supplied must be correct, and the group name should be added to the appropriate level in the tree structure at the bottom of groups.py/radical.py/polycyclic.py/etc.

The group that you have written must be a subset of the parent group that it references in the tree. You may only further specify things, or specify additional surrounding structures, but you can not change anything in the existing structure. The ordering of the atoms and bonds must also match line by line, or else it wouldn't work (you can be technically correct here but not syntactically correct).

A common mistake that I find myself making is overspecifying the parent structures too early. For example, it is common instinct to draw single bonds and specify single bonded carbons. I remember myself specifying the s2_6_7_ben group with benzene bonds on one side and single bonds on the other side, and it worked properly to estimate benzocycloheptene. Later, I wanted to make a group for benzocycloheptadiene, and it didn't work because the 7 membered ring was already specified with all single bonds, and I tried to add a double bond to the child structure.

Always use [S,D,T,B] bonds if you're not sure, and specify the C atom or R!H atom times unless appropriate.

EstimateThermo doesn't use the specified group

This is commonly tied with the previous problem. If a group isn't written properly or specified properly, or if it's parent isn't written or specified properly, the ThermoEstimator will not be able to use the group.

Updated Group additivity value estimates do not match training data

Depending on how they do not match, you will have to adjust your strategy accordingly. If the updated group additivity value estimates are only off by a little in entropy but not in anything else, it means symmetry was not implemented properly in RMG, or wasn't taken care of properly in the development of group additivity values. Recall that RMG has an algorithm to calculate symmetry when generating species thermochemistry using group additivity value, and group additivity values do not intrinsically carry any symmetry effects. This means the training data used to construct group additivity values must not contain any symmetry effects. This often means setting external symmetry, rotor symmetry, and optical isomers to 1, regardless of what the actual symmetry number may actually be.

Mistakes can often occur when working with spreadsheets and spreadsheets of numbers. Make sure all numbers are implemented in the correct order. Also make sure ThermoEstimator.py is using the correct thermochemistry groups for the estimation.

If your average error of estimation is 0 with a wide margin of error, it may mean that the group additivity values added were not specific enough. It is recommended to further specify the different group values to achieve better training accuracy.

On the Topic of Developing Training Reactions

Unit test says cannot identify reaction

The participating atoms in a reaction need to be specified accurately. In some cases such as `R_Addition_Multiple Bond`, this is very intuitive, because there are never more than 3 atoms involved. In intramolecular reaction families, such as `Intra_H_Migration`, this may be more complicated. Check the recipe at the top, and look through other examples to make sure all the numbers (*1, *2, etc.) are implemented properly.

generateReactions.py script is not picking up training reaction

If `generateReactions` doesn't pick up an exact match of a training reaction, then there are either two of the same training reaction, or the training reaction isn't implemented properly.

If the script does not pick up an analogous match, there may be another node on the reaction tree that is closer than the test case. There may also be multiple reactions matching that node of the tree, in that case you may want to further specify your reaction groups. Read the output file for `generateReactions.py` for more details.

On the topic of developing new training groups

Often times, the reaction trees may not contain sufficient specificity for your new training reaction to be distinct from an analogous reaction. In this case, a new training group must be added. The script written by Max "`analyzeTrainingReactions.ipynb`" can be used to check whether if multiple training reactions match the same reaction group, and will give a useful visualization to decide whether if a new group should be developed.

Reaction group is not accessible

Similar to the group additivity section, the reaction groups have to be properly implemented. Again, the proper structures need to be drawn, and the appropriate entry must be added to the correct level of the tree.

Similar rules apply. Children must be a subset of the parent. The lines of atom specification must be exactly the same. The parent must not be over specified. You know the rules by now; read the group additivity section for more.

Aromatic Reaction Groups aren't being used

One of the many reasons would be that the adjacency lists used for the associated training reactions were written in single/double bond notations. You want to convert everything to using benzene bonds. The RMG website doesn't automatically output in benzene bonds; you will want to use the scripts "dictionaryToAromatic.py" or "thermo_library_aromatic_adjlists.ipynb" to do this conversion. Scripts written by Max.

On the Topic of Generating RMG Models

A reaction that I thought was for sure going to happen isn't included

Many reasons. If you are relying on automatic generation to find your reaction, the first thing that could be missing is that an entire reaction family is excluded or not included in the first place.

Next, it is possible that a reaction you think for sure is happening actually didn't make it past the flux criteria. Check the edge, see how many competing reactions are taking place. I would suggest to seed the mechanism with all the species involved in the reaction to make sure that the reaction is at least implemented correctly.

Which brings us to if you are on a seeded mechanism. If all species of that reaction are seeded, everything was in the core to start with. Your choices narrow down; again, the reaction family or library might not have been included, or the reaction may not have been implemented correctly in the database.

RMG won't start

Make sure you fetched, pulled, made clean.

And if all of that fails, check the error message for hints. The most common thing I tend to miss is a comma or an indentation at a key place, like in the input file, in a group that I just wrote, or in a training reaction that I just implemented.

Concentration of a species does not match experiments/literature

Sensitivity analysis of the species with respect to all reactions and all thermochemistry of the model. Find the key species and reactions that control the species' concentration.

Check for the sources to see if any of these species or reactions come from a questionable source. If it says Lai et al. CBS-QB3 calculation, there's not a lot you can do, but if there is no documentation, or if the groups used to come up with the species thermochemistry or rate

coefficient doesn't actually represent your system (missing features), it is a good idea to update said group, and generate some of your own training data.

If this does not work, it is possible that key reactions are missing that have caused the concentration of said species to be inaccurate. For example, in the biphenyl system, we updated the thermochemistry and kinetics of the relevant pathways based on sensitivity analysis, but did not yield successful results. This would be a good time to consult Professor Green to brainstorm for a few new reaction pathways; in my case, he came up with pathway (5), and someone should generate some training data for that.

Last step is to blame the experiment or literature.

RMG won't converge

When dealing with systems as large as the hexylbenzene system, it's just common that RMG won't converge. If the new reactions that RMG is generating aren't really changing the overall product composition of the system, it really doesn't matter that the model has not fully converged based on the flux criteria.